eXPRESS Polymer Letters Vol.4, No.1 (2010) 1
Available online at www.expresspolymlett.com
DOI: 10.3144/expresspolymlett.2010.1

Preface

T. Czigány[*]*, Gy. Bánhegyi, J. Karger-Kocsis*

Department of Polymer Engineering, Budapest University of Technology and Economics, Műegyetem rkp. 3., H-1111, Budapest, Hungary

Dear Readers,

Now you are reading the first, January issue of the fourth volume. Each New Year starts with some retrospection and account on the one hand and with expectations for the future on the other hand. ***eXPRESS Polymer Letters*** has 'survived' the first three years, characterized by continuously growing acceptance and international respect of the journal. The past three years can be called a success story; three, as in the tales, proved to be a lucky number. In addition to luck, however, we needed good papers, strict and fast peer reviewing, exact, predictable and fault-free editing and publication. Expressed in numbers it means that we usually inform the authors within 48 hours, whether the article has been accepted for reviewing or not. The reviewing process is finished within 4 weeks, the authors are notified of the results (usually about 3 referees review an article). The acceptance or returning of the corrected manuscript is usually done within 72 hours, the proof of the finally accepted article is generally sent to the author within 2–4 weeks, which is usually published in the journal in the final form (with page and DOI numbers) within 2–3 weeks (all numbers are averages). It means that a submitted paper may appear in ***eXPRESS Polymer Letters*** within as short timespan as 2–3 months provided that the authors cooperate, i.e. correct the manuscripts and the proofs fast.

About 100 articles are published annually in the journal, which has 'imploded' into the scientific community (as shown by the references). ***eXPRESS Polymer Letters*** has been indexed among others by SCOPUS since 2008, and by Thomson Reuters since 2009. The articles appeared in the Web of Science from the beginning, i.e. from 2007 on, where citations increased exponentially (20 in 2007, 106 in 2008, about 400 in 2009). This growing international acceptance might be due to the strict peer reviewing process. Accordingly, ca. 70% of the manuscripts submitted so far from 53 countries have been rejected.

Continuously increasing popularity of ***eXPRESS Polymer Letters*** is shown by the fact that in 2009 several hundred readers visited our website daily to download articles, to check out conference dates, or simply to get acquainted with the site. Many colleagues use our website as a kind of 'home page' as the 'related journals' menu links to the websites of other journals.

Based on all these facts we are eagerly looking forward the Journal Citation Report of Thomson Reuters, to appear in the summer of 2010, which surely will contain the first impact factor of ***eXPRESS Polymer Letters*** for the year 2009. We are looking forward to the further cooperation with our authors, referees and readers. The editors wish you a lot of success in year 2010. *Sincerely yours*,

Dr. Gy. Bánhegyi Prof. Dr.-Ing. Dr.hc. J. Karger-Kocsis
Prof. Dr. T. Czigány

[*]Corresponding author, e-mail: czigany@eik.bme.hu

eXPRESS Polymer Letters Vol.4, No.1 (2010) 2–8
Available online at www.expresspolymlett.com
DOI: 10.3144/expresspolymlett.2010.2

Investigation on glassy skin formation of porous polystyrene fibers electrospun from DMF

M. M. Demir

Department of Chemistry, İzmir Institute of Technology, Gülbahçe Köyü, Urla 35430 İzmir, Turkey

Received 20 August 2009; accepted in revised form 5 October 2009

Abstract. Micrometer and submicrometer diameter of polystyrene (PS) fibers were electrospun from various dimethyl formamide (DMF) solutions at different weight fractions under 35% relative humidity. Increasing polymer fraction in the solution results in a gradual morphological transition from beads-with-incipient to bead-free fibers and also increases the diameter. The formation of uniform glassy skin presumably due to radial capillary flow within the liquid jet was confirmed by scanning electron microscope. The thickness of the skin varies with the weight fraction of PS; therefore, it was normalized with respect to average fiber diameter (AFD). The skin gets thinner as the weight fraction of PS increases. In addition, the fibers exhibit highly porous internal structure and smooth surface along with slight porosity. The development of porosity is attributed to liquid-liquid phase separation of water molecules in atmospheric moisture and DMF.

Keywords: *nanomaterials, electrospinning, capillary flow, humidity, porosity*

1. Introduction

Electrospinning has been proven as a robust technique to produce polymeric fibers whose diameter is on the order of a few tens to hundreds of nanometers [1]. In a typical process, a high electrical potential is applied between a polymer solution placed into a reservoir and a grounded conductive target. When the applied electrical force overcomes surface tension of the solution droplet at the nozzle of the reservoir, a charged jet is ejected from the droplet. The jet becomes thinner as it flows through the collector due to both solvent evaporation and continuous electrical force stretching. The polymer concentration gradually increases on the surface of the jet due to solvent loss. This process eventually leaves a dense, skin-like external boundary along the perimeter of the resulting fiber. While it has been accepted that a thin and mechanically distinct skin is formed initially on the charged liquid jet during solidification of fibers [2], experimental results exhibiting the formation of glassy skin on electrospun fibers have not been reported. In this work, we have verified this phenomenon by microscopic observations on electrospun PS fibers and quantified the skin thickness with respect to average fiber diameter (AFD).

A nonwoven fiber mat having a high surface area to volume ratio on the order of 1–100 m^2/g is achieved by electrospinning, which offers numerous existing and potential applications in filtration [3], catalysis [4, 5], and tissue engineering [6]. The surface area of the mats can be further enlarged when surface and/or interior porosity is developed within the electrospun filaments [7, 8]. Two main approaches have been employed to produce porosity in the fibers. One approach is leaching one of the phases out from a bicomponent fiber systems for example polymer blends [9, 10] and the fibers remain rough and porous. Using similar methodology, not only polymeric but also porous *ceramic* fibers can be

*Corresponding author, e-mail: mdemir@iyte.edu.tr

readily obtained by calcination of polymeric component from binary polymer/metal salt systems [11]. Another approach to produce porosity in electrospun fibers is to use highly volatile co-solvents [9, 12]. Rapid solvent evaporation causes phase separation into polymer-rich and solvent-rich domains. The evaporation of volatile co-solvents leaves behind voids thereby porosity along the fiber volume is achieved. This approach was extended to electrospinning of hydrophobic polymers dissolved in a water-compatible solvent in a humid environment [13] because the liquid-liquid phase separation can occur even in the presence of small amount of nonsolvent [14], *e.g.* moisture in air. The charged jet uptakes water from the vapor, which acts as a nonsolvent for the polymers. The miscibility of water with solvent causes formation of liquid-liquid phase separation and finally porous features within the fibers occur. Recently, Pai *et al*. reported interior porosity of polystyrene fibers prepared from DMF at different levels of humidity and influence of this internal morphology on mechanical strength and stiffness of the electrospun fibers [15]. The same group also pointed out the development of wrinkled surface topography of fibers that result from buckling instability of the charged jet in poly(acrylonitrile) (PAN) and PS. Rabolt *et al*. investigated the influence of polymer/solvent properties using a variety of solvents on fibers surface morphology [16] and demonstrated the formation of pores on the surface of PS fibers electrospun in humid environment [17]. Here, we electrospun PS from DMF solution at 35% relative humidity and also demonstrated that the resulting fibers have both interior and surface porosity.

2. Experimental

Polystyrene (PS) (M_n = 170 kg/mol M_w = 350 kg/mol) and dimethylformamide (DMF) (ACS reagent, >99%) were provided from Aldrich and Fluka, respectively. They were used without further purification. Four different weight fraction solutions (0.05, 0.10, 0.15, and 0.25) were prepared. These clear solutions were subjected to electrospinning at 3 kV/cm using a power supply, Gamma Voltage ES 40P-20 W. In all experiments, the instrumental parameters were unchanged such that the applied voltage and source-to-target distance were 15 kV and 5 cm, respectively. Flow rate (~3 mL/h) was controlled by an infusion pump. The fibers were imaged by scanning electron microscopy (SEM) of Philips XL-30S FEG. The diameter of PS fibers was obtained from SEM images using image J software from at least measurement of 100 polystyrene fibers. In order to examine the internal structure of the fibers, electrospun mats were kept in liquid nitrogen for a while to decrease temperature far below the glass transition temperature of PS and the constituent fibers were broken. The broken end of the fibers was found in electrospun mat by SEM and cross sectional morphology was examined using ultrahigh resolution mode. Two sources of uncertainties may be affecting the observations of skin thickness. First, the SEM images appear to be tilted, therefore the thickness may not be measured properly. To minimize the effect of tilting, the thickness was measured from several points of the skin and the results were averaged out. Second, the border between skin and bulk was not clear especially for the fibers obtained at low polymer fractions. This is because the measured thickness value was normalized with respect to AFD for true comparison.

3. Results and discussion

Chain entanglement is one of the important parameters for stability of liquid jet in electrospinning [18, 19]. It is the effect of ϕ_p and M where ϕ_p is volume fraction and M is weight average molecular weight. The entanglement can be quantified with entanglement number in solution, $(n_e)_{soln} = (\phi_p M_w/M_e)$ using ρ = 1.05 g/cm^3 and M_e = 16 600 g/mol. SEM images of PS fibers electrospun from four solutions of different weight fractions are presented in Figure 1. The structure of the fibers varies significantly with the polymer weight fraction. At the lowest fraction (0.05), the charged jet is unstable and bead-with-incipient fibers were obtained (panel **a**). The formation of incipient fibers suggests some degree of chain entanglement in solution, $(n_e)_{soln}$ <1. At 0.10, beads-on-string morphology is achieved. The solution entanglement number calculated for this condition is ~2. Increasing the polymer fraction to 0.15 yields continuous structure in which the occurrence of beads diminished gradually and their shape becomes more spindle-like (panel **c**). At this fraction, chain entanglement number is $(n_e)_{soln}$ ~3 and the liquid jet was fully stabilized. Further

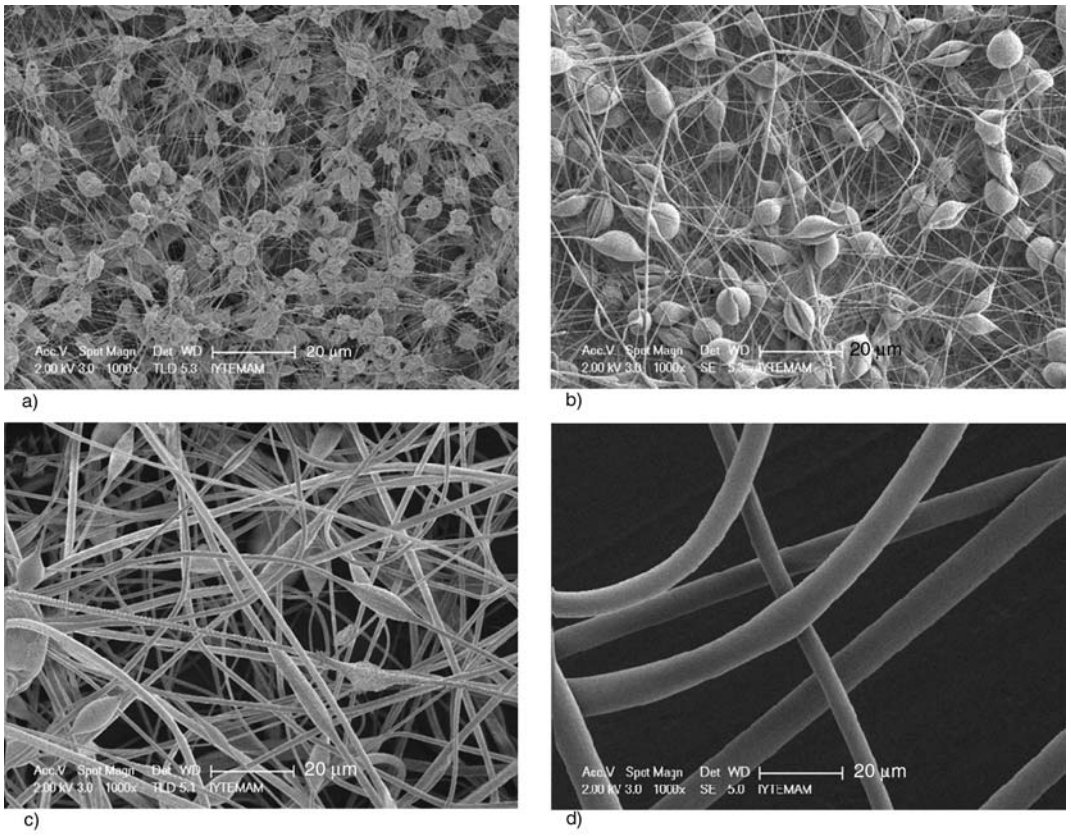

Figure 1. SEM images of PS fibers obtained from DMF solutions at different weight fractions under 35% relative humidity. (a) 0.05, (b) 0.10 (c) 0.15, and (d) 0.25

increase of fraction to 0.25 increases viscosity of solution due to extensive chain entanglements, $(n_e)_{soln}$ ~4.8. Hence, continuous and bead-free thick fibers were produced. The general trend of morphological transition presented here is consistent with literature, which was obtained for electrospinning of both PS and some other polymer/solvent systems [18].

The dependences of AFD and skin thickness normalized with respect to AFD on PS weight fraction are demonstrated in Figure 2. A power law relationship was found between AFD and weight fraction such that AFD ~(weight fraction)$^{2.4}$. This expression is very close to the one we reported previously for polyurethane urea/DMF system [20]. At the most dilute solution (0.05), the diameter of bead-with-incipient fibers is ~100 nm. An apparent broken end of fiber was not observed since the mat is mainly composed of beads on the order of several µm. However, a cross sectional morphology is gradually developed as the polymer fraction in solution increases. Panel **a**, **b**, and **c** of Figure 3 show broken end of the fibers obtained from solutions of 0.10, 0.15, and 0.25, respectively. The skin

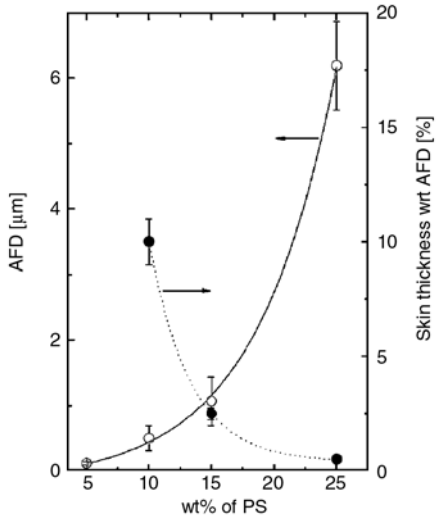

Figure 2. Average fiber diameter (AFD) and skin thickness of fibers normalized with respect to AFD as functions of weight fraction of PS

layer is much thinner than the diameter of fibers and its thickness varies with the fraction of PS in electrospinning solution. To make a true comparison, it was normalized with respect to AFD (right y-axis of Figure 2). In contrast to AFD, the normalized skin thickness is inversely proportional with weight fraction of PS. In other words, the skin layer

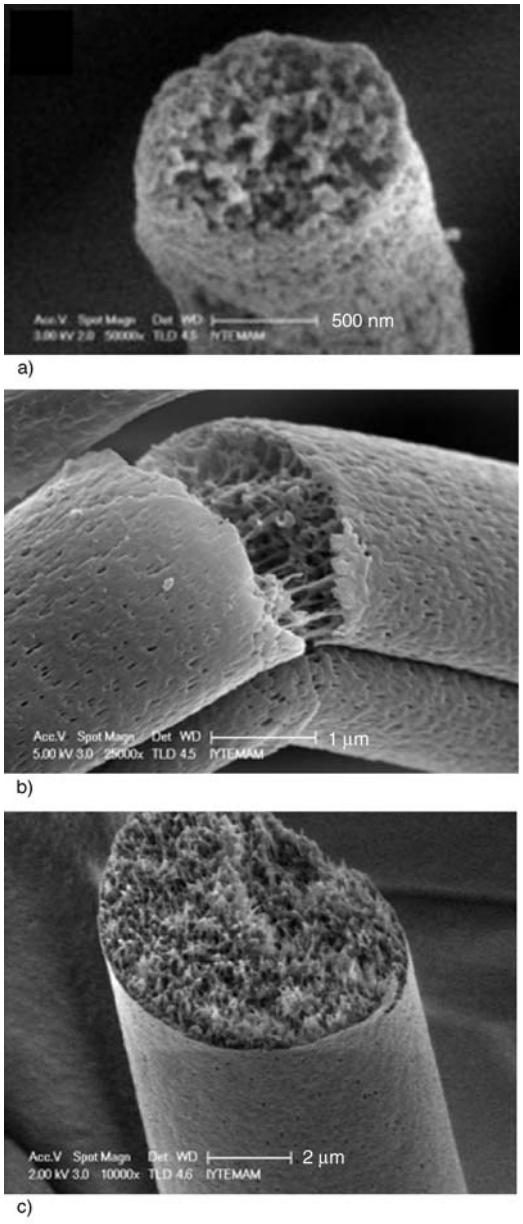

Figure 3. Crossectional profiles of PS fibers electrospun from solutions at (a) 0.10, (b) 0.15, and (c) 0.25 weight fraction

gets thinner and sharper as the weight fraction increases.

The characteristic skin formation of electrospun fibers can be attributed to radial capillary flow of solution through the surface of the liquid jet. When a drop of a polymer solution is deposited on a substrate, polymer molecules are concentrated at the edge of the droplet although the molecules are initially homogeneously dispersed over the entire dispersion [21]. Solvent evaporates and the liquid evaporating from the edge is replenished by liquid from the interior. The resulting outward flow can carry the dispersed solid ingredients through the perimeter of the droplet. A ring made up of the ingredients is achieved after complete evaporation of solvent. We have verified this phenomenon for tiny droplet of dilute polystyrene solutions on an atomically flat mica surface [22]. In electrospinning, we propose that polymer molecules concentrate on the external boundary of the liquid jet due to capillary flow and causes characteristic formation of glassy skin during evaporation of solvents. In fact, this phenomenon could take place within the solution droplet at the nozzle of the container prior to jet formation. In addition to capillary effect, charge repulsion within the liquid jet may also contribute this radial flow. In dilute polymer solutions where viscosity is low, the flow deposits polymeric ingredient to the surface of liquid jet. Evaporation of solvent on the outhermost layer leaves behind a dense skin. The solution in the core of these semi-solidified fibers appears to be solvent rich. A liquid-liquid phase separation taking place between atmospheric moisture in air and DMF lead to the formation of large solvent rich domains. Complete evaporation of solvent from the core finally imparts large internal voids covered with thick polymer skin with respect to AFD. On the other hand, at high polymer fractions, viscosity of solution increases due to extensive chain entanglements; therefore the effect of evaporative flow does not occur as strongly as in the dilute solution and only limited amount of polymer molecules is carried to the boundary. Rapid solvent evaporation on the surface results in a thin skin layer. For example, the thickness of the layer is around 1% of the average diameter of the fiber at 0.25 fraction. The presence of low fraction of solvent sets in liquid-liquid separation with smaller domains in the core of the jet. Thus, smaller voids with homogeneous distribution throughout the cross section of the fibers are developed.

Figure 4a shows cross section of polystyrene fibers electrospun from DMF solution at 0.25. A thin uniform skin surrounding a homogeneously porous core is evident. Even though the fiber core remains robust, the skin of fiber is fractured down as indicated with a white arrow. This observation suggests the brittle and glassy nature of the skin. Figure 4b presents higher magnified image of a representative fiber. Two types of pores here can be identified: i) the interior porosity whose size is approximately 100 nm, ii) the surface porosity in the range of 30–70 nm. Specific surface area of the fibers was found

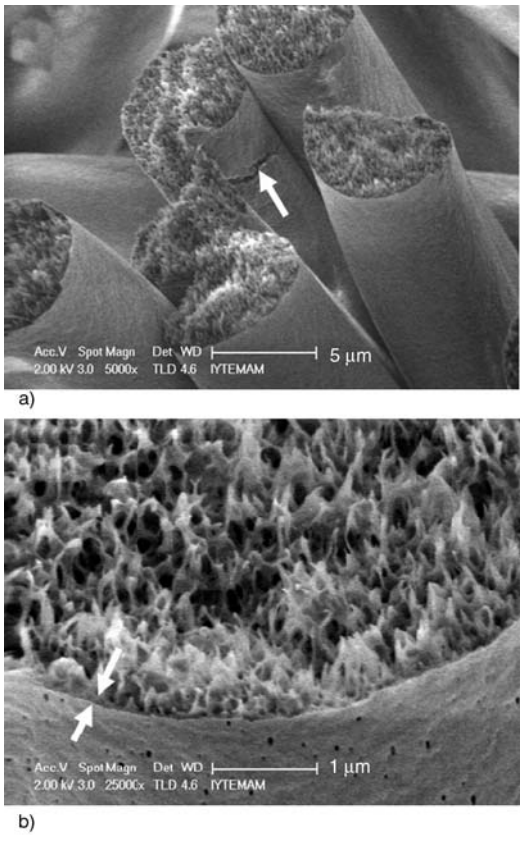

Figure 4. Crossectional SEM images of the electrospun fibers prepared from solution at 0.25 (a) 5 000× and (b) 25 000×

3.89 m^2/g by BET nitrogen absorption. This value is more than six times higher than the theoretical surface area of smooth PS fibers (0.62 m^2/g) where the fibers have 6.19 µm in diameter on average with no beads. Based on the SEM images, the interior porosity appears to be stronger than the surface porosity. Therefore, the contribution of former porosity to the surface area of entire system is expected to be much higher than that of the latter one.

Although electrospinning process is very fast and polymer molecules are far from equilibrium, this porous morphology may be a consequence of phase separation occurring between moisture in air and DMF. This phenomenon is very well-known and widely discussed in literature [16]. There are two relevant phase separation mechanisms in the course of fiber evolution: thermally induced phase separation (TIPS) and vapor-induced phase separation (VIPS). The former is associated with the rapid solvent evaporation that lowers the local temperature on the liquid jet although the temperature of spinning environment is unchanged. The evaporative cooling leads to condensation of moisture in air and the formation of breath figures [23]; therefore, pores occur only on the surface of the fibers. The latter is ascribed to the presence of water vapor in the surrounding air which acts as nonsolvent. The polymer solution undergoes phase separation by diffusion of water vapor. The pore formation is governed by polymer fraction. Increasing fraction of polymer increases the internal pore formation, which is consistent with our results. Since electrospun PS fibers we have produced have both interior and surface porosity, we can conclude that both phase separation mechanisms coexist in formation of PS fibers. However, VIPS appears to have stronger contribution compared to TIPS. It has to be noted that the formation of fused structure or wrinkled surface morphology due to the difference between evaporation rate of water and DMF was not observed.

4. Conclusions

The formation of uniform glassy skin on porous electrospun PS fibers was demonstrated. Capillary flow of polymer solution through the external boundary of charged liquid jet may be the main contributing mechanism in skin formation. The thickness of skin normalized with respect to AFD was found to be inversely proportional to the weight fraction of polymer in solution. The electrospun solutions experience absorption of water from humid environment into the polymer/ solvent system. Porosity is induced by phase separation resulting from the rapid evaporation of water molecules from polystyrene/DMF system. The resulting electrospun mats contain three types of pores at different length scales. The first type of pore is the interstitial spaces between the fibers, which is on the order of micrometer. The other two are surface and internal pores of fibers and their size is in nanometer scale. This feature fits with the needs of various applications concerning high surface area such as filtration, catalysts, sensors, membrane and adsorption of living cells for scaffolds in tissue engineering. Similar porous structure possibly occurs for a sort of polymers where DMF and water act as solvent and nonsolvent, respectively.

Acknowledgements

The author thanks members of IYTE–MAM for microscope images and BET analysis and M. Çelik for his contribution to the initial stage of the experiments. M.M.D. acknowledges the financial support of The Scientific and Technological Research Council of Turkey (TUBITAK) career development project encoded with TBAG-107T795.

References

[1] Reneker D. H., Yarin A. L.: Electrospinning jets and polymer nanofibers. Polymer, **49**, 2387–2425 (2008). DOI: 10.1016/j.polymer.2008.02.002

[2] Koombhongse S., Liu W. X., Reneker D. H.: Flat polymer ribbons and other shapes by electrospinning. Journal of Polymer Science Part B: Polymer Physics, **39**, 2598–2606 (2001). DOI: 10.1002/polb.10015

[3] Yoon K., Kim K., Wang X. F., Fang D. F., Hsiao B. S., Chu B.: High flux ultrafiltration membranes based on electrospun nanofibrous PAN scaffolds and chitosan coating. Polymer, **47**, 2434–2441 (2006). DOI: 10.1016/j.polymer.2006.01.042

[4] Demir M. M., Gulgun M. A., Menceloglu Y. Z., Erman B., Abramchuk S. S., Makhaeva E. E.: Khokhlov A. R., Matveeva V. G., Sulman M. G.: Palladium nanoparticles by electrospinning from poly(acrylonitrile-*co*-acrylic acid)-$PdCl_2$ solutions. Relations between preparation conditions, particle size, and catalytic activity. Macromolecules, **37**, 1787–1792 (2004). DOI: 10.1021/ma035163x

[5] Demir M. M., Ugur G., Gülgün M. A., Menceloglu Y. Z.: Glycidyl-methacrylate-based electrospun mats and catalytic silver nanoparticles. Macromolecular Chemistry and Physics, **209**, 508–515 (2008). DOI: 10.1002/macp.200700544

[6] Nisbet D. R., Forsythe J. S., Shen W., Finkelstein D. I., Horne M. K.: Review paper: A review of the cellular response on electrospun nanofibers for tissue engineering. Journal of Biomaterials Applications, **24**, 7–29 (2009). DOI: 10.1177/0885328208099086

[7] Zhang Y. Z., Feng Y., Huang Z-M., Ramakrishna S., Lim C. T.: Fabrication of porous electrospun nanofibres. Nanotechnology, **17**, 901–908 (2006). DOI: 10.1088/0957-4484/17/3/047

[8] McCann J. T., Marquez M., Xia Y. N.: Highly porous fibers by electrospinning into a cryogenic liquid. Journal of the American Chemical Society, **128**, 1436–1437 (2006). DOI: 10.1021/ja056810y

[9] Bognitzki M., Frese T., Steinhart M., Greiner A., Wendorff J. H., Schaper A., Hellwig M.: Preparation of fibers with nanoscaled morphologies: Electrospinning of polymer blends. Polymer Engineering and Science, **41**, 982–989 (2001). DOI: 10.1002/pen.10799

[10] Moon S., Choi J., Farris R. J.: Highly porous polyacrylonitrile/polystyrene nanofibers by electrospinning. Fibers and Polymers, **9**, 276–280 (2008). DOI: 10.1007/s12221-008-0044-y

[11] McCann J. T., Li D., Xia Y. N.: Electrospinning of nanofibers with core-sheath, hollow, or porous structures. Journal of Materials Chemistry, **15**, 735–738 (2005). DOI: 10.1039/b415094e

[12] Han S. O., Son W. K., Youk J. H., Lee T. S., Park W. H.: Ultrafine porous fibers electrospun from cellulose triacetate. Materials Letters, **59**, 2998–3001 (2005). DOI: 10.1016/j.matlet.2005.05.003

[13] Wang L. F., Pai C-L., Boyce M. C., Rutledge G. C.: Wrinkled surface topographies of electrospun polymer fibers. Applied Physics Letters, **94**, 151916/1–151916/3 (2009). DOI: 10.1063/1.3118526

[14] Matsuyama H., Teramoto M., Nakatani R., Maki T.: Membrane formation via phase separation induced by penetration of nonsolvent from vapor phase. I. Phase diagram and mass transfer process. Journal of Applied Polymer Science, **74**, 159–170 (1999).

[15] Pai C-L., Boyce M. C., Rutledge G. C.: Morphology of porous and wrinkled fibers of polystyrene electrospun from dimethylformamide. Macromolecules, **42**, 2102–2114 (2009). DOI: 10.1021/ma802529h

[16] Megelski S., Stephens J. S., Chase D. B., Rabolt J. F.: Micro- and nanostructured surface morphology on electrospun polymer fibers. Macromolecules, **35**, 8456–8466 (2002). DOI: 10.1021/ma020444a

[17] Casper C. L., Stephens J. S., Tassi N. G., Chase D. B., Rabolt J. F.: Controlling surface morphology of electrospun polystyrene fibers: Effect of humidity and molecular weight in the electrospinning process. Macromolecules, **37**, 573–578 (2004). DOI: 10.1021/ma0351975

[18] Shenoy S. L., Bates W. D., Frisch H. L., Wnek G. E.: Role of chain entanglements on fiber formation during electrospinning of polymer solutions: Good solvent, non-specific polymer-polymer interaction limit. Polymer, **46**, 3372–3384 (2005). DOI: 10.1016/j.polymer.2005.03.011

[19] Wang C., Hsu C-H., Lin J-H.: Scaling laws in electrospinning of polystyrene solutions. Macromolecules, **39**, 7662–7672 (2006). DOI: 10.1021/ma060866a

[20] Demir M. M., Yilgor I., Yilgor E., Erman B.: Electrospinning of polyurethane fibers. Polymer, **43**, 3303–3309 (2002).
DOI: 10.1016/S0032-3861(02)00136-2

[21] Deegan R. D., Bakajin O., Dupont T. F., Huber G., Nagel S. R., Witten T. A.: Capillary flow as the cause of ring stains from dried liquid drops. Nature, **389**, 827–829 (1997).
DOI: 10.1038/39827

[22] Demir M. M., Erman B.: Dimensions of polystyrene particles deposited on mica from dilute cyclohexane solution at different temperatures. Macromolecules, **35**, 7986–7992 (2002).
DOI: 10.1021/ma020676+

[23] Srinivasarao M., Collings D., Philips A., Patel S.: Three-dimensionally ordered array of air bubbles in a polymer film. Science, **292**, 79–83 (2001).
DOI: 10.1126/science.1057887

eXPRESS Polymer Letters Vol.4, No.1 (2010) 9–16
Available online at www.expresspolymlett.com
DOI: 10.3144/expresspolymlett.2010.3

Synthesis and properties of starch-g-poly(maleic anhydride-co-vinyl acetate)

*C. M. Xiao**, *J. Tan, G. N. Xue*

College of Material Science and Engineering of Huaqiao University, Quanzhou, 362021, China

Received 26 August 2009; accepted in revised form 5 October 2009

Abstract. Starch-g-poly(maleic anhydride-co-vinyl acetate) (SMV) was synthesized via the esterification reaction of starch with the copolymer of maleic anhydride and vinyl acetate. The carboxylic unit percentage (CUP) of SMV was tailored with reaction conditions, and it ranged from 29.8 to 46.9%. The structure and the morphology of the copolymers were characterized with Fourier Transform Infrared spectroscopy and X-ray diffraction analysis. It was found that SMV could form complex with some metal cations such as Ca^{2+}, Pb^{2+} and Hg^{2+} or cationic polyelectrolyte chitosan, and precipitate from the solution. The weight of precipitation increases with an increase of the CUP of SMV. In addition, a physically cross-linked hydrogel of SMV/poly(vinyl alcohol) (PVA) was obtained by freeze/thaw technique. Scanning electron microscopy exhibited the hydrogel was uniform. The gel exhibited pH-responsive re-swelling. The maximum swelling-ratio values of SMV/PVA (9:1, wt/wt) gel were 3.29 and 5.34 in HCl (pH 1.0) and phosphate-buffer saline (PBS) (pH 12) respectively.

Keywords: *tailor-made polymers, starch, functionalization, properties*

1. Introduction

As an annually renewable and biodegradable agriculturally derived biopolymer, starch has been receiving growing attention since 1970s [1, 2]. For conserving the petrochemical resources and reducing environmental pollution, many efforts have been exerted to develop starch-based polymers as alternatives of petroleum-based polymers [3–6]. Regenerated from carbon dioxide and water by photosynthesis in plants [7], the totally biodegradable [8], inexpensive and renewable [9] starch is considered as a promising candidate for developing sustainable materials.

However, it is the intrinsic structure and performance of starch itself makes the dream of obtaining polymers of suitable performance from the earth difficult to come true. Starch is the mixture of two homopolymers of D-glucose, linear amylose and branched amylopectin [2, 7–8]. There are two or three hydroxyl groups in each glucose residue, which render pure starch hydrophilic and poor in its dimensional stability and processability [10]. Thus, native starch is not used directly.

To improve the end-use properties, starch has been modified through the non-covalent blending or oxidation, hydrolysis, and substitution [11]. Chemical modifications of starch are generally carried out via the reaction with hydroxyl groups in the starch molecule [12]. The derivatives have physicochemical properties that differ significantly from the parent starch and maintain its biodegradability. Consequently, substituting the hydroxyl groups with some groups or chains is an effective means to prepare starch-based materials to suit various needs.

Esterification is one of the most important methods to synthesize starch-based polymers [13]. Starch half-esters can be prepared via reaction, such as

*Corresponding author, e-mail: congmingxiao@hqu.edu.cn

acetylation or succinylation, of starch with anhydrides [14]. An attractive feature of such derivatives is that they usually contain carboxyl groups, which may exhibit some special performances. Carboxymethylation and etherification are another major ways to introduce carboxyl groups onto starch chains [15–17].

In the documented esterification or caboxymethylation methods, each hydroxyl group of starch is transformed into a substituted group that only contains one carboxyl group. Herein, a simple but effective route, i.e. the esterification reaction of starch with a copolymer of maleic anhydride and vinyl acetate, to incorporate numerous carboxyl groups onto starch backbone is presented. The carboxylic derivative of starch, starch-g-poly(maleic anhydride-co-vinyl acetate), shows valuable properties such as cation binding and pH-sensitivity.

2. Experimental

2.1. Materials

All chemicals, with the exception of polyvinyl alcohol (PVA, kindly donated by Fujian Chemical Fiber and Chemical Factory, China) were obtained from Shanghai Chemical Agents Ltd. Co., China. Water-soluble starch was dried before use. Vinyl acetate (VAc) was purified by distillation. Maleic anhydride (MAn, m.p. 54–55°C) and N,N′-azobisisobutyronitrile (AIBN) were purified by recrystallization from benzene and ethanol respectively. Chitosan (CS, minimum 90% deacetylation), polyvinyl alcohol (PVA, degree of hydrolysis of 99%), sodium hydroxide, calcium chloride, plumbum acetate, hydrargyrum nitrate, 95% ethanol, benzene, hydrochloric acid (HCl) and acetic acid were all analytical grade reagents and used as received.

2.2. Synthesis of carboxylation agent

The carboxylation agent, copolymer of maleic anhydride and vinyl acetate (MV), was prepared by radical copolymerization using AIBN as initiator [18]. Briefly, MAn (16.11 g, 0.164 mol) and benzene (20 ml) were added into a 250 ml three-necked flask and kept constant stirring at 65°C until MAn completely dissolved. Then a mixture of VAc (15.6 ml, 0.164 mol), AIBN (2.5885 g) and benzene (15 ml) was added dropwise into the solution within 1.5 h. Some benzene (50 ml) was added when the solution became turbid. The reaction mixture was allowed to react for 5 h with agitation. It was cooled, filtered, dried and extracted with benzene in a Soxhlet apparatus for 24 h. The dried powder was pure copolymer MV.

The sample was weighed, kept in NaOH (30 ml, 0.09674 M) at 70°C for 4 h, and titrated with HCl (0.07289 M) in the presence of thymol blue. Then the content of MAn in MV could be calculated according to Equation (1):

$$\mathrm{MAn}[\%] = \frac{(30 \cdot C_{\mathrm{NaOH}} - V_{\mathrm{HCl}} \cdot C_{\mathrm{HCl}}) \cdot 9.8}{2m} \quad (1)$$

where C, V and m were the concentration, volume and weight of NaOH, HCl and MV respectively. The average MAn% was taken from four samples.

2.3. Synthesis of starch-g-poly(maleic anhydride-co-vinyl acetate)

Starch-g-poly(maleic anhydride-co-vinyl acetate) (SMV) were synthesized via the esterifiation reaction of starch with MV. Typically, starch (4.0 g) was mixed with MV in different feeding ratios and dissolved in ca. 15 ml water. The solution was carefully heated to remove the majority of water, then the concentrated slimy mixture was kept in an air oven at 100°C. At predetermined time, the reaction mixture was removed, extracted with 95% ethanol and dried to obtain the product SMV.

The sample was weighed, kept in NaOH (30 ml, 0.09674 M) at 60°C for 3 h, and titrated with HCl (0.07289 M) in the presence of thymol blue. Then the carboxylic unit percentage (CUP) of SMV could be calculated according to Equation (2) [19]:

$$\mathrm{CUP} = \frac{(30 \cdot C_{\mathrm{NaOH}} - V_{\mathrm{HCl}} \cdot C_{\mathrm{HCl}}) \cdot 45 \cdot 100}{m \cdot 1000} \quad (2)$$

where C, V and m were the concentration, volume and weight of NaOH, HCl and SMV respectively. The average CUP was taken from four samples. SMV–xx.x in the following represented the CUP of a SMV sample is xx.x%, e.g. the CUP of SMV-45.5 was 45.5%.

SMV (0.5000 g) was dissolved in NaOH (50 ml, 0.1 M) and neutralized with HCl (0.1 M). Some more distilled water was added till the volume of

the solution was 100 ml. Then the intrinsic viscosity of SMV was measured using an Ubbelohde viscometer at 30°C.

2.4. Preparation of SMV/PVA complex hydrogels

A mixture (0.4 g) of PVA and SMV-46.9 in the ratios of 1:9, 3:7, and 5:5 (wt/wt) was dissolved in 5 ml distilled water respectively. The solution was poured into moulds. Then it was subjected to two repeated freeze/thaw cycles, 16 h at –16°C and 5 h at 25°C. The obtained hydrogels were dried under vacuum at 37°C to constant weight.

2.5. Cation-binding property of SMV

SMV-45.5 (0.005 g/ml) solution was mixed with 10 ml calcium chloride, plumbum acetate or mercury nitrate aqueous solution (0.01 g/ml) in different ratio respectively. After being kept for 30 min, the formed precipitation was filtered, dried and weighed. The cation-binding property of SMV-29.8, SMV-33.7, SMV-38.6 and SMV-42.3 were examined by assuming the best ratio between SMV and cation-contained solution.

Chitosan was dissolved in 1% acetic acid and mixed with SMV-29.8, SMV-33.7, SMV-38.6, SMV-42.3 and SMV-46.4 aqueous solution in the ratio of 1:1 (wt/wt of chitosan:SMV) respectively. The precipitation was filtered, dried and weighed.

2.6. pH-responsive re-swelling behavior of SMV/PVA complex hydrogels

The dried SMV-46.9/PVA gels were weighed and placed in vials that contained 3 ml HCl (0.1 M, pH 1.0) and maintained at 37°C. At timed intervals, the samples were removed; the surface liquid of the samples was blotted up with soft paper and the samples were weighed. HCl was replaced with phosphate-buffer saline (PBS) (0.1 M, pH 12) when the weight of the samples became constant, and then the aforementioned procedure was repeated. The swelling ratio (SR) of the samples was calculated from the weight of sample at different time (W_t) and the weight of dried sample (W_d) accoding to Equation (3):

$$SR = \frac{W_t}{W_d} \tag{3}$$

An average of triplicate measurements was taken.

2.7. Spectroscopic and morphological characterization

Powdered MV, starch, and SMV were mixed with dry KBr and compressed into disk respectively. Then, Fourier transform infrared spectra (FTIR) of the samples were recorded using a Nexus 470 FTIR spectrometer (Thermo Nicolet, USA).

X-ray diffraction (XRD) analysis profiles of dried starch, MV and SMV powder were collected with a Bruker D8-Advanced diffractometer (Bruker, Germany) using Nickel-filtered CuK_α radiation (λ = 0.15406 nm) and scanned from 2 to 60°C at a scan speed of 2°/min.

The Au-coated cross-section of SMV-46.9/PVA gels was examined with a Hitachi S-3500N scanning electron microscope (Hitachi, Tokyo, Japan).

3. Results and discussion

3.1. Synthesis of starch-g-poly(maleic anhydride-co-vinyl acetate)

As mentioned above, esterification is an effective way to transform the hydroxyl groups of starch into carboxyl groups. It is used to synthesize starch-based anionic polyelectrolyte too, and the copolymer MV is used as a carboxylation agent. It is found that the percent content of MAn unit in MV is 44.4% and the copolymer is water-soluble. The reactive groups in the chain of MV make it useful for carboxylation. To ensure that MV is uniformly mixed with starch and to focus the examination on the reaction between two reactants, soluble starch i.e., amylose is used as a raw material. The esterification is carried out gradually by water evaporation in an air oven. As a result, starch-g-poly(maleic anhydride-co-vinyl acetate) is readily obtained by two simple steps (Figure 1). More MV added or longer reaction time will increase the CUP of SMV, and CUP will level off when equal weights of reactants fed or 72 h used (Figure 2). In addition, CUP of SMV is 29.8, 36.2 and 46.2% when equal weight of MV and starch is kept at 80, 90 and 100°C for

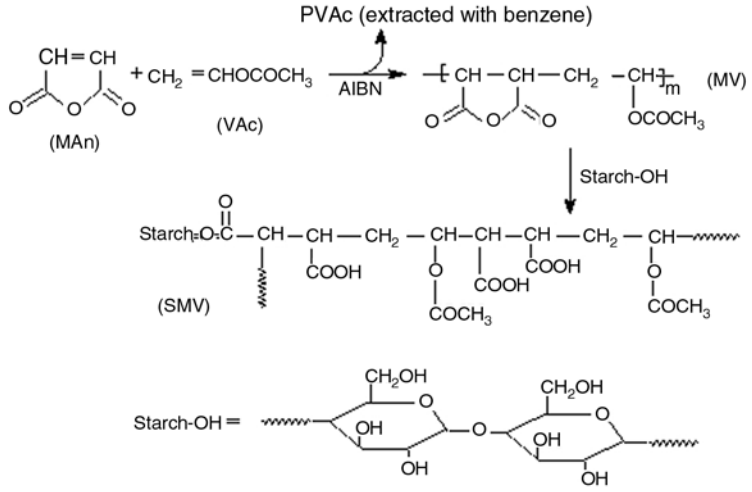

Figure 1. The synthesis of starch-g-poly(maleic anhydride-co-vinyl acetate)

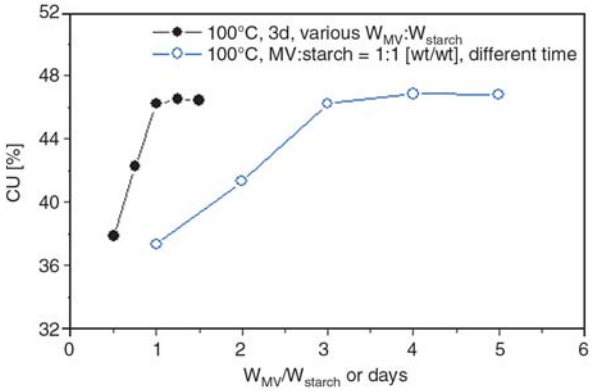

Figure 2. The effect of feeding ratio of reagents and reaction time on the carboxylic unit percentage of starch-g-poly(maleic anhydride-co-vinyl acetate)

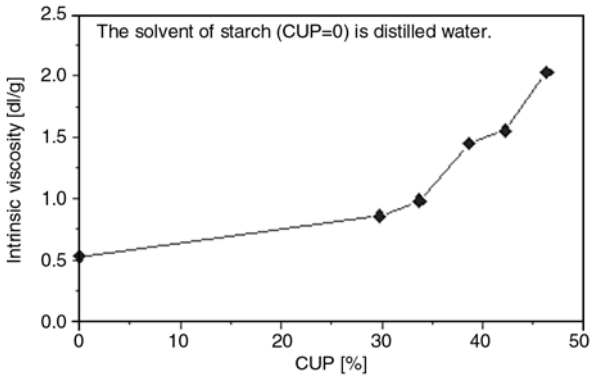

Figure 3. The relationship between the carboxylic unit percentage of starch-g-poly(maleic anhydride-co-vinyl acetate) and its intrinsic viscosity

72 h respectively. In other words, the content of carboxyl groups in starch can be easily tailored with reaction conditions such as reaction time, reaction temperature and the feeding ratios. Not higher than 100°C is suggested for reaction temperature to avoid adverse reactions such as cross-linking, oxidation or decomposition.

3.2. Characterization of starch-g-poly(maleic anhydride-co-vinyl acetate)

SMV is water-soluble and its solubility can be enhanced with NaOH. The intrinsic viscosity ([η]) of SMV is determined in presence of a little sodium chloride formed during preparing the solution. It is known that [η] of the copolymer of MAn is in proportion to its molecular weight [20]. On the other hand, the more MV reacted with starch, the higher CUP and molecular weight of SMV will be. Thus, the [η] of SMV increases with the increase of CUP of SMV (Figure 3), and this indicates the esterification of MV and starch is successfully carried out as expected.

As the difference between the structure of starch and SMV is quite obvious, the structure of SMV can be simply verified with FTIR (Figure 4). The characteristic peaks appeared at 1855 and 1783, 1735 and 1236 cm^{-1} on the spectra of MV are attributed to the anhydride group of MAn unit and the ester group of VAc unit respectively. Owing to the hydrolysis of some anhydride groups during storage [18], an absorption band appears around 3505 cm^{-1}. Comparing the FTIR spectra of SMV with starch and MV, the characteristic peaks of the unreacted hydroxyl groups and formed carboxyl groups, carbonyl groups and ester groups are found at 3450, 1773, 1245 and 1020 cm^{-1} on the spectra of SMV respectively.

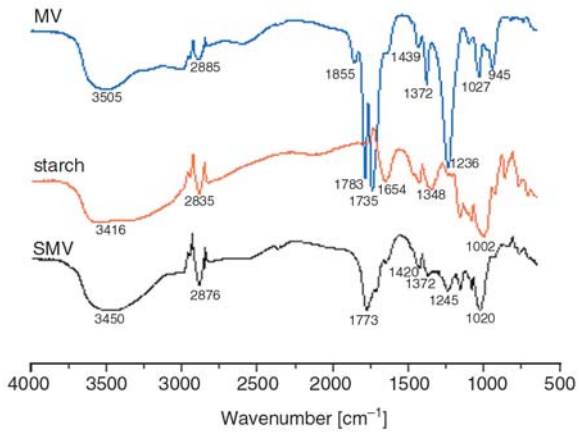

Figure 4. FTIR spectra of starch, copolymer of maleic anhydride and vinyl acetae and starch-g-poly(maleic anhydride-co-vinyl acetate)

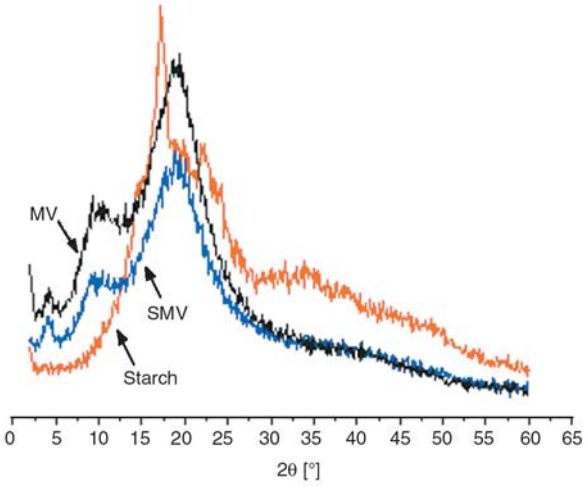

Figure 5. X-ray diffraction analysis profiles of starch, copolymer of maleic anhydride and vinyl acetae and starch-g-poly(maleic anhydride-co-vinyl acetate)

XRD analysis results (Figure 5) show that starch, MV and SMV are all semicrystalline. There are two sharp peaks exhibited at ca.17 and 22° on the XRD pattern of starch. The XRD profile of SMV is similar to that of MV whereas different from the one of starch. Both the sharp peaks of MV and SMV appear at about 10 and 19°. These phenomena indicate that the chemical structure and morphology of starch is evidently changed after modification.

3.3. Properties of starch-g-poly(maleic anhydride-co-vinyl acetate)

The carboxyl groups existed in SMV may be changed into negatively charged groups in the solution, which enable SMV binding multivalent-metal

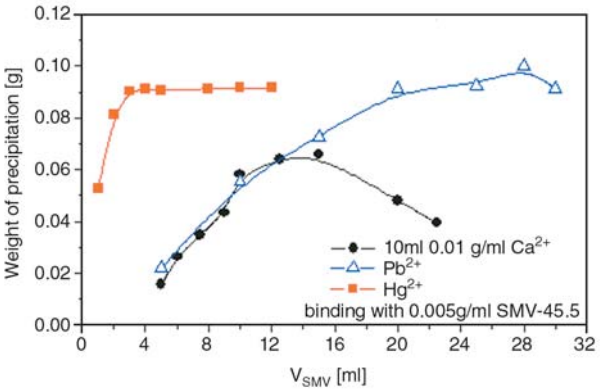

Figure 6. The effect of dosage of starch-g-poly(maleic anhydride-co-vinyl acetate) solution on its metal cations' chelation

cations [21]. Actually, a precipitation is formed when the SMV solution is mixed with the solution containing Ca^{2+}, Pb^{2+} or Hg^{2+}. Noting that some of chelating agent SMV will remain in solution due to its water-solubility, the weight of precipitation instead of adsorption capacity is used to investigate the interaction of SMV and cations. As shown in Figure 6, the weight of precipitation is increased with the amounts of SMV added and appears a maximum value for each cation. Since the amount of cations in solution is fixed, the volume of SMV-45.5 solution that forms the maximum weight of precipitation can be regarded as the best one for chelating metal cations. Then 15, 28 and 10 ml SMV solution is assumed to chelate Ca^{2+}, Pb^{2+} or Hg^{2+} in 10 ml 0.01 g/ml salt solution respectively. As carboxyl groups are the functional groups for binding cations, the weight of precipitation increase with an increase of CUP of SMV (Figure 7). The results also reveal that the amount of carboxyl groups incorporated onto starch chains is high

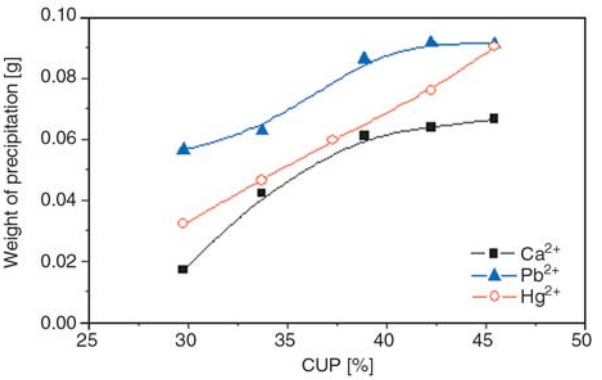

Figure 7. The effect of the carboxyl groups' content of starch-g-poly(maleic anhydride-co-vinyl acetate) solution on its metal cations' chelation

enough to make uncross-linked SMV binding metal cations.

Chitosan can be positively charged in aqueous solution. The electrostatic attraction and additional secondary interaction such as hydrogen bonds between the cationic amino groups of chitosan and the anionic groups of the other polyelectrolyte will produce polyelectrolyte complex (PEC) [22]. The fact, that precipitation is observed when mixing SMV solution with chitosan solution, once more confirms SMV is an anionic polyelectrolyte. Evidently, more carboxyl groups in SMV will enhance the interaction between two oppositely charged polyelectrolytes and obtain more precipitation. The experimental results shown in Figure 8, SMV of higher CUP will form more precipitation with equal weight of chitosan, is consistent with formation mechanism of PEC. The weight of precipitation is almost kept the same when CUP of SMV is higher than 38.6%, which may be attributed to amino groups of chitosan have been saturated with carboxyl groups.

The pH-sensitive re-swelling behavior of dried SMV-46.9/PVA gels also proves the amount of carboxyl groups on SMV is high enough [23]. After subjecting to several freeze/thaw cycles [24], the solution containing SMV and PVA can be transformed into hydrogels. As can be seen in Figure 9, a uniform, soft and elastic SMV-46.9/PVA hydrogel is successfully prepared via such a physical cross-linking method. Scanning electron microscopy shows that no phase separation happened within the hydrogels (Figure 10). As might have been expected, SR of SMV-46.9/PVA gels in PBS are much greater than that in HCl. Moreover, the higher the content of SMV-46.9, the more evident pH-sensi-

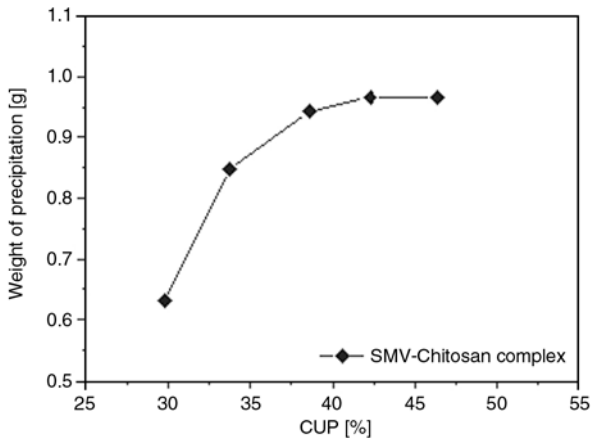

Figure 8. The effect of the carboxyl groups' content of starch-g-poly(maleic anhydride-co-vinyl acetate) solution on its complexation with chitosan

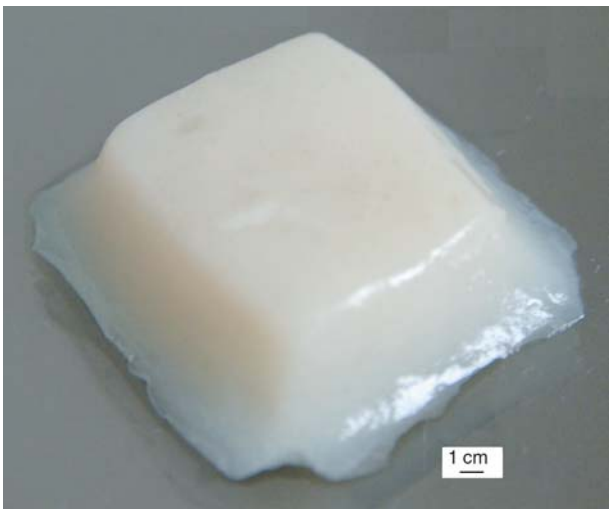

Figure 9. The appearance of starch-g-poly(maleic anhydride-co-vinyl acetate)/PVA hydrogel

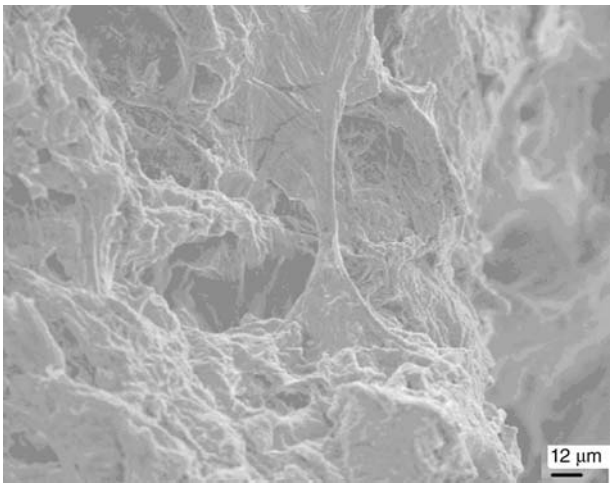

Figure 10. Scanning electron microscopy of the cross-section of starch-g-poly(maleic anhydride-co-vinyl acetate)/PVA hydrogel

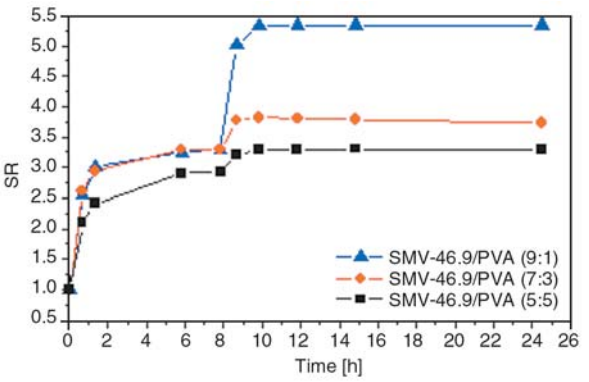

Figure 11. Re-swelling behaviors of starch-g-poly(maleic anhydride-co-vinyl acetate)/PVA gels in HCl (0.1 M, pH 1.0) and phosphate-buffer saline (PBS) (0.1 M, pH 12) at 37°C

tive re-swelling will be exhibited (Figure 11). The maximum SR values of SMV-46.9/PVA gels prepared in the ratio of 9:1, 7:3 and 5:5 (wt/wt) are 3.29 and 5.34, 3.29 and 3.81, 2.92 and 3.30 in HCl (0.1 M, pH 1.0) and in PBS (0.1 M, pH 12) respectively. Undoubtedly, it is the incorporation of SMV-46.9 that renders the gels shows pH-responsive.

4. Conclusions

A convenient two-steps route including radical copolymerization of maleic anhydride with vinyl acetate and subsequent esterification with starch is carried out to incorporate numerous carboxyl groups onto starch chains. The starch-based derivative SMV shows some unique properties such as binding metal cations, forming PEC with a polycationic biopolymer and endowing complex hydrogel pH-responsive re-swelling. The experimental results validate not only that the amount of carboxyl groups incorporated onto starch chains by using the approach presented is high enough, but also suggests that SMV will be a good candidate for environmental or biomedical applications.

These reactions can be easily performed and are controllable, and can be used to modify naturally occurring native starch. Starch, chitosan and PVA are biodegradable. In addition, vinyl acetate units are almost distributed singly in the side-chain of SMV. Thus, synthesis of SMV and formation of PEC with chitosan or hydrogel with PVA may elicit a direction to improve the performance of starch without sacrificing its biodegradable nature.

References

[1] Lu D. R., Xiao C. M., Xu S. J.: Starch-based completely biodegradable polymer materials. Express Polymer Letters, **3**, 366–375 (2009).
DOI: 10.3144/expresspolymlett.2009.46

[2] Pareta R., Edirisinghe M. J.: A novel method for the preparation of starch films and coatings. Carbohydrate Polymers, **63**, 425–431 (2006).
DOI: 10.1016/j.carbpol.2005.09.018

[3] Park J-S., Yang J-H., Kim D-H., Lee D-H.: Degradability of expanded starch/PVA blends prepared using calcium carbonate as the expanding inhibitor. Journal of Applied Polymer Science, **93**, 911–919 (2004).
DOI: 10.1002/app.20533

[4] Schwach E., Avérous L.: Starch-based biodegradable blends: Morphology and interface properties. Polymer International, **53**, 2115–2124 (2004).
DOI: 10.1002/pi.1636

[5] Stepto R. F. T.: Understanding the processing of thermoplastic starch. Macromolecular Symposia, **245–246**, 571–577 (2006).
DOI: 10.1002/masy.200651382

[6] Lu Y. S., Weng L. H., Cao X. D.: Morphological, thermal and mechanical properties of ramie crystallites-reinforced plasticized starch biocomposites. Carbohydrate Polymers, **63**, 198–204 (2006).
DOI: 10.1016/j.carbpol.2005.08.027

[7] Teramoto N., Motoyama T., Yosomiya R., Shibata M.: Synthesis, thermal properties, and biodegradability of propyl-etherified starch. European Polymer Journal, **39**, 255–261 (2003).
DOI: 10.1016/S0014-3057(02)00199-4

[8] Araújo M. A., Cunha A. M.: Enzymatic degradation of starch-based thermoplastic compounds used in protheses: identification of the degradation products in solution. Biomaterials, **25**, 2687–2693 (2004).
DOI: 10.1016/j.biomaterials.2003.09.093

[9] Zhang J-F., Sun X. Z.: Mechanical properties of poly(lactic acid)/starch composites compatibilized by maleic anhydride. Biomacromolecules, **5**, 1446–1451 (2004).
DOI: 10.1021/bm0400022

[10] Choi E-J., Kim C-H., Park J-K.: Synthesis and characterization of starch-g-PCL copolymer. Macromolecules, **32**, 7402–7408 (1999).
DOI: 10.1021/ma981453f

[11] Biswas A., Willet J. L., Gordon S. H., Finkenstadt V. L., Cheng H. N.: Complexation and blending of starch, poly(acrylic acid), and poly(*N*-vinyl pyrrolidone). Carbohydrate Polymers, **65**, 397–403 (2006).
DOI: 10.1016/j.carbpol.2006.01.035

[12] Bao J. S., Xing J., Phillips D. L., Corke H.: Physical properties of octenyl succinic anhydride modified rice, wheat, and potato starches. Journal of Agricultural and Food Chemistry, **51**, 2283–2287 (2003).
DOI: 10.1021/jf020371u

[13] Vargha V., Truter P.: Biodegradable polymers by reactive blending transesterification of thermoplastic starch with poly(vinyl acetate) and poly(vinyl acetate-co-butyl acrylate). European Polymer Journal, **41**, 715–726 (2005).
DOI: 10.1016/j.eurpolymj.2004.10.044

[14] Biswas A., Shogren R. L., Kim S., Willett J. L.: Rapid preparation of starch maleate half-esters. Carbohydrate Polymers, **64**, 484–487 (2006).
DOI: 10.1016/j.carbpol.2005.12.013

[15] Lazik W., Heinze T., Pfeiffer K., Albrecht G., Mischnick P.: Starch derivatives of a high degree of functionalization VI. Multistep carboxymethylation. Journal of Applied Polymer Science, **86**, 743–752 (2002).
DOI: 10.1002/app.10983

[16] Heinze T., Koschella A.: Carboxymethyl ethers of cellulose and starch – A review. Macromolecular Symposia, **223**, 13–39 (2005).
DOI: 10.1002/masy.200550502

[17] Gnte C., Lazik W., Heinze T.: Tararic acid starch ether: A novel biopolymer-based polyelectrolyte. Macromolecular Rapid Communications, **24**, 927–931 (2003).
DOI: 10.1002/marc.200300042

[18] Štaudner E., Kyselá G., Kruppová T., Turayová Z.: Study of the stability of maleic anhydride-vinyl acetate copolymers. European Polymer Journal, **33**, 463–465 (1997).
DOI: 10.1016/S0014-3057(96)00166-8

[19] Spridon D., Panaitescu L., Ursu D., Uglea C. V., Popa L., Ottenbrite R. M.: Synthesis and biocompatibility of maleic anhydride copolymers: 1. Maleic anhydride-vinyl acetate, maleic anhydride-methyl methacrylate and maleic anhydride-styrene. Polymer International, **43**, 175–181 (1997).
DOI: 10.1002/(SICI)1097-0126(199706)43:2<175::AID-PI734>3.0.CO;2-I

[20] Nemtoi G., Beldie C., Tircolea C., Popa I., Cretescu I., Humelnicu I., Humelnicu D.: Behaviour of the poly(maleic anhydride-co-vinyl acetate) copolymer in aqueous solutions. European Polymer Journal, **37**, 729–735 (2001).
DOI: 10.1016/S0014-3057(00)00161-0

[21] Guilherme M. R., Reis A. V., Paulino A. T., Fajardo A. R., Muniz E. C., Tambourgi E. B.: Superabsorbent hydrogel based on modified polysaccharide for removal of Pb^{2+} and $Cu2^{+}$ from water with excellent performance. Journal of Applied Polymer Science, **105**, 2903–2909 (2007).
DOI: 10.1002/app.26287

[22] Berger J., Reist M., Mayer J. M., Felt O., Gurny R.: Sturcture and interactions in chitosan hydrogels formed by complexation or aggregation for biomedical applications. European Journal of Pharmaceutics and Biopharmaceutics, **57**, 35–52, 2004.
DOI: 10.1016/S0939-6411(03)00160-7

[23] Mitsumata T., Suemitsu Y., Fujii K., Fujii T., Taniguchi T., Koyama K.: pH-response of chitosan, κ-carrageenan, carboxymethyl cellulose sodium salt complex hydrogels. Polymer, **44**, 7103–7111 (2003).
DOI: 10.1016/j.polymer.2003.09.001

[24] Patachia S., Florea C., Friedrich Chr., Thomann Y.: Tailoring of poly(vinyl alcohol) cryogels properties by salts additiona. Express Polymer Letters, **5**, 320–331 (2009).
DOI: 10.3144/expresspolymlett.2009.40

eXPRESS Polymer Letters Vol.4, No.1 (2010) 17–25
Available online at www.expresspolymlett.com
DOI: 10.3144/expresspolymlett.2010.4

Preparation and characterization of organic-inorganic hybrid nanomaterials using polyurethane-*b*-poly[3-(trimethoxysilyl) propyl methacrylate] via RAFT polymerization

*S. Z. Guo, C. Zhang, W. Z. Wang, T. X. Liu**

Key Laboratory of Molecular Engineering of Polymers of Ministry of Education, Department of Macromolecular Science, Laboratory of Advanced Materials, Fudan University, Shanghai 200433, P. R. China

Received 13 May 2009; accepted in revised form 11 October 2009

Abstract. A series of novel block-type amphiphilic copolymers have been prepared by copolymerizing methacrylate end-capped oligo-urethane and 3-(trimethoxysilyl) propyl methacrylate (TPM) via the sol-gel process. Copolymers with well-defined end groups and narrow polydispersity were prepared through Reversible Addition Fragmentation Chain Transfer (RAFT) polymerization. As-synthesized copolymer was characterized ^{1}H nuclear magnetic resonance (^{1}H NMR), gel permeation chromatography (GPC), Fourier transform infrared (FTIR). The copolymer precursors self-assembled in form of spherical micelles (in selective solvents) have been hydrolyzed and then condensed via sol-gel process in order to generate polyurethane-silica (PU-SiO_2) hybrid materials. The hybrid copolymers thus prepared possess excellent thermal stability and mechanical property. The structures and properties of the copolymer precursors and their hybrid copolymers were characterized by thermogravimetric analysis (TGA), tensile test and atomic force microscopy (AFM).

Keywords: *nanomaterials, polyurethane, organic-inorganic hybrids, RAFT polymerization, self-assembly*

1. Introduction

Self-assembly of amphiphilic diblock copolymers and associated nano-science afford unique opportunities to create revolutionary material combinations. Wide variety of aggregates (e.g., spheres, vesicles, large compound spheres and vesicles) with different sizes can be obtained in selective solvents through sol-gel process [1–8]. These novel materials can have improved (mechanical, thermal etc.) properties arising from the synergism of the components and their interesting morphologies. In addition, well-defined polymer-nanoparticle hybrids with controlled architectures also have promising potential applications such as microreactors, microcapsules, and drug delivery systems [9–14]. Recently, increasing attention has been paid to the incorporation of an inorganic network by covalent bond such as a silica phase into an organic polymer matrix to produce monolithic, transparent hybrid nanoballs without macroscopic phase separation. Researchers have shown that these nanoballs may be incorporated as building-block fillers or cores into other polymers to form hybrid organic-inorganic copolymers with improved compatibility and hence elasticity. In addition, optimal dispersion of silica nanoballs within the polymer serves as reinforcing nanofiller with high surface coverage. Up to now, a large number of methods have been reported to prepare organic-inorganic hybrid nanoballs. One of the methods mentioned above, the

*Corresponding author, e-mail: txliu@fudan.edu.cn

sol-gel method, permits access to hybrid nanoballs through a very simple one-pot procedure. TPM with reactive trimethoxysilane groups is widely used in the preparation of organic-inorganic hybrid nanomaterials [15–19]. With a base catalyst, the R-Si$(OCH_3)_3$ groups can be easily hydrolyzed into R-Si$(OH)_3$ which can subsequently transform into cross-linked polysilsesquioxane nanocages by condensation, thus producing organic-inorganic hybrid nanoballs [7, 20, 21]. Recently, some research interests have sparked in the studies of self-assembly of copolymers based on poly[3-(trimethoxysilyl) propyl methacrylate] (PTPM). For example, Chen et al. reported the preparation and self-assembly behavior of novel organic-inorganic hybrid nanoparticles with a complex hollow structure based on a reactive amphiphilic diblock copolymer, poly(ethylene oxide)-*b*-poly[3-(trimethoxysilyl) propyl methacrylate] (PEO-*b*-PTPM) [22].

Polyurethanes (PU), as organic matrices, have received most attention for their versatile properties and a variety of starting materials. Therefore, the tailor-made properties of this class of materials can be obtained from well-designed combinations of monomeric materials, catalysts, auxiliary compounds. Polyurethanes can be tailored to meet the highly diversified demands of modern technologies such as coatings, adhesives, reaction injection molding, fibers, foams, rubbers, and thermoplastic elastomers. The linear structures of segmented PU take the form of $(A\text{-}B)_n$. The soft segment part B represents the polyester or polyether macrogels with molecular weights ranging from 1000 to 3000; and the hard segment part A is consisted of low-molecular weight diol or diamine being able to react with diisocyanate. Because of the incompatibility between the hard segments and the soft ones, PU undergoes microphase separation resulting in a hard-segment domain, soft-segment matrix, and urethane-bonded interphase. The hard-segment domains act as physical cross-links in the soft-segment matrix. The primary driving force of phase separation is the strong intermolecular interaction of the urethane units, which are capable of forming intermolecular hydrogen bonds. Upon mechanical deformation, a portion of the soft segments is stressed by uncoiling and the hard segments align themselves in the stress direction. The reorientation of the hard segments and consequently the powerful hydrogen bonding contribute to enhance the tensile strength, elongation and tear resistance values. Some polyurethane-silica hybrids have been prepared and reported, such as PU composites containing alkoxysilane groups [7, 23], PU composites containing POSS (polyhedral oligomeric silsesquioxane) nanocages [24, 25]. In the present paper, inorganic-organic diblock copolymers are prepared by incorporating 3-(trimethoxysilyl) propyl methacrylate (TPM) to vinyl-terminated PU macromonomers.

Recent progress in controlled 'living' free-radical polymerization techniques, such as atom transfer radical polymerization (ATRP) [26], nitroxide-mediated radical polymerization (NMP) [27], and reversible addition-fragmentation chain transfer (RAFT) polymerization [28–30], has created new avenues for the synthesis of structured polymers with predefined molecular weights, well-defined end groups, and narrow polydispersity. Polymerizations of vinyl monomers via RAFT have already been reported [31]. It may be of interest to prepare polyurethane-silica hybrid polymers using RAFT, since the copolymer of TPM and PU could combine the reactive groups, nontoxic, highly biocompatible and inorganic properties of TPM with the properties of PU.

Herein, the present study focuses on the synthesis of a diblock copolymer of PU-*b*-PTPM using cumyl dithiobenzoate (CDB) based RAFT in tetrahydrofuran (THF) solution and investigation of the self-assembly behaviors of the resultant polymer in THF/methanol mixture. As is known, PU-*b*-PTPM copolymer can form micelles with PU as the corona and the hydrophobic block as the core; and the siloxane part on the copolymer precursor can form a kind of stable polysilsesquioxane nanocages by hydrolysis and condensation reaction. This inorganic nanocages incorporated into the PU matrix by covalent bond increase the compatibility between the PU matrix and inorganic parts, thus improve the properties of the hybrid nanocomposites.

2. Experimental

2.1. Materials

Dibutyl tin dilaurate, 2-hydroxypropyl acrylate (HPA), methyl ethyl ketone (MEK), THF (purchased from Sinopharm Chemical Reagent Co., Ltd China), isophorone diisocyanate (IPDI, from Alfa

Aesar) and isophorone diamine (Fluka), 3-(trimethoxysilyl) propyl methacrylate (TPM, purchased from Acros Organics), 2,2′-Azobisisobutyronitrile (AIBN, purchased from Shanghai Shisihewei Chemical Co.) were used without further purification. Poly(diethylene adipate) (PDA, purchased from Jiangdu Longchuan Wear-Resistant Polymer Materials Co., Ltd China) was dried under vacuum at 80°C for 1 h before use. Cumyl dithiobenzoate (CDB) was synthesized according to the literature procedure [32] and recrystallized twice using petroleum ether. All the rest materials were purchased from Aldrich and used as received unless stated otherwise.

2.2. Synthesis of double-bond end-capped polyurethane macroinitiator

IPDI (29.96 mmol) and PDA (14.98 mmol) were added into a reaction flask with MEK as solvent, followed by heating up to 75°C, and then the solution (solid content: 90 wt%) was reacted in the presence of dibutyl tin dilaurate (0.02 wt%) at the same temperature for 3 h to synthesize the NCO-terminated prepolymer. After MEK was injected into the flask to adjust the solid content to be 30 wt%, the solution was allowed to cool down to room temperature. Then, the chain extender IPDA (12.91 mmol) was slowly charged into the system. After 1 h, HPA (2.00 mmol) was added into the system at 50°C and the temperature was kept there for 10 h, and polyurethane macroinitiator with vinyl end-capped was prepared. Then, the obtained solution was cooled down to room temperature and immediately used for further copolymerization with TPM.

2.3. Synthesis of copolymer of PU-*b*-PTPM by RAFT

The polymerization procedure and the recipes are presented in Figure 1 and Table 1, respectively. The polymerization procedure mediated by CDB

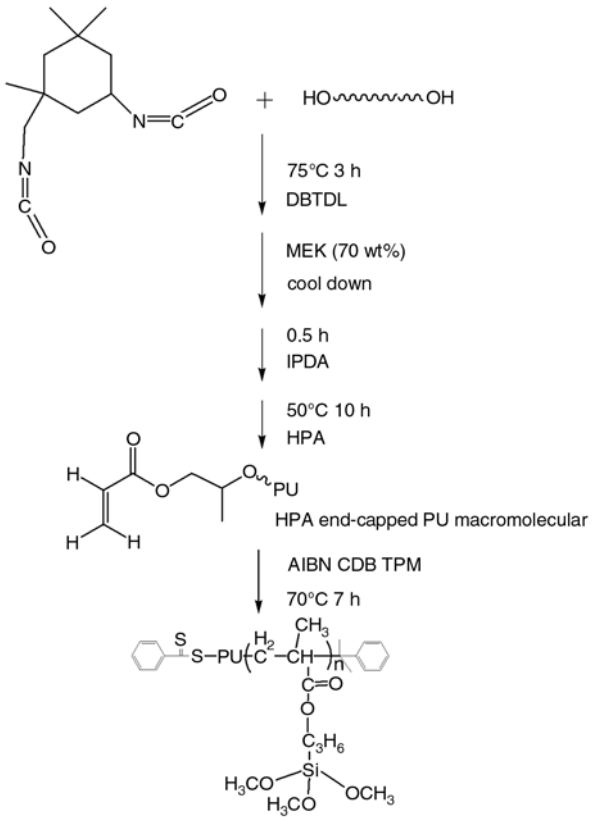

Figure 1. Synthesis procedure of PU-*b*-PTPM

procedure was as follows (as shown in Figure 1): polyurethane macroinitiator (5.0 g, $1.75 \cdot 10^{-4}$ mol), AIBN (25 mg, $1.52 \cdot 10^{-4}$ mol), TPM (0.5 g, $2.01 \cdot 10^{-3}$ mol) and CDB (76 mg, $2.79 \cdot 10^{-4}$ mol) were transferred into a 25 ml flask, and the THF solution was degassed with three cycles of freezing pump thawing to remove the oxygen. The reaction mixture was then warmed to 70°C. After 7 h, the polymerization was stopped by cooling to room temperature by liquid nitrogen and then the flask was opened. The mixture was soon precipitated into 250 ml of anhydrous methanol to remove the catalyst such as dibutyl tin dilaurate and unreacted TPM. Finally, the PU-*b*-PTPM diblock copolymers were obtained. The contents of TPM monomer in the copolymers can be roughly estimated to be 14, 19 and 32, respectively, by GPC results. The copolymers thus obtained were labeled as PU-A, PU-B, and PU-C correspondingly.

Table 1. Recipes for synthesis and the results obtained from GPC experiments

Code	PU [mol]	TPM [mol]	CDB [mol]	AIBN [mol]	M_w [Dalton]	PDI
PU	$1.75 \cdot 10^{-4}$	–	$2.79 \cdot 10^{-4}$	$1.52 \cdot 10^{-4}$	28600	1.63
PU-A	$1.75 \cdot 10^{-4}$	$2.01 \cdot 10^{-3}$	$2.79 \cdot 10^{-4}$	20/2.8/1.5	32100	1.49
PU-B	$1.75 \cdot 10^{-4}$	$4.02 \cdot 10^{-3}$	$2.79 \cdot 10^{-4}$	40/2.8/1.5	33400	1.44
PU-C	$1.75 \cdot 10^{-4}$	$6.03 \cdot 10^{-3}$	$2.79 \cdot 10^{-4}$	60/2.8/1.5	36600	1.41

2.4. Self-assembly and gelation of amphiphilic diblock copolymers

Dilute solutions were prepared by dissolving PU-*b*-PTPM in distilled THF which was a common solvent for both blocks with mechanical stirring. Subsequently, anhydrous methanol, which was a poor solvent for PU blocks but good solvent for PTPM blocks, was added to the solution dropwise by a syringe at a rate of 1 drop every 10 s under vigorous stirring to induce formation of polymer micelles with PU as the corona and the hydrophobic block as the core. The micelles were prepared at a polymer concentration of 0.50 wt% in the THF/methanol (w/w: 90/10) mixtures. After 5 h, triethylamine (TEA) as the catalyst (0.4 wt%) was dropped into the above solutions to induce the hydrolysis and condensation of the PTPM blocks in the polymeric aggregates, and then the PTPM blocks were transferred into the crosslinked polysilsesquioxane nanocages. The solution was stirred at room temperature for five days, and thus these organic-inorganic hybrid nanomaterials were obtained conveniently by the sol-gel process.

2.5. Instrumentation

Molecular weight characterization was performed on a HP1100 GPC instrument equipped with a Zorbax HV1618 column connected to a refractive-index detector (G1362A) and a UV detector (G1315A). THF was used as eluent at a flow rate of 1.0 ml/min at 35°C. Polystyrene standards were used for the calibration.

^{1}H NMR spectra were measured by using a MERCURYPLUS400 (U.S.A. VARIAN) spectrometer. All samples were dissolved in chloroform-D isotope for NMR measurements.

FTIR spectra of the dried copolymer precursor films were recorded on a Nicolet Nexus 470 FTIR spectrometer. All the samples were taken before the gelation step for FTIR, ^{1}H NMR, GPC measurements.

After gelation, all the samples were dissolved in THF and dropped onto mica flake. After solvent evaporation, the film samples obtained were used for AFM observations. Atomic force microscope (AFM) (Digital Instruments NanoScope IV) was operated with 10×10 μm scanner under tapping mode. AFM imaging technique can provide a representative analysis covering individual micron-sized particles, such as the diameter and height of particles, surface roughness, etc. [37]. Therefore, the particles that protrude from the polyurethane sample surface may be imaged by using AFM.

The films were finally punched into dog-bone shaped specimens using a punch cutter with a dimension of 55×4×1 mm^3 (GB-T13022-1991). The tensile tests were carried out using a CMT4000 Series Floor-standing Electromechanical Universal Testing Machine at room temperature with a crosshead speed of 100 mm/min. Property values reported here represent averaged results of at least five specimens. The thermal decomposition studies were performed from room temperature to 600°C using a Perkin-Elmer Pyris TGA-1 under nitrogen environment at a heating rate of 20°C/min.

3. Results and discussion

3.1. Synthesis and characterization of PU-b-PTPM copolymer precursors

GPC traces are shown in Figure 2. Molecular weight is shown on a logarithmic scale and the value of the peak intensity is normalized. The molecular weight (M_w) and the polydispersity (PDI) data obtained are summarized in Table 1. As shown in Figure 2, all the peaks are symmetric, and no shoulder peak was observed, indicating the polymerization occurred as expected. The peak was also shifted gradually to higher molecular weight and the PDI became narrower with the increase of the feed ratio of TPM (Table 1), indicating that the RAFT polymerization occurred and the well controlled copolymers were obtained. Polyurethane prepared by condensation polymerization, as

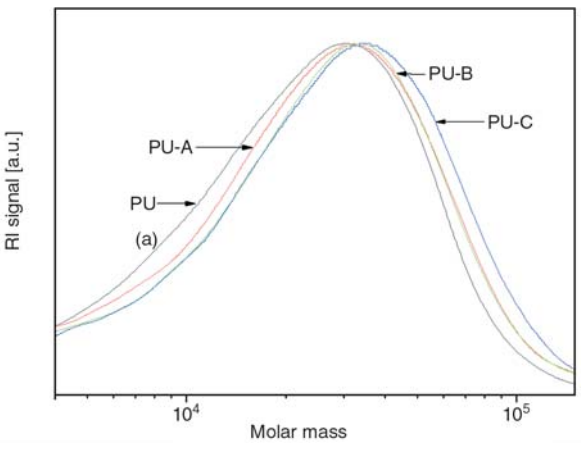

Figure 2. Gel permeation chromatograms of PU and PU-PTPM copolymer precursors

known, has a high PDI. After incorporation of structured TPM block by RAFT polymerization, the PDI decreases with the increase of TPM contents. A gradient growth can also be found as shown in Figure 2 and Table 1, which corresponds to the gradient feed of TPM monomer. According to the M_w results, different TPM chain contents were incorporated into polyurethane, thus obtaining PU-A, PU-B, and PU-C.

Figure 3 shows the ^{1}H NMR spectra of the copolymer precursors. The chemical shifts appearing at 3.4 ppm are associated with methyl protons of Si–OCH_3. The H of methylene group adjacent to the oxygen atom of glycol in the PU chain, showed a chemical shift at 3.4–3.5 ppm. The H of the methylene adjacent to the methylene connected with oxygen atom of trimethoxy and the H of the methylene adjacent to the methylene connected with carbonyl in the PU chain showed a chemical shift at 1.60–1.68 ppm. The H of the methylene adjacent to

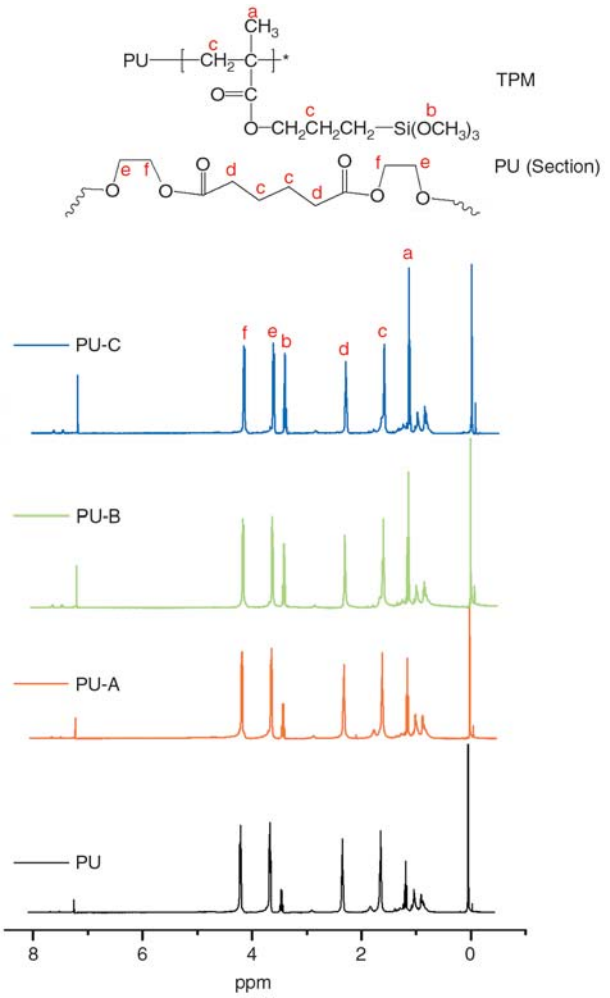

Figure 3. ^{1}H NMR spectra of PU and PU-PTPM copolymer precursors

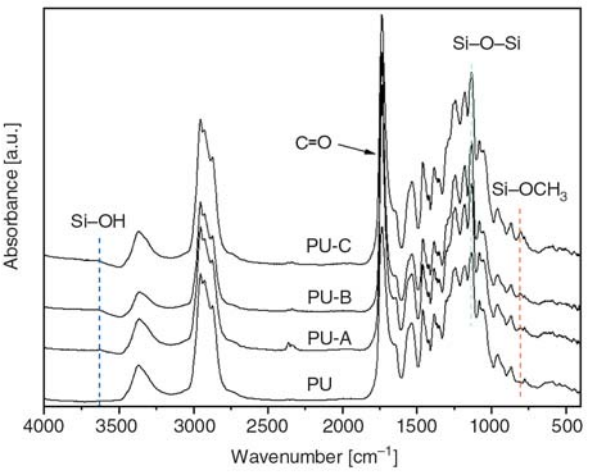

Figure 4. FTIR spectra of PU and PU-PTPM copolymer precursors

the oxygen atom of carbonyl in the PU chain showed a chemical shift at 2.30–2.45 ppm. The H of methyl groups on the cyclohexyl and the H of methyl groups on the TPM exhibited a chemical shift at 1.15–1.25 ppm. Although ^{1}H NMR spectra of TPM are overlapped with ^{1}H NMR spectra of polyurethane, gradient increase for chemical shifts at 3.4–3.5 ppm and 1.15–1.25 ppm can still be seen, indicating that a series of block copolymers were successfully prepared with well controlled molecular weights.

The FTIR spectra of PU-PTPM copolymer precursors shown in Figure 4 are generally similar. Gelation of PTPM was easily occurred when exposed to the air, thus we can observe weak Si–OH peaks in FTIR curves. The weak and broad Si–OH band between 3650 and 3500 cm^{-1} is formed in the hydrolysis reaction of the alkoxy groups of TPM. The Si–OH peak at 940 cm^{-1} was overlapped with PU matrix. The peak at 805 cm-1 and the peak at 1087 cm^{-1} are probably from the Si–OCH_3 group. The intensity of this peak, appearing in all the hybrid copolymer precursors, increases from PU-A to PU-C, which demonstrates that TPM groups were successfully incorporated into PU via RAFT and the TPM content in the copolymer precursors was gradually increased. Although the characteristic absorption bands of Si–O–Si bond around 1130 cm^{-1} were overlapped with PU matrix, an increased peak intensity was observed due to the condensation of the Si–OH group. The C=O absorption from both the TPM groups and PU can be clearly observed at 1730 cm^{-1}.

3.2. Identification and characterization of PU-silica hybrid materials

The thermal stability of PU was characterized by TGA. The TGA curves of PU and its nanocomposites are shown in Figure 5. The decomposition of PU took place in two stages. The initial step of degradation in stage I is primarily the decomposition of the hard segment, which involves the dissociation of urethane to the original polyol and isocyanate or of the urea group to the original amine and isocyanate, then forms a primary amine, alkyne and carbon dioxide. Stage I occurs at about 200–370°C and is influenced by the content of hard segment. The consequent stage II proceeds by the depolycondensation and polyol degradation mechanisms, and is affected by the content of soft segment. Figure 5 also presents the thermal stability of neat PU and its nanocomposites. When 50% weight loss was selected for comparison, the decomposition temperatures increase from 405°C for neat PU to 423°C for PU-C, indicating the enhancement of thermal stability by incorporating crosslinked silica moiety into PU matrix. The hydrolysis and condensation of alkoxysilane would form crosslinking networks (Si–O–Si) which possess excellent thermal stability over 600°C [25, 33]. The initial decomposition temperature (here taking the temperature at 10% weight loss) of PU-B was about 342°C and higher than that of neat PU (332°C), also suggesting that the thermal stability of the nanocomposite was greatly enhanced compared with neat PU. Compared to neat PU, the higher residue content of all the nanocomposites at high temperature (600°C) was attributed to the excellent thermal stability of inorganic silica (Si–O–Si) part, which would be accumulated on the surface of the polymer and thus prevent from further thermal decomposition of the inner organic network.

The mechanical properties of PU and its nanocomposites were evaluated by tensile tests at room temperature. The stress-strain curves are shown in Figure 6 and the results obtained are summarized in Table 2. In comparison with the unmodified PU, the TPM-containing nanocomposites exhibited significant increase in both tensile modulus and tensile strength with increasing the TPM content. This increase can be interpreted on the basis of two factors: i) the nano-reinforcement effect from polysilsesquioxane spheres, and ii) the increase in crosslinking density of the networks formed by the hydrolysis and condensation of alkoxysilane [34, 35]. The nano-reinforcement of polysilsesquioxane spheres could be ascribed to the restriction of nano-sized polysilsesquioxane spheres on the deformation of the macromolecular chains. Accordingly, due to the reinforcement, the elongation-at-break also decreases initially with the content of TPM similarly. It may be ascribed to the deformation mechanism of PU [36]. In case of PU composed of hard and soft segment domains, the hard segment domain, sensitive to applied stress, can be tilted

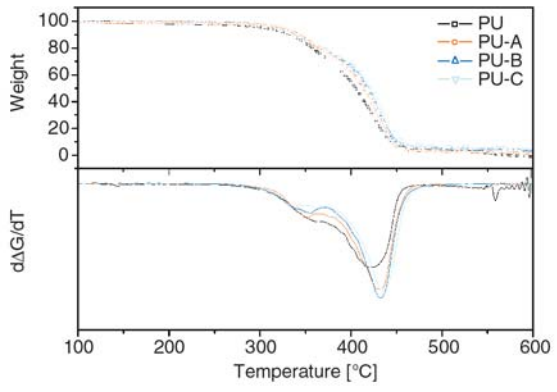

Figure 5. TGA curves of PU and its nanocomposites

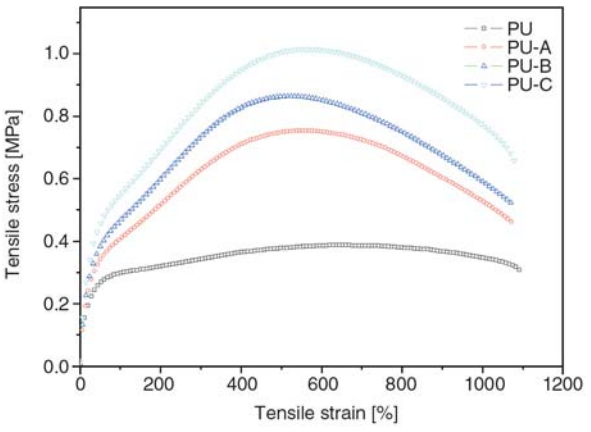

Figure 6. Typical stain–stress curves of PU and its nanocomposites

Table 2. Mechanical properties of synthesized PUs

Sample	Tensile modulus [MPa]	Tensile strength [MPa]	Elongation-at-break [%]
PU	1.43 ± 0.08	0.41 ± 0.02	1372.5 ± 46.7
PU-A	1.61 ± 0.06	0.71 ± 0.04	1032.4 ± 49.7
PU-B	1.75 ± 0.04	0.85 ± 0.02	1004.5 ± 63.9
PU-C	1.95 ± 0.08	0.97 ± 0.04	1038.0 ± 35.9

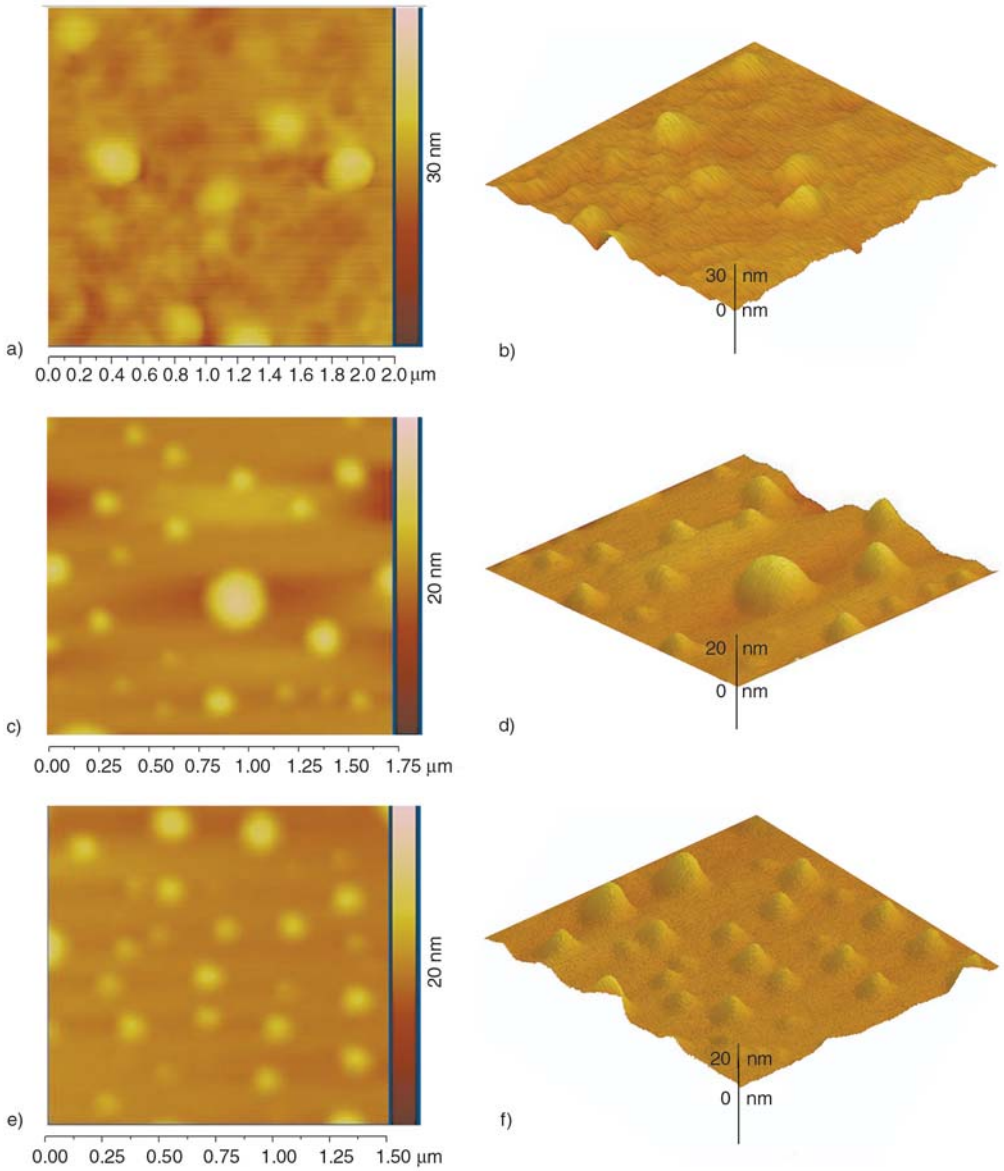

Figure 7. Height-contrast 2D (left) and corresponding 3D (right) AFM images of PU based nanocomposites

toward the stretching direction at low strain; and at high strain, the hard segment domain may align parallel to the stretching direction. Thus, PU can maintain its stress capacity in the relatively high strain without any breakdown of amorphous soft chains. However, the incorporation of polysilsesquioxane spheres hinders the deformation of soft segments in PU and thus leads to lower elongation-at-break.

As shown in Figure 7 from PU-A to PU-C, with increasing the TPM content, the silica spheres undergo a change from lower number with larger diameter to higher number with smaller and homogeneous diameter. The soft surface of polyurethane leads to the unclear image. Moreover, the silica spheres are covered by polyurethane, resulting in fuzzy boundary of the particles. However, as confirmed by AFM images, the silica spheres with different sizes (about 80–200 nm) are formed during the hydrolysis and condensation. The sphere morphology was influenced by the TPM content in the copolymer. With the increase of TPM incorporation, the silica spheres were smaller and distributed more homogeneously. Thus, the thermal stability and the mechanical properties were enhanced from PU-A to PU-C.

4. Conclusions

In this work, a series of alkoxysilane-containing copolymers with a gradient change in molecular weight were prepared by RAFT, and PDI became

narrower with the increase of the feed ratio of TPM. After gelation process, the silica particles were uniformly dispersed in the copolymer matrix, and their sizes were in the nanoscale from the AFM results. The thermal stability of the hybrid copolymers was increased with increasing the content of silica spheres. The mechanical property of PU matrix was improved greatly due to the reinforcement effect of polysilsesquioxane nanospheres and the increase in crosslinking density of the silica spheres. Therefore, we can tune the performance of the hybrid nanocomposites by adjusting the configuration of polysilsesquioxane by RAFT polymerization (e.g., via feed ratio).

Acknowledgements

This work is supported by the Shanghai Leading Academic Discipline Project (Project Number: B113).

References

[1] Dislich H.: New routes to multicomponent oxide glasses. Angewandte Chemie International Edition, **10**, 363–369 (1971).
DOI: 10.1002/anie.197103631

[2] Zhulina E. B., Borisov O. V.: Self-assembly in solution of block copolymers with annealing polyelectrolyte blocks. Macromolecules, **35**, 9191–9203 (2002).
DOI: 10.1021/ma020865s

[3] Shen H., Eisenberg A.: Control of architecture in block-copolymer vesicles. Angewandte Chemie International Edition, **39**, 3310–3312 (2000).
DOI: 10.1002/1521-3773(20000915)39:18<3310::AID-ANIE3310>3.0.CO;2-2

[4] Okada A., Usuki A., Kurauchi T., Kamigaito O.: Polymer-clay hybrids. ACS Symposium Series, **585**, 55–65 (1995).

[5] Han Y-H., Taylor A., Mantle M. D., Knowles K. M.: Sol-gel-derived organic-inorganic hybrid materials. Journal of Non-Crystalline Solids, **353**, 313–320 (2007).
DOI: 10.1016/j.jnoncrysol.2006.05.042

[6] Jang J., Park H.: *In situ* sol-gel process of polystyrene/silica hybrid materials: Effect of silane-coupling agents. Journal of Applied Polymer Science, **85**, 2074–2083 (2002).
DOI: 10.1002/app.10747

[7] Jiang H. M., Zheng Z., Song W. H., Li Z. M., Wang X. L.: Alkoxysilane functionalized polyurethane/polysiloxane copolymers: Synthesis and the effect of end-capping agent. Polymer Bulletin, **59**, 53–63 (2007).
DOI: 10.1007/s00289-007-0748-y

[8] Rodríguez-Hernández J., Chécot F., Gnanou Y., Lecommandoux S.: Toward 'smart' nano-objects by self-assembly of block copolymers in solution. Progress in Polymer Science, **30**, 691–724 (2005).
DOI: 10.1016/j.progpolymsci.2005.04.002

[9] Zhou J. F., Wang L., Dong X. C., Yang Q., Wang J. J., Yu H. J., Chen X.: Preparation of organic/inorganic hybrid nanomaterials using aggregates of poly(stearyl methacrylate)-*b*-poly(3-(trimethoxysilyl) propyl methacrylate) as precursor. European Polymer Journal, **43**, 1736–1743 (2007).
DOI: 10.1016/j.eurpolymj.2006.09.022

[10] Wu C., Xu T., Yang W.: Synthesis and characterizations of novel, positively charged poly(methyl acrylate)-SiO_2 nanocomposites. European Polymer Journal, **41**, 1901–1908 (2005).
DOI: 10.1016/j.eurpolymj.2005.02.031

[11] Hsiue G-H., Kuo W-J., Huang Y-P., Jeng R-J.: Microstructural and morphological characteristics of PS-SiO_2 nanocomposites. Polymer, **41**, 2813–2825 (2000).
DOI: 10.1016/S0032-3861(99)00478-4

[12] Zhang Y. W., Jiang M., Zhao J. X., Wang Z. X., Dou H. J., Chen D. Y.: pH-responsive core-shell particles and hollow spheres attained by macromolecular self-assembly. Langmuir, **21**, 1531–1538 (2005).
DOI: 10.1021/la047912p

[13] Pilon L. N., Amies S. P., Findlay P., Rannard S. P.: Synthesis and characterization of shell cross-linked micelles with hydroxy-functional coronas: A pragmatic alternative to dendrimers? Langmuir, **21**, 3808–3813 (2005).
DOI: 10.1021/la047046g

[14] Zhao Q., Han B., Wang Z., Gao C., Peng C., Shen J.: Hollow chitosan-alginate multilayer microcapsules as drug delivery vehicle: Doxorubicin loading and in vitro and in vivo studies. Nanomedicine: Nanotechnology, Biology and Medicine, **3**, 63–74 (2007).
DOI: 10.1016/j.nano.2006.11.007

[15] Du J., Chen Y.: Atom-transfer radical polymerization of a reactive monomer: 3-(trimethoxysilyl)propyl methacrylate. Macromolecules, **37**, 6322–6328 (2004).
DOI: 10.1021/ma0359382

[16] Du J. Z., Chen Y. M.: Organic-inorganic hybrid nanoparticles with a complex hollow structure. Angewandte Chemie, **116**, 5194–5197 (2004).
DOI: 10.1002/ange.200454244

[17] Du J., Chen Y., Zhang Y., Han C. C., Fischer K., Schmidt M.: Organic/inorganic hybrid vesicles based on a reactive block copolymer. Journal of the American Chemical Society, **125**, 14710–14711 (2003).
DOI: 10.1021/ja0368610

[18] Sayari A., Hamoudi S.: Periodic mesoporous silica-based organic-inorganic nanocomposite materials. Chemistry of Materials, **13**, 3151–3168 (2001).
DOI: 10.1021/cm011039l

[19] Du J. Z., Chen Y. M.: Preparation of organic/inorganic hybrid hollow particles based on gelation of polymer vesicles. Macromolecules, **37**, 5710–5716 (2004). DOI: 10.1021/ma0497097

[20] Park J-W., Thomas E. L.: A Surface-reactive rod-coil diblock copolymer: Nano- and micropatterned polymer brushes. Journal of the American Chemical Society, **124**, 514–515 (2002). DOI: 10.1021/ja017116v

[21] Park J-W., Thomas E. L.: Multiple ordering transitions: Hierarchical self-assembly of rod-coil block copolymers. Advanced Materials, **15**, 585–588 (2003). DOI: 10.1002/adma.200304591

[22] Du J. Z., Chen Y. M.: Organic-inorganic hybrid nanoparticles with a complex hollow structure. Angewandte Chemie International Edition, **43**, 5084–5087 (2004). DOI: 10.1002/anie.200454244

[23] Ni H., Aaserud D. J., Simonsick W. J. Jr., Soucek M. D.: Preparation and characterization of alkoxysilane functionalized isocyanurates. Polymer, **41**, 57–71 (2000). DOI: 10.1016/S0032-3861(99)00160-3

[24] Kannan R. Y., Salacinski H. J., De Groot J., Clatworthy J. I., Bozec L., Horton M., Butler P. E., Seifalian A. M.: The antithrombogenic potential of a polyhedral oligomeric silsesquioxane (POSS) nanocomposite. Biomacromolecules, **7**, 215–223 (2006). DOI: 10.1021/bm050590z

[25] Liu Y., Ni Y., Zheng S.: Polyurethane networks modified with octa(propylglycidyl ether) polyhedral oligomeric silsesquioxane. Macromolecular Chemistry and Physics, **207**, 1842–1851 (2006). DOI: 10.1002/macp.200600241

[26] Hua D. B., Sun W., Bai R. K., Lu W. Q., Pan C. Y.: Study on controlled/living free-radical polymerization of methyl acrylate in the presence of benzyl 9H-carbazole-9-carbodithioate under thermal condition. European Polymer Journal, **41**, 1674–1680 (2005). DOI: 10.1016/j.eurpolymj.2005.01.022

[27] Charleux B., Nicolas J., Guerret O.: Theoretical expression of the average activation-deactivation equilibrium constant in controlled/living free-radical copolymerization operating via reversible termination. Application to a strongly improved control in nitroxide-mediated polymerization of methyl methacrylate. Macromolecules, **38**, 5485–5492 (2005). DOI: 10.1021/ma050087e

[28] Xia J., Zhang X., Matyjaszewski K.: Synthesis of star-shaped polystyrene by atom transfer radical polymerization using an 'arm first' approach. Macromolecules, **32**, 4482–4484 (1999). DOI: 10.1021/ma9900378

[29] Chiefari J., Mayadunne R. T. A., Moad C. L., Moad G., Rizzardo E., Postma A., Skidmore M. A., Thang S. H.: Thiocarbonylthio compounds (SC(Z)S-R) in free radical polymerization with reversible addition-fragmentation chain transfer (RAFT polymerization). Effect of the activating group Z. Macromolecules, **36**, 2273–2283 (2003). DOI: 10.1021/ma020883+

[30] Pyun J., Matyjaszewski K.: Synthesis of nanocomposite organic/inorganic hybrid materials using controlled/'living' radical polymerization. Chemistry of Materials, **13**, 3436–3448 (2001). DOI: 10.1021/cm011065j

[31] Smulders W., Gilbert R. G., Monteiro M. J.: A kinetic investigation of seeded emulsion polymerization of styrene using reversible addition-fragmentation chain transfer (RAFT) agents with a low transfer constant. Macromolecules, **36**, 4309–4318 (2003). DOI: 10.1021/ma026020y

[32] Le T. P., Moad G., Rizzardo E., Thang S. H.: Polymerization with living characteristics. PCT International Application, WO9801478 AI 980115 (1998).

[33] Liu P., Song J., He L., Liang X., Ding H., Li Q.: Alkoxysilane functionalized polycaprolactone/polysiloxane modified epoxy resin through sol-gel process. European Polymer Journal, **44**, 940–951 (2008). DOI: 10.1016/j.eurpolymj.2007.12.014

[34] Cho J. W., Lee S. H.: Influence of silica on shape memory effect and mechanical properties of polyurethane-silica hybrids. European Polymer Journal, **40**, 1343–1348 (2004). DOI: 10.1016/j.eurpolymj.2004.01.041

[35] Nomura Y., Sato A., Sato S., Mori H., Endo T.: Synthesis of novel moisture-curable polyurethanes end-capped with trialkoxysilane and their application to one-component adhesives. Journal of Polymer Science Part A: Polymer Chemistry, **45**, 2689–2704 (2007). DOI: 10.1002/pola.22025

[36] Valentová H., Sedlaková Z., Nedbal J., Ilavský M.: Formation, structure, thermal and dynamic mechanical behaviour of ordered polyurethane networks based on mesogenic diol. European Polymer Journal, **37**, 1511–1517 (2001). DOI: 10.1016/S0014-3057(01)00017-9

[37] Uricanu V., Donescu D., Banu A. G., Serban S., Olteanu M., Dudau M.: Organic-inorganic hybrids made from polymerizable precursors. Materials Chemistry and Physics, **85**, 120–130 (2004). DOI: 10.1016/j.matchemphys.2003.12.024

eXPRESS Polymer Letters Vol.4, No.1 (2010) 26–31
Available online at www.expresspolymlett.com
DOI: 10.3144/expresspolymlett.2010.5

Characterisation of solution cast cellulose nanofibre – reinforced poly(lactic acid)

D. Y. Liu[1], *X. W. Yuan*[1*], *D. Bhattacharyya*[1], *A. J. Easteal*[2]

[1]Department of Mechanical Engineering, The University of Auckland, Auckland, New Zealand
[2]Department of Chemistry, The University of Auckland, Auckland, New Zealand

Received 14 August 2009; accepted in revised form 12 October 2009

Abstract. Cellulose nanofibres, 20 nm in diameter and 300 nm long, were prepared by acid hydrolysis of flax yarns. Composite films containing 2.5 and 5.0 wt% flax cellulose (FC) fibres were prepared by solution casting of mixtures of poly(lactic acid) (PLA) solution and cellulose nanofibre suspension in chloroform. The resulting composite films and solution cast pure PLA film, with thickness of around 160 μm, showed good transparency. For composites with 2.5 and 5.0 wt% FC, the tensile strength increased by 25 and 59% and tensile modulus by 42 and 47%, respectively, compared to pure PLA film. The composite film with 2.5 wt% FC combined high strength and ductility with tensile strength of 24.3 MPa and 70% elongation at break. Flax cellulose appeared to facilitate nucleation and subsequent crystallisation of PLA more effectively in the amorphous composites than in the crystalline composites.

Keywords: *polymer composites, poly(lactic acid) (PLA), nanocellulose, biopolymer*

1. Introduction

Biopolymers are attractive materials because they are biodegradable, recyclable and compostable, and are regarded as the best replacement for conventional packaging materials in respect of energy resources and environmental impact. PLA is a versatile biopolymer made from the renewable agricultural raw material corn, and shows good potential for applications in packaging, and the automotive and biomedical fields. For the packaging industry in particular, PLA has significant potential because of the combination of high clarity and stiffness, and excellent printability, and because it can be manufactured using readily available production technology. PLA is being commercialised as a food packaging polymer for short shelf-life products in common applications such as containers, drinking cups, and overwrap and lamination films [1]. However, the thermal properties and water vapour and gas barrier properties of PLA are inferior to those of conventional petroleum-based polymers [2, 3].

To tailor the properties of PLA it is desirable to combine the polymer with reinforcing elements. Much research is focused on the use of natural fibres as reinforcements for polymer composites, because natural fibres are renewable and abundant [4]. Purified cellulose fibres with one nano-scale dimension have more potential as reinforcing fillers in polymer matrices due to their good mechanical properties with very high bending strength, and stiffness (e.g. Young's modulus of about 150 GPa [5, 6]). Cellulose in nano-scale has been investigated extensively [7] for preparation of polymer composites and is available from various sources, such as cotton, tunicate, bacteria, ramie and wood. The high aspect ratio and good dispersability of cellulose enhance barrier properties to gases and vapours, because the presence of the impermeable

*Corresponding author, e-mail: xw.yuan@auckland.ac.nz

crystalline fibres can increase the travel path for gas or vapour movement through the composite (detour factor) and lead to slower diffusion processes [8, 9]. Thus, preparation of composites with nano-scale fillers has been considered a promising method to improve gas barrier properties and mechanical properties without affecting transparency for packaging applications [10].

In the present work, cellulose fibres, 20 nm in diameter and 400 nm long, were obtained from flax yarns by the sulphuric acid hydrolysis method. Pure PLA and its composite films with 2.5 and 5.0 wt% flax cellulose (FC) were prepared by casting PLA solution, and mixtures of cellulose suspension and PLA solution. The objective of the study was to investigate the effects of addition of nano-FC on the properties of the PLA matrix. The morphology, structure, thermal and mechanical properties are presented in this paper.

2. Experimental methods

2.1. Materials

Poly(lactic acid) (PLA), 2002 D, was purchased in pellet form from Natureworks Co., Minnetonka, USA. Bleached flax yarns were purchased from Jayashree Textiles, Kolkata, India. Microcrystalline cellulose powder was supplied by Sigma-Aldrich Inc., St. Louis, USA. Sodium hydroxide was purchased from Ajax Finechem Pty Ltd., Taren Point, Australia. Sulphuric acid with concentration 95–97%, and chloroform (purity 99.0–99.4%, lab grade) were bought from Merck KGaA, Darmstadt, Germany.

2.2. Preparation of flax nanocellulose fibres

Bleached flax yarns were boiled in distilled water for 30 min and oven-dried to constant weight. The dried yarns were then soaked for 30 min in 1% (w/w) aqueous NaOH at 80°C, and were washed again in running water, i.e. in an alkali-free environment. An aqueous suspension of nanocellulose fibres was prepared by acid hydrolysis for 4 h in 55 wt% sulphuric acid at 55°C with continuous stirring. After completion of the hydrolysis, the flask was cooled in ice-cold water. The aqueous suspension of fibres was diluted and repeatedly washed by centrifugation, then neutralised with 1.0 wt% aqueous NaOH. The suspension was then frozen and freeze dried for 48 h.

2.3. Preparation of neat PLA and PLA composite films

The neat PLA films were prepared by casting PLA solution in chloroform at a concentration of 5.0 wt%. The PLA/chloroform mixtures were continuously stirred at room temperature until the pellets were fully dissolved. The composite films were obtained by mixing a 5 wt% suspension of FC in chloroform with varying proportions of the PLA solution, and stirring for 12 h. The mixtures were then poured into Petri dishes and chloroform was allowed to evaporate at ambient temperature and pressure. The resulting films were finally oven dried for 12 h at 40°C.

2.4. Characterisation

The structure of hydrolysed flax cellulose was investigated using transmission electron microscope (TEM – Philips CM 12, Holland). A droplet of the diluted suspension was allowed to float on and eventually flow through a copper grid covered with a carbon film. The samples were then stained by allowing the grids to float in a 2.0 wt% solution of uranyl acetate for 1 min. X-ray diffraction (XRD – Bruker D 8 Advance, Germany) measurements were performed using CuK_α radiation at a scan speed $0.02°\cdot s^{-1}$ from 5 to 50°. The tensile properties were evaluated with an Instron universal testing machine (model 5567, USA), with a 200 N load cell. The crosshead speed was maintained at $50\ mm\cdot min^{-1}$ during testing. The samples were 15 mm wide and 85 mm long, and the distance between the grips was 60 mm. The results presented here are the average values of six individual samples. Thermal behaviour was investigated by a differential scanning calorimeter (DSC, TA Instruments Q1000, USA) using approximately 7.0 mg of sample material. For heating-cooling-heating measurements, the following procedure was performed: isotherm at 0°C for 1 min; heat at $10°C\cdot min^{-1}$ from 0 to 200°C; isotherm at 200°C for 1 min; cool at $5°C\cdot min^{-1}$ from 200 to 0°C.

3. Results and discussion

The TEM micrographs in Figure 1 show that sulphuric acid hydrolysis of FC caused breakdown of the fibres into rod-like fragments. The amorphous parts were selectively hydrolysed, and the crystalline parts remained unaffected. The average diameter and length for individual cellulose fibres were measured as 20 and 300 nm, respectively. Treating cellulose with sulphuric acid involves esterification of hydroxyl groups by sulphate ions [11]. Introduction of sulphate groups along the surface of the crystallites will result in a negative charge of the surface. This anionic stabilization via the attraction/repulsion forces of the electrical double layers at the crystallites is probably the reason for the stability of the colloidal suspensions of the crystallites [12]. However, upon drying the crystalline fragments were rod-like and aggregated to some extent. The aggregation might have resulted from the formation of hydrogen bonds from the hydroxyl groups and the high surface energy of the cellulose nanofibres.

The X-ray diffraction patterns of freeze dried flax cellulose powder and non-hydrolysed flax cellulose (bleached flax yarns), shown in Figure 2, are typical cellulose I structures. The patterns of commercial microcrystalline cellulose are also shown for comparison. The crystallinity index was calculated according to Equation (1) [13]:

$$I_c\,[\%] = \frac{I_{(200)} - I_{(am)}}{I_{(200)}} \cdot 100 \qquad (1)$$

where $I_{(200)}$ is the counter reading at peak intensity at a 2θ angle close to 22.8° representing the crystalline part and amorphous part, and $I_{(am)}$ is the counter reading at peak intensity at a 2θ angle around 18.6° representing the amorphous part in the cellulose fibres. Use of Equation (1) from Figure 2 gives for the freeze dried flax cellulose the crystallinity index I_c = 82%, a little lower than those of non-hydrolysed flax yarns (I_c = 83%) and commercial microcrystalline cellulose (I_c = 85%). The lower crystallinity index of hydrolysed flax cellulose is because degradation of crystalline cellulose has probably occurred due to the hydrolysis in order to obtain isolated nanofibres [14].

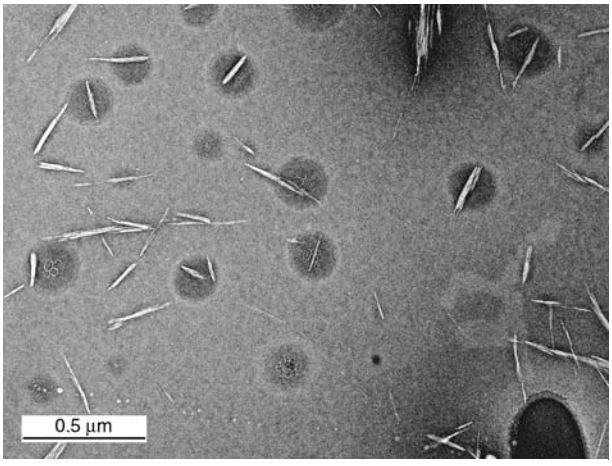

Figure 1. Transmission electron micrograph of flax cellulose nanofibres using sulphuric acid hydrolysis

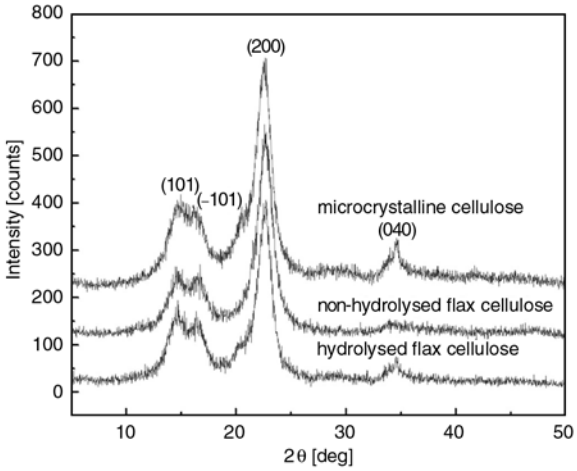

Figure 2. X-ray diffraction patterns of non-hydrolysed flax cellulose (bleached flax yarns) and freeze-dried flax cellulose. Commercial microcrystalline cellulose is shown for comparison.

Representative stress-strain curves of the pure PLA and PLA-FC composites are shown in Figure 3. From the tensile results shown in Figure 3, it is apparent that the composites show improvement in tensile modulus (measured between strains of 0.05

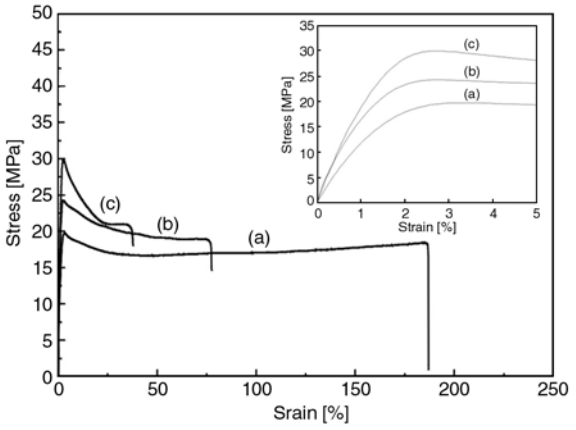

Figure 3. Stress-strain curves of pure PLA and composite films. The inset shows the stress-strain behaviour at low strains.

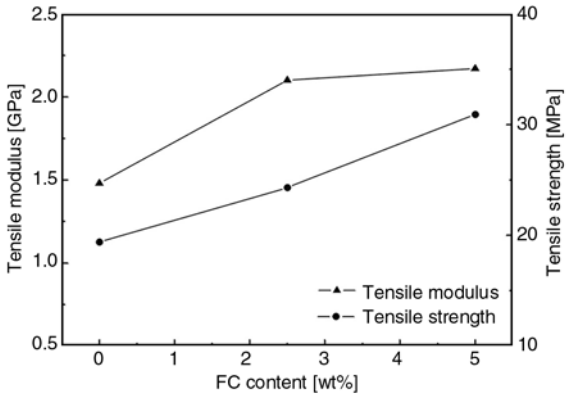

Figure 4. Tensile properties of PLA and PLA-FC composites

and 0.25%) and tensile strength, compared to pure PLA. The tensile strength of pure PLA film and PLA films containing 2.5 and 5.0 wt% FC was measured as 19.4, 24.3, and 30.9 MPa, respectively. Thus FC increased the tensile strength of PLA by 25 or 59% with the addition of 2.5 or 5.0 wt%, respectively. The tensile modulus is measured as 1.48, 2.10, and 2.17 GPa for pure PLA film and PLA films with 2.5 and 5.0% FC addition, respectively. Thus FC increased the tensile modulus by 42 or 47% with the addition of 2.5 or 5.0 wt% respectively (Figure 4). However, the elongation at break (ductility) decreased from 194% for neat PLA film to 70 and 40% for the composites with 2.5 and 5.0 wt% FC, respectively. The composite film with 2.5 wt% flax cellulose combined high strength and ductility with tensile strength of 24.3 MPa and 70% elongation at break.

To investigate the effects of flax cellulose fibres on the thermal behaviours of PLA matrix, a DSC study was performed on the pure PLA and PLA-FC composite films. The thermal parameters, such as, glass transition onset temperature (T_g), cold crystallisation onset temperature (T_c), and melting onset temperature ($T_{m)}$ were measured from the DSC curves. The degree of crystallinity of the PLA in the composites was evaluated by the percent crystallinity of PLA in the composites, X_c, which can be calculated by Equation (2) [15]:

$$X_c\,[\%] = \frac{\dfrac{\Delta H_m + \Delta H_c}{X_{PLA}}}{\Delta H_m^c} \cdot 100 \qquad (2)$$

where ΔH_m and ΔH_c are enthalpies of fusion and crystallisation, respectively, and $\Delta H_m^c = 93\ \mathrm{J \cdot g^{-1}}$ is the enthalpy of fusion of 100% crystalline poly(lactic acid) [16], and X_{PLA} is the weight fraction of PLA in the composite. The DSC scans (first heating scan) of pure PLA and PLA-FC composite films are depicted in Figure 5. The as-cast composite films show very similar thermal behaviour to that of neat PLA film. No obvious glass transition and crystallisation were observed upon heating up to 200°C. The enthalpy of fusion decreases from 19.6 $\mathrm{J \cdot g^{-1}}$ for pure PLA film to 19.4 and 18.9 $\mathrm{J \cdot g^{-1}}$ for PLA film containing 2.5 and 5.0 wt% FC, respectively, which probably results from the lower content of PLA matrix. The calculated percent crystallinity X_c of the three samples is almost the same, indicating that flax cellulose did not change the crystallinity of PLA during the solution casting process. The thermal parameters for the first heating run are tabulated in Table 1.

However, different thermal behaviour shown in Figure 6 was seen during the second heating run after the samples had been cooled at 5°C·min^{-1}

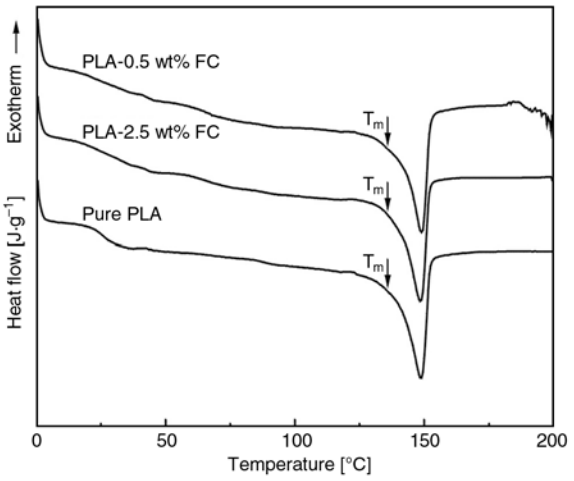

Figure 5. Thermal behaviour of pure PLA, PLA-2.5 wt% FC and PLA-5.0 wt% FC composites during the first heating scan

Table 1. DSC results for pure PLA and PLA-FC composites from the first and second heating runs

Composition	T_g [°C]	T_c [°C]	T_m [°C]		ΔH_m [J·g^{-1}]		ΔH_c [J·g^{-1}]	X_c [%]	
			1nd	2nd	1nd	2nd		1nd	2nd
Neat PLA	56.0	117.3	139.9	141.8	19.6	0.16	0.14	21.1	0.0
PLA-2.5 wt% FC	55.5	112.1	140.1	142.2	19.4	1.81	1.42	21.4	0.4
PLA-5.0 wt% FC	55.3	108.7	141.2	142.4	18.9	2.81	1.90	21.4	1.0

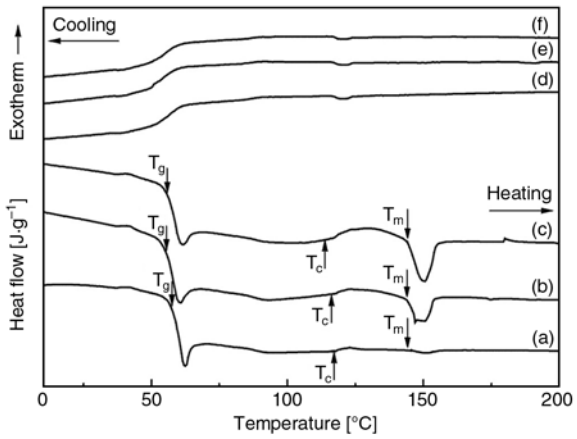

Figure 6. The cooling behaviour of pure PLA (a), PLA-2.5 wt% FC (b) and PLA-5.0 wt% FC (c) composites and heating behaviour of PLA (d), PLA-2.5 wt% FC (e) and PLA-5.0 wt% FC (f) during the second heating scan

from 200°C. The three samples show a well defined glass transition, 'cold' crystallisation and melting, which are different in several respects from the thermal behaviour in the first heating scan. The composite films show a broader cold crystallisation temperature range and lower cold crystallisation onset temperature than those of the pure PLA film. The thermal parameters of this heating run are listed in Table 1. The glass transition onset temperature (T_g) of the three samples is almost same, between 55–56°C. The enthalpy of crystallisation and fusion of PLA-FC increased with addition of flax cellulose to PLA matrix, compared to pure PLA film. The composite films show higher percent crystallinity of 0.4 and 1.0% for the films containing 2.5 and 5.0 wt% FC, respectively. The onset crystallisation temperature decreased to 112 and 109°C for the composite films with 2.5 and 5.0 wt% FC, respectively, compared with 117°C for the pure PLA film. This behaviour indicates that the flax cellulose nano-fibre can induce crystal nucleation of the PLA polymer, which implies that this flax cellulose material can probably be used as a nucleating agent for PLA.

The different effect of flax cellulose on the thermal behaviour of PLA matrix during the same heating process is probably related to the different microstructures of the starting sample before heating. From Figure 6, the structure of pure PLA film is almost fully amorphous, because the areas under the cold crystallisation exotherm and melting endotherm are very similar, and the enthalpy of fusion is very small. Moreover, the originally cast films for the first heating run were crystalline because no cooling was applied to the casting process, providing enough time for crystallisation of dissolved polymer, while the films after cooling at 5°C·min^{-1} from 200°C for the second heating run were almost amorphous because the crystallisation was retarded during the cooling process, which is shown in Figure 6 that there is no obvious crystallisation from the cooling curves. This indicates that the influence of flax cellulose on the thermal behaviour of PLA matrix is related to the sample's history.

4. Conclusions

A suspension of cellulose nanocrystals was prepared from flax yarns by acid hydrolysis and used as reinforcement in a PLA matrix for preparation of composite films by a convenient casting method. The nanocrystal contents used were 2.5 and 5.0 wt%. The tensile strength increased 25 and 59% for PLA composites containing 2.5 and 5.0 wt% flax cellulose, respectively, while the tensile modulus increased 42 and 47% for those composites. However, the elongation at break (ductility) decreased from 194% for neat PLA film to 70 and 40% for the composites with 2.5 and 5.0 wt% FC, respectively. The composite film with 2.5 wt% flax cellulose combines high strength and ductility with tensile strength of 24.3 MPa and 70% elongation at break. Flax cellulose appeared to facilitate nucleation and subsequent crystallisation of PLA more effectively in the amorphous composites than in crystalline composites.

Acknowledgements

The authors are thankful for the financial support provided by the University of Auckland.

References

[1] Kale G., Auras R., Singh S. P.: Degradation of commercial biodegradable packages under real composting and ambient exposure conditions. Journal of Polymers and the Environment, **14**, 317–334 (2006). DOI: 10.1007/s10924-006-0015-6

[2] Petersen K., Nielsen P., Olsen M.: Physical and mechanical properties of biobased materials-starch, polylactate and polyhydroxybutyrate. Starch, **53**, 356–361 (2001).
DOI: 10.1002/1521-379X(200108)53:8<356::AID-STAR356>3.0.CO;2-7

[3] Bastioli C.: Global status of the production of biobased packaging materials. Starch, **53**, 351–355 (2001).
DOI: 10.1002/1521-379X(200108)53:8<351::AID-STAR351>3.0.CO;2-R

[4] Oksman K., Skrifvars M., Selin J-F.: Natural fibres as reinforcement in polylactic acid (PLA) composites. Composites Science and Technology, **63**, 1317–1324 (2003).
DOI: 10.1016/s0266-3538(03)00103-9

[5] Šturcová A., Davies G. R., Eichhorn S. J.: Elastic modulus and stress-transfer properties of tunicate cellulose whiskers. Biomacromolecules, **6**, 1055–1061 (2005).
DOI: 10.1021/bm049291k

[6] Cao X. D., Dong H., Li C. M.: New nanocomposite materials reinforced with flax cellulose nanocrystals in waterborne polyurethane. Biomacromolecules, **8**, 899–904 (2007).
DOI: 10.1021/bm0610368

[7] Azizi Samir M. A. S., Alloin F., Dufresne A.: Review of recent research into cellulose whiskers, their properties and their application in nanocomposite field. Biomacromolecules, **6**, 612–626 (2005).
DOI: 10.1021/bm0493685

[8] Lagaron J. M., Catalá R., Gavara R.: Structural characteristics defining high barrier polymeric materials. Materials Science and Technology, **20**, 1–7 (2004).
DOI: 10.1179/026708304225010442

[9] Khalil H. P. S. A., Shahnaz Sharifah B. S., Ratnam M. M., Ahmad F., Nik Fuaad N. A.: Recycled polypropylene (RPP) wood saw dust (WSD) composites-Part1: The effect of different filler size and filler loading on mechanical and water absorption properties. Journal of Reinforced Plastics and Composites, **25**, 1291–1303 (2006).
DOI: 10.1177/0731684406062060

[10] Alexandra M., Dubois P.: Polymer-layered silicate nanocomposites: Preparation, properties and uses of a new class of materials. Materials Science and Engineering: R: Reports, **28**, 1–63 (2000).
DOI: 10.1016/S0927-796X(00)00012-7

[11] Yao S. J.: Sulfation kinetics in the preparation of cellulose sulphate. Chinese Journal of Chemical Engineering, **7**, 47–55 (1999).

[12] Marchessault R. H., Morehead F. F., Koch M. J.: Some hydrodynamic properties of neutral suspensions of cellulose crystallites as related to size and shape. Journal of Colloid Science, **16**, 327–344 (1961).
DOI: 10.1016/0095-8522(61)90033-2

[13] Segal S., Creely J. J., Martin A. E., Conrad C. M.: Am empirical method for estimating the degree of crystallinity of native cellulose using the X-ray diffractometer. Textile Research Journal, **29**, 786–794 (1959).
DOI: 10.1177/004051755902901003

[14] Bondeson D., Mathew A., Oksman K.: Optimization of the isolation of nanocrystals from microcrystalline cellulose by acid hydrolysis. Cellulose, **13**, 171–180 (2006).
DOI: 10.1007/s10570-006-9061-4

[15] Ke T. Y., Sun X. Z.: Physical properties of poly (lactic acid) and starch composites with various blending ratios. Cereal Chemistry, **77**, 761–768 (2000).
DOI: 10.1094/CCHEM.2000.77.6.761

[16] Fisher E. W., Sterzel H. J., Wegner G.: Investigation of the structure of solution grown crystals of lactide copolymers by means of chemical reactions. Colloid and Polymer Science, **251**, 980–990 (1973).
DOI: 10.1007/BF01498927

eXPRESS Polymer Letters Vol.4, No.1 (2010) 32–38
Available online at www.expresspolymlett.com
DOI: 10.3144/expresspolymlett.2010.6

Synthesis of biodegradable thermoplastic elastomers (BTPE) based on ε-caprolactone

V. T. Lipik[1], *L. K. Widjaja*[1], *S. S. Liow*[1], *S. S. Venkatraman*[1], *M. J. M. Abadie*[*1,2]

[1]School of Materials Science & Engineering, Block N4.1, Level 1, Room # 15, 50 Nanyang Avenue, Nanyang Technological University, Singapore 639798, Singapore
[2]Laboratory of Polymer Science & Advanced Organic Materials LEMP/MAO, CC 021, Université Montpellier II, Sciences et Techniques du Languedoc, Place Eugène Bataillon, 34095 Montpellier cedex 05, France

Received 20 August 2009; accepted in revised form 18 October 2009

Abstract. Aiming to mimic blood vessels, biodegradable thermoplastic elastomer (BTPE) is designed to be elastic, flexible and tough. A series of biodegradable triblock copolymers and poly(ester-urethanes) (PEU) based on ε-caprolactone have been synthesized and studied. The crystallinity of the poly(ε-caprolactone) used as soft segment has been disrupted by incorporating either L-lactide (L-LA) units or trimethylene carbonate (TMC) units. Our studies suggest that soft segment composition does affect the mechanical properties significantly.

Keywords: *polymer synthesis, tailor-made polymers, biodegradable polymers, mechanical properties*

1. Introduction

Although thermoplastic elastomers (TPE) have been known since 1970s by the trade name KRATON®, intensive research for biodegradable TPE just started recently and there are not many commercial elastomeric biodegradable materials in the market today. Biodegradable thermoplastic elastomers with elastomeric mechanical properties, remoldability, wide range of biodegradation rates, and cytocompatibility are always desired for numerous biomedical applications, most predominantly as cardiovascular assist devices, controlled drug delivery and tissue engineering scaffolds [1, 2].

In last decade, researches on biodegradable copolymers [3, 4] and polyurethanes [5, 6] have robustly grown because they may offer good elasticity and unique properties that favor the development of new biomedical materials. However, one of the potential drawbacks of these elastomers is that their rubbery property is restricted by crystalline structures in soft segment. Conventional biomedical copolymers or polyurethanes under studies are made of polycaprolactone (PCL) and/or poly(ethylene glycol) diol as soft segment [6, 7], these semi-crystalline chains in soft segment give rise to lower chain mobility.

In this project, biodegradable TPE having soft block and hard block are being prepared. Two alternatives are investigated where the soft segment is prepared by using coordinated anionic ring opening polymerization (CAROP) of ε-caprolactone mixed with L-Lactide (L-LA) or trimethylene carbonate (TMC), with stannous octoate as biocompatible FDA approved catalyst [4] and diol as the initiator or by a combination of CAROP of ε-caprolactone mixed with L-LA and polycondensation reactions. The first option is to copolymerize the hard segment with L-LA to get a tri-block copolymer whereas the second optional is to polycondensate the dihydroxy poly(ε-caprolactone-co-LLA) with

*Corresponding author, e-mail: marc@ntu.edu.sg

diisocyanate to make a multiblock poly(ester-urethane). For the initial stages of this project, attempts were made at synthesizing the soft block of TPE using random copolymer of ε-caprolactone and L-LA or TMC with various compositions. The target is to make the soft block to be completely amorphous or at least having minimum crystallinity, thus giving the triblock a large elongation. Then this soft block will be coupled either with the hard block made of L-LA or condensed with diisocyanate, which will act as an anchor point to give the elastic property of the TPE.

2. Experimental section

2.1. Materials

Epsilon-caprolactone (CL) monomer (99%) was purchased from Fluka, Singapore, and used without further purification. L-lactide (L-LA) was obtained from Sigma Aldrich, Singapore. It was freshly purified by recrystallization in ethyl acetate, dried in 40°C vacuum oven for 24 hours before every synthesis. Trimethylene carbonate (TMC) was purchased from Boehringer Ingelheim. The initiator, 2,2-dimethyl 1,3-propanediol (purum, >99.0%) was purchased from Fluka, Singapore. It was dried in 40°C vacuum oven for 24 hours for water elimination prior to use because it absorbs moisture from the air easily. The catalyst, tin (II) 2-ethylhexanoate ($SnOct_2$) was purchased from Sigma Aldrich, Singapore. It was stored over molecular sieves (0.4 nm). Anhydrous toluene (99.8%), which was obtained from Sigma Aldrich, Singapore, was used as solvent in the copolymerization reaction. It was used as received. Ethyl acetate, which was obtained from Aik Moh Chemical, Singapore, was stored over molecular sieves (0.4 nm).

In polycondensation reaction, the hard segment, hexamethylene diisocyanate, HMDI, (puriss, >99.0%) was purchased from Fluka, Singapore, and used as received. The chain extender, 1,4-butanediol (99%) was obtained from Alfa Aesar, was stored over molecular sieves (0.4 nm).

2.2. Synthesis

ABA triblock copolymers, where A is a PLLA hard segment and B is the soft segment made of random copolymer of ε-CL and L-LA or TMC were prepared by one-step living coordinated anionic ring-opening polymerization. The syntheses were done in a two necks round bottom flask (100 ml) equipped with thermometer, condenser and magnetic stirrer. The flask was purged with nitrogen,

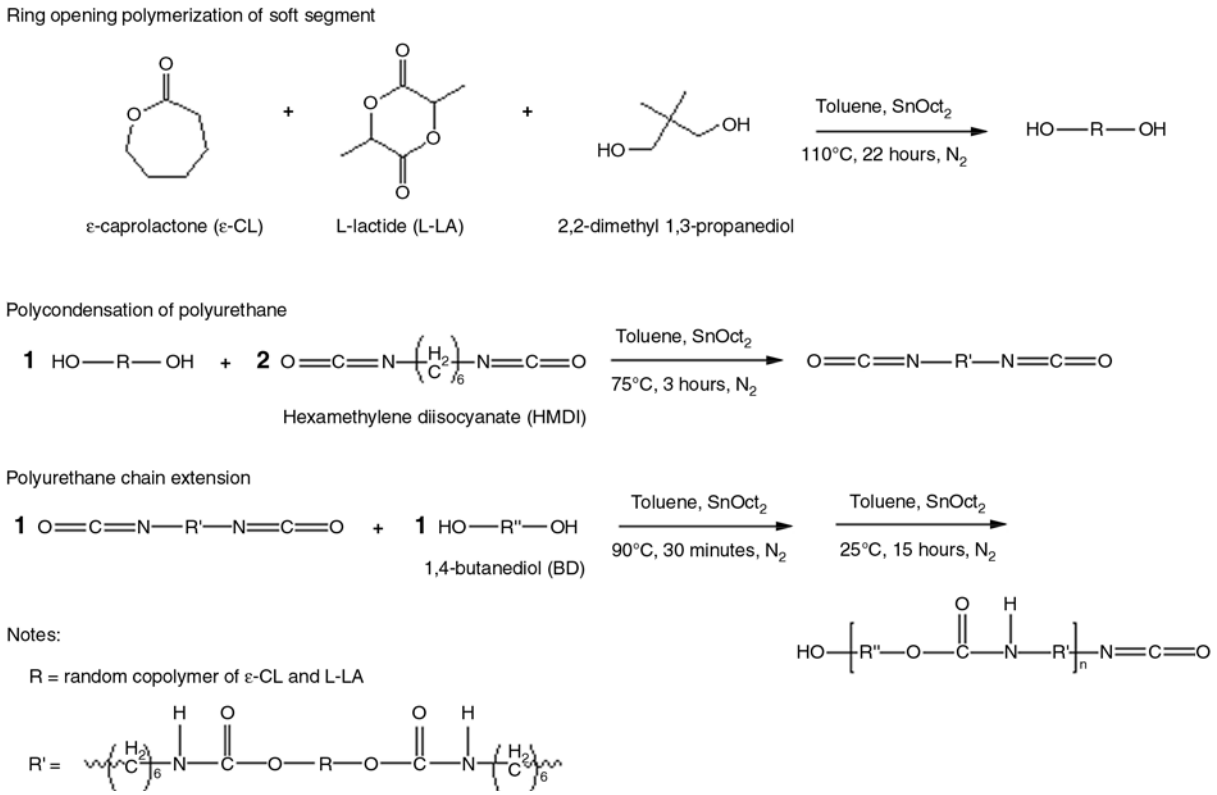

Figure 1. PEU synthesis routes

vacuumed twice and after that was kept under the nitrogen atmosphere. A mixture of ε-capolactone and L-LA or TMC monomers were added to the toluene and then a certain amount of propane-diol was added according to the desired degree of polymerization, lastly $SnOct_2$ as catalyst was added to the mixture and the flask was immersed into silicone oil bath with temperature of 140°C for 24 hours. After that, a defined quantity of L-LA was added to the flask and the mixture was kept another 24 hours. Polymer was precipitated in methanol and dried under vacuum for 3 days.

Multiblock poly(ester-urethanes) were prepared by polycondensation of soft segment with HMDI and chain extension by 1,4-butanediol. The polyurethanes used in this study were synthesized by two-step method in nitrogen atmosphere. Briefly, the stoichiometry of the reaction was set to 2:1:1 hard segment (HMDI): soft segment (HO–PCL-co-PLLA–OH): chain extender (BD). Simultaneously with the soft segment polymerization, HMDI was injected into the soft segment solution at 75°C. After the mixture was allowed to react for 3 hours, the mixture temperature was raised to 90°C while 1,4-butanediol was added dropwise into the flask. This temperature was maintained for 30 minutes under vigorous stirring (>1000 rpm). The mixture was then cooled down to room temperature while the chain-linking reaction was continued for another 15 hours. After the reaction was completed, the product was poured into a Teflon® dish. It was air dried in hood at room temperature for 24 hours, and vacuum dried at 55°C for 48 hours. Detailed chemical schemes are shown in Figure 1.

2.3. Measurement

The molar masses data were obtained by size exclusion chromatography (Agilent 1100 Series) using chloroform as the eluent at a flow rate of 1 $ml \cdot min^{-1}$. Polystyrene standards were used to calibrate the molar mass. Thermal analysis was carried out on a TA Instruments Model Q10 DSC machine. Tensile test was carried out using the INSTRON 5848 microtester and its software INSTRON Bluehill. The dog-bone shape specimens were pulled in the vertical direction at a rate of 50 mm/min and a minimum of 5 specimens per sample were tested. For cyclic tests, which were also performed at room temperature, one sample was tested. The dog shape bone sample was pulled in vertical direction with the rate 10 mm per minute. The rate of recovery was the same.

3. Results and discussions

3.1. Triblocks based on ε-caprolactone & L-lactide

Due to high crystallinity of the soft segment, triblock PLLA-b-(PCL-co-PLLA)-b-PLLA having a molar mass of 5000 Da/5000 Da/5000 Da, represented as 5-5-5 kDa, has demonstrated a poor elongation 5% at maximum load.

A series of soft segments as random copolymers containing a variable amount of lactide have been synthesized – Table 1. The hard block is pure PLLA.

In Table 1, PCL crystallinity (3rd column) is the crystallinity of the soft block whereas PLLA crystallinity (4th column) is the total crystallinity of the

Table 1. Data on triblock PLLA-b-(PCL-co-PLLA)-b-PLLA

PLLA-b-P(CL-LLA)-b-PLLA	%LLA in PCL [mol]	PCL crystallinity [%] soft block	PLLA crystallinity [%] copolymer	M_n by SEC [Da] (DI)	Elongation at maxim load [E%]	Young's modulus [MPa]	Max tensile stress [MPa]
5-10-5 sample#1	10	7.69	10.32	13 330 (1.24)	22.94	12.01	4.22
5-10-5 sample#2	25	0.25	11.55	40 060 (1.22)	146.37	2.50	2.24
5-10-5 sample#3	50	0	10.98	26 840 (1.16)	35.19	7.03	2.75
5-10-5 sample#4	75	0	20.14	18 939 (1.32)	1.53	47.77	2.97
10-10-10 sample#5	25	0	23.81	43 055 (1.21)	90.77	5.29	5.62
10-10-10 sample#6	50	0	26.93	26 158 (1.16)	48.23	18.34	8.05
10-10-10 sample#7	75	0	32.84	24 984 (1.92)	0.84	244.00	2.23

PLLA contained in the triblock copolymer. We observe that best mechanical properties are achieved – sample#2, for a small amount of crystallinity of the soft block, i.e. 0.25%. The crystallinity of the soft block plays a central role defining the properties of polymer.

We also observe Table 1 – samples#5, #6 and #7 – that the mechanical properties depend on the content of L-LA in the soft block. More L-LA in the soft block reduces PCL segment length and therefore brings hardness to the copolymer and elongation at break decreases and modulus increases.

Best elongation is obtained for the triblock PLLA-b-(PCL-co-PLLA)-b-PLLA with molar mass 5 kDa/10 kDa/5 kDa at 25% molar of lactide in the soft segment. After optimization, the best elongation obtained – 171% – Figure 2, is for molar mass 6.5 kDa/10 kDa/6.5 kDa with 25% of lactide in the middle part of the triblock.

Shape recovery behavior has been done on the best sample – sample#2, presented Table 1. Measured degree of recovery was 77% after 100% of elongation.

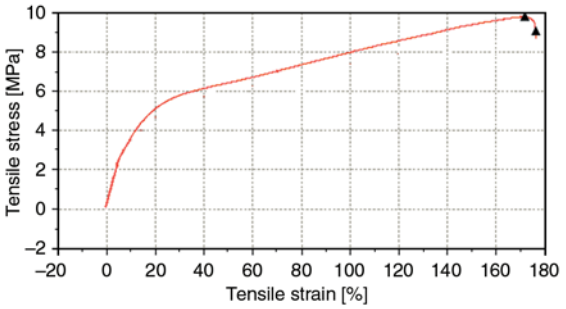

Figure 2. Instron test of copolymer triblock with the structure PLLA-b-(PCL-co-PLLA)-b-PLLA, 6.5 kDa/10 kDa/6.5 kDa, 25% of L-lactide in the middle block

From Table 1, we have observed that crystallinity of hard block affects elongation and modulus. To improve mechanical properties of the triblock copolymer, we have reduced the crystallinity of the hard block by incorporating ε-caprolactone in the PLLA at the second step of the synthesis. We have studied the influence of CL in the hard segment PLLA. Results are presented Table 2.

From Table 2, optimum value is obtained for sample#4 where the presence of 30% of CL in the hard segment gives best elongation at break. It also shows that the presence of more than 30% of CL in the hard block gives excessive softness to the block copolymer.

Therefore if we add more ε-caprolactone, it brings softness. But if we add less ε-caprolactone, polymer contains more L-LA and becomes hard. Only one direction gives softness. At small quantity of CL in PLLA, polymers losses in elongation and cause PLLA hardness.

3.2. Triblock based on ε-caprolactone and trimethylene carbonate [8, 9]

Various triblock copolymers with middle block made of random copolymer of ε-CL and TMC with molar ratio 50:50 and 75:25, and outer block of PLLA have been synthesized and studied – Tables 3 and 4. What have been varied here were the molar masses of the middle block and the outer block. It can be seen that for the middle block of

Table 2. Triblock 10-10-10 kDa, (PLLA-co-PCL)-b-(PCL-co-PLLA)-b-(PLLA-co-PCL). DI stands for polydispersity index

Polymer PLLA-PCL-PLLA [kDa]	%LLA in PCL soft block	%CL in PLLA hard block	Crystallinity of PLLA hard block [%]	Elongation at maxim load [E%]	M_n by SEC [Da] (DI)
10-10-10 sample#1	10	0	37.27	228	32 536 (1.17)
10-10-10 sample#2	10	10	26.22	271	30 910 (1.28)
10-10-10 sample#3	10	20	23.70	385	32 994 (1.18)
10-10-10 sample#4	10	30	11.87	525	33 004 (1.21)
10-10-10 sample#5	10	50	3.97	370	27 504 (1.29)

Table 3. Data on triblock PLLA-b-(PCL-co-PTMC)-b-PLLA, ratio TMC/ε-CL = 50/50

PLLA-PCL-PLLA [kDa]	%TMC in PCL [mol]	Crystallinity [%]	Elongation at max load [E%]	Young's modulus [MPa]	Tensile strength [MPa]	M_n by SEC [Da] (DI) in bracket
5-10-5 sample#1	50	23	29	8.3	2.6	16 470 (1.63)
10-20-10 sample#2	50	21	60	10.8	4.6	31 150 (1.57)
10-40-10 sample#3	50	4	74	3.5	1.5	37 780 (1.48)
20-40-20 sample#4	50	17	520	12.5	4.5	49 160 (1.22)

Table 4. Data on triblock PLLA-b-(PCL-co-PTMC)-b-PLLA, ratio TMC/ε-CL = 25/75

PLLA-PCL-PLLA [kDa]	%TMC in PCL [mol]	Crytallinity soft block [%]	Crystallinity hard block [%]	Elongation at maxim load [E%]	Young's modulus [MPa]	Tensile strength [MPa]	M_n by SEC [Da] (DI) in bracket
20-40-20 sample#1	25	0.3%	15.5%	812	23.8	7.9	41 580 (1.24)
40-80-40 sample#2	25	5.8%	14.0%	1084	32.0	12.3	56 110 (1.40)

targeted molecular mass 10 kDa – sample#1, and 20 kDa – sample#2, the resulting middle block managed to reach the target, while for targeted 40 kDa – samples#3 and #4, the result was slightly lower, probably due to the presence of trace hydroxyl group-containing impurities in the reactants and reaction system which is getting more significant as the molar mass increases.

Mechanical property wise, Table 3 shows that molar mass and the length of PLLA block played a major role. For triblock with targeted middle block of 10 kDa, increasing the L-LA content from 1.5 to 3 (with respect to CL content of 1), resulted in having a polymer which was too brittle to be made into a film. Meanwhile for middle block of 20 kDa, decreasing the L-LA content from 1.5 to 0.75 gave rise to a polymer which was too soft to be made into a film. Comparing between those with same L-LA content but different molar mass, it was observed that increasing the molar mass would result in increasing both the tensile strength and the maximum elongation of the triblock – samples#3 and #4 from Table 3 it can also be seen that the triblock having molar mass of 20 kDa/40 kDa/20 kDa – sample#4, has a good mechanical properties with elongation up to 520%.

Table 4 shows two triblock copolymers with middle block of random copolymer of PCL and PTMC with ε-CL:TMC molar ratio of 75:25. From the previous section, it was shown that triblock with targeted molar mass of 20 kDa/40 kDa/20 kDa – sample#1, gave the best tensile strength and elongation, so here, the focus will be on triblock having that molar mass and higher. Preliminary study showed that the random copolymer of PCL and PTMC with molar ratio 75:25 was a semi crystalline polymer with T_g around –58°C and T_m around 30°C. So it was expected that the triblock had 2 T_m, one from PLLA and the other from P(ε-CL-co-TMC).

Looking at the mechanical properties, a significant increase can be observed by increasing the molar ratio of CL:TMC:CL 50:50 to 25:75 for molar mass of 20 kDa/40 kDa/20 kDa – sample#1, Table 4 (compare Tables 3 and 4). An attempt to synthesize higher molar mass of 40k-80-40k – sample#2, Table 4, resulted in further increase in tensile strength and elongation, although the actual molar mass of the polymer was far below the targeted. This might be due to transesterification reactions which were caused by catalyst during the propagation reactions. Nevertheless, a polymer with a good mechanical property having tensile strength of 12.3 MPa and elongation of 1084% managed to be achieved.

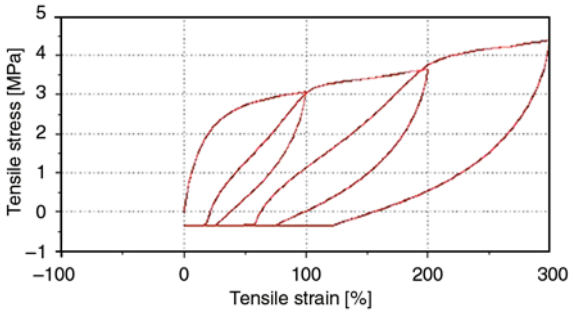

Figure 3. Cyclic test of triblock PLLA-b-(PCL-co-PTMC)-b-PLLA, ratio TMC/ε-CL = 25/75 at room temperature

Shape recovery behavior has been done on the best sample – sample#2, presented Table 4. Measured degree of recovery – Figure 3, according to the cyclic test was 82.1% after 100% of elongation and 70.5% after 200% of elongation. After the 300% elongation, the sample was taken out from the Instron machine and after 10 minutes the final measured recovery was 89.7%.

3.3. Multiblock poly(ester-urethane) elastomers PEU [10]

In a first step hydroxyl-terminated random copolymers of polycaprolactone and poly(L-lactide) were synthesized by ring opening polymerization, which is initiated by 2,2-dimethyl 1,3-propanediol. The molar fraction of L-LA in the soft segment is in mole 75, 50 and 25% respectively. Characteristics of soft segment were shown in Table 5.

Table 5. Characteristics of soft segment

Sample ID	%LLA in PCL [mole]	M_n by SEC [Da]	DI
PCL25	75	9 410	1.31
PCL50	50	11 050	1.29
PCL75	25	12 070	1.30

From hydroxyl-terminated random copolymer of PCL and PLLA serving as soft segment – Table 5, a series of degradable polyurethanes PEU are synthesized from HMDI and 1,4-butanediol (BD) serving as hard segment and chain extender, respectively. SEC results showed – Table 5. PEU molar masses were ranged from 48 to 57 kDa. Soft segment composition may not affect molar weights of PEU since the molar masses obtained were similar. Narrow molar mass distribution was observed suggesting a balance stoichiometry in the synthesis.

T_g was slightly higher than their respective soft segments. All T_gs were below room temperature, suggesting that all PEU have elastomeric characteristics at body temperature. No melting peak was detected due to absence of crystalline structures in these polyurethanes. Table 6 showed the bulk properties of PEU.

Tensile stress-strain curves measured for all the PEU, and commercial non-biodegradable thermoplastic elastomers (TPE) such as SBS and ether-based PU were studied. Comparing among PEU, higher lactide content (PUCL25 – sample#1) results in significant increase in strain at break: e.g. increase lactide content 3 times from 25 to 75 mol%, strain at break increased 7.1 times from 114 to 811%. We also observe for this sample a strain recovery from cyclic test – Figure 4, of 77.9%. In contrast to commercial SBS and ether-based PU, PUCL25 showed better tensile properties but similar elongation, 738% for SBS and 843% for ether PU.

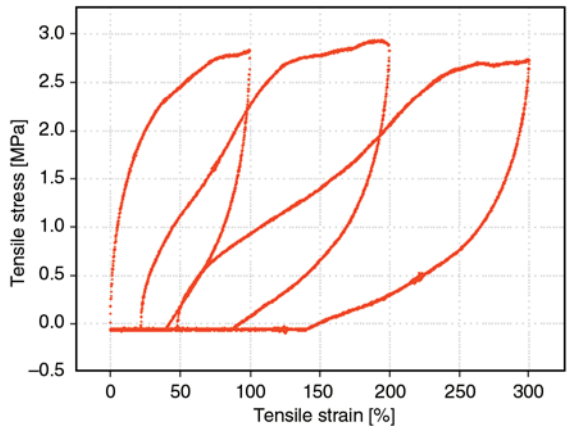

Figure 4. Cyclic test of PUCL25 at room temperature, with rate of deformation 100% per minute

On the other hand, PUCL50 – sample#2 and PUCL75 – sample#3 showed strain in the range of human vein and artery (150–200% strain at break). Despite of the good mechanical properties, toxicity of PEU that based on HMDI as chain coupling agent is still debatable in recent literatures. The potential toxicity could be due to the formation of HMDA during the degradation of urethane linkages [11]. As a result, our group will be focusing on the development of more biocompatible PEU that based on 1,4-diisocyanatobutane (BDI) or lysine diisocyanate (LDI) because they degrade into putrescine and lysine, respectively.

4. Conclusions

Triblock copolymers of ε-CL, TMC, and L-LA with different molar ratio and molar mass were synthesized by the ring-opening bulk copolymerization, using stannous octoate as catalyst. The molecular structures, thermal properties, as well as the mechanical properties of the triblocks changed considerably with composition.

Our study shows that increasing the moar mass will enhance the mechanical properties considerably. For the middle block poly(ε-caprolactone), monomers such as L-LA and TMC are good candidates to disrupt the crystallinity of the soft block; the molar ratio ε-CL:TMC of 75:25 gave a better mechanical properties than 50:50, most probably due to the ε-CL being more elastic and tough compared to TMC.

Table 6. Characteristics of multiblock poly(ester-urethane) elastomers PEU

Sample ID	%L-LA in PCL [mol]	Ultimate tensile strength [MPa]	Elongation at maxim load [E%]	Young's modulus [MPa]	M_n by SEC [Da] (DI)	Strain recovery from cyclic test [%]
PUCL25 sample#1	75	6.29	811	17.33	48,070 (1.33)	77.9
PUCL50 sample#2	50	0.95	262	6.89	56,570 (1.43)	Not tested
PUCL75 sample#3	25	0.50	114	2.40	51,220 (1.47)	Not tested

This study also suggest that multiblock copolymers seem to have a better potentiality in term of mechanical properties that triblock copolymers as maximum strain up to 811% with strain recovery near 80% can be achieved.

References

[1] Venkatraman S., Boey F., Lao L. L.: Implanted cardiovascular polymers. Natural, synthetic and bio-inspired. Progress in Polymer Science, **33**, 853–874 (2008).
DOI: 10.1016/j.progpolymsci.2008.07.001

[2] Amsden B.: Curable, biodegradable elastomers: Emerging biomaterials for drug delivery and tissue engineering. Soft Matter, **3**, 1335–1348 (2007).
DOI: 10.1039/b707472g

[3] van der Mee L., Helmich F., de Bruijn R., Vekemans J. A. J. M., Palmans A. R. A., Meijer E. W.: Investigation of lipase-catalyzed ring-opening polymerizations of lactones with various ring sizes, kinetic evaluation. Macromolecules, **39**, 5021–5027 (2006).
DOI: 10.1021/ma060668j

[4] Wu X. S.: Synthesis and properties of biodegradable lactic/glycolic acid polymers. in 'Encyclopedic handbook of biomaterials and bioengineering' (ed.: Wise D. L.) Marcel Dekker, New York, 1015–1054 (1995).

[5] Younes H. M., Bravo-Grimaldo E., Amsden B. G.: Synthesis, characterization and in vitro degradation of a biodegradable elastomer. Biomaterials, **25**, 5261–5269 (2004).
DOI: 10.1016/j.biomaterials.2003.12.024

[6] Tatai L., Moore T. G., Adhikari R., Malherbe F., Jayasekara R., Griffiths I.: Thermoplastic biodegradable polyurethanes: The effect of chain extender structure on properties and *in-vitro* degradation. Biomaterials, **28**, 5407–5417 (2007).
DOI: 10.1016/j.biomaterials.2007.08.035

[7] Guan J., Sacks M. S., Beckman E. J., Wagner W. R.: Synthesis, characterization, and cytocompatibility of elastomeric, biodegradable poly(ester-urethane)ureas based on poly(caprolactone) and putrescine. Journal of Biomedical Materials Research, **61**, 493–503 (2002).
DOI: 10.1002/jbm.10204

[8] Shen Y. Q., Shen Z. Q., Zhang Y. F., Huang Q. H., Shen L. F., Yuan H. Z.: Random copolymerization of ε-caprolactone and trimethylene carbonate with rare earth catalysts. Journal of Applied Polymer Science, **64**, 2131–2139 (1997).
DOI: 10.1002/(SICI)1097-4628(19970613)64:11<2131::AID-APP9>3.0.CO;2-K

[9] Zhu K. J., Hendren R. W., Jensen K., Pitt C. G.: Synthesis, properties, and biodegradation of poly(1,3-trimethylene carbonate). Macromolecules, **24**, 1736–1741 (1991).
DOI: 10.1021/ma00008a008

[10] Kylmä J., Seppälä J. V.: Synthesis and characterization of a biodegradable thermoplastic poly(ester-urethane) elastomer. Macromolecules, **30**, 2876–2882 (1997).
DOI: 10.1021/ma961569g

[11] Tuominen J., Kylmä J., Kapanen A., Venelampi O., Itävaara M., Seppälä J.: Biodegradation of lactic acid based polymers under controlled composting conditions and evaluation of the ecotoxicological impact. Biomacromolecules, **3**, 445–455 (2002).
DOI: 10.1021/bm0101522

eXPRESS Polymer Letters Vol.4, No.1 (2010) 39–46
Available online at www.expresspolymlett.com
DOI: 10.3144/expresspolymlett.2010.7

Memory effect of polymer dispersed liquid crystal by hybridization with nanoclay

E. H. Jeong[1], *K. R. Sun*[2], *M. C. Kang*[1], *H. M. Jeong*[3], *B. K. Kim*[2*]

[1]National Core Research Center for Hybrid Materials Solution, Pusan National University, Busan 609-735, Korea
[2]Department of Polymer Science and Engineering, Pusan National University, Busan 609-735, Korea
[3]Department of Chemistry, University of Ulsan, Ulsan 680-749, Korea

Received 17 August 2009; accepted in revised form 20 October 2009

Abstract. The electro-optical performances of polymer dispersed liquid crystal (PDLC) were investigated in the presence of organically modified clays. With the addition and increasing amount of modified clay, driving voltage and memory effect, viz. transparent state of the film after the electricity is off simultaneously increased due most likely to the increased viscosity. Among the two types of modifier, 4-(4-aminophenyl) benzonitrile having greater chemical affinity with LC than hexylamine, gave finer dispersion of clay in liquid crystal, greater viscosity, larger driving voltage and response time, and greater memory effect.

Keywords: *polymer composites, PDLC, polyurethane acrylates, clay, memory effect*

1. Introduction

Polymer dispersed liquid crystals (PDLC) have been intensively studied as electro-optical display materials during the last few decades since they can be switched electrically from a light scattering state to a transparent state without polarizers and alignment layers [1, 2]. Improved electro-optical properties have been reported for new applications [3, 4]. Fan *et al.* [5] reported scattering-free PDLC for infrared light modulator. Nicoletta *et al.* [6] investigated application of PDLC for electro-chromic device by doping some electro-chromic materials. Regarding the electro-optic performance, low molar mass surfactant such as octanoic acid has also been used to reduce the operating voltage.

Nowadays, nanocomposites employing spatially confined liquid crystals are of great interest due to the prospects of their application in opto-electric devices, photonic crystals, depolarizers, scattering displays, information storage and recording devices and windows with adjustable transparency [7–10]. It has been shown that in such systems applied external electric field causes transparent state which under some conditions can be retained after the field is off , which is called memory effect [11]. The memory effect can be utilized for large area outdoor displays with high power consumption, which can significantly be reduced by utilizing the memory effect of PDLC with the field off.

For spherical aerosol particles, it has been found that essential contribution to the memory effect is achieved due to formation of ordered branched network of the aerosol particles in the liquid crystal matrix [12].

The present work reports the memory effect of modified clay in PDLC, where modification was made with two different organic surfactants, viz. 4-(4-aminophenyl) benzonitrile (AB), and hexylamine (HA), and the effect has been studied by scanning electron microscopy (SEM) morphology,

*Corresponding author, e-mail: bkkim@pnu.edu

contact angle, transmittance, switching voltage, response time of the film.

2. Experimental

2.1. Materials and preparations of modified clay

The sodium montmorillonite (MMT) having cation exchange capacity of 92.6 meq/100 g of the clay was purchased from the Southern Clay (Gonzales, TX). MMT was added to water / ethanol (75/25 by vol%) solution at 70°C and stirred for 4 h. A 4-(4-aminophenyl) benzonitrile (AB), and hexylamine (HA) (Figure 1) were respectively added to hydrochloric acid and stirred for 24 h. The modified clay was filtered and washed repeatedly in the water/ethanol solution and dried for 12 h.

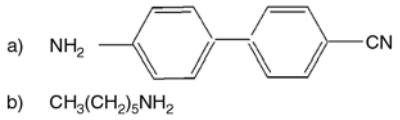

Figure 1. Chemical structures of clay modifiers: AB (a) and HA (b)

The LC-clay nanocomposite were prepared by dissolving a small amount (0.5, 1.0, 1.5 and 2.0 wt%) of clay in a commercially available cyano-based nematic LC mixture, E7 from Merck.

2.2. Polyurethane prepolymer synthesis

Bifunctional polypropylene glycol (PPG) having number average molecular weight of 750 was dried at 80°C, 0.1 mm Hg for several hr until no bubbling was observed. Extra pure grade of hexamethylene diisocyanate (HDI) was used without further purifications. Molar excess of HDI was reacted with PPG for over 1 h at 80°C to obtain NCO-terminated prepolymer. Then the reaction mixture was cooled down to 40°C and hydroxyl ethyl acrylate (HEA) was added to obtain HEA-capped polyurethane acylate (PUA) oligomers [13, 14]. Basic formulation to prepare the PUA oligomer is given in Table 1.

The PUA oligomers are highly viscous and immiscible with LC. To this 2-ethyl hexyl acrylate (EHA) and trimethylol propane triacrylate (TMPTA) were added to form a miscible mixture with LC, leading to a composition of oligomer/EHA/TMPTA = 4/2/4 [15].

E7 (BL001, Merck), an eutectic mixture of three cyanobiphenyl and a cyanoterphenyl with n_0 = 1.5216, n_e = 1.7462, and TNI = 61°C was used as LC. LC-modified clay mixture was added to the prepolymer mixture at a fixed composition of LC-modified clay/prepolymer = 4/6 by weight, together with a photo-initiator viz. Darocur 1173.

2.3. Cell fabrication

The reactive mixtures were mechanically mixed before they were filled into the indium-tin-oxide (ITO) coated cell by capillary action. Cell thickness was adjusted to 10 μm using glass bead spacers. Then, the mixtures were cured using a UV crosslinker (1.8 mW/cm^2, 365 nm) to give three dimensionally networked PUA matrix. The UV cured PDLC films sandwiched between two ITO coated cells were placed normal to the direction of collimated beam of He/Ne laser (wavelength of 632.8 nm) to measure the electro-optical properties of the cell.

Table 1. Formulations for the preparation of PDLC films

PU acrylate oligomer			Dilluent	Virgin clay	Modifier	Content of clay [wt%]	LC	Remark
Polyol	Diisocyanate	End-capping acrylate	EHA	Cloisite Na$^+$		0.0	E7	None
						0.5		[a]DC05
						1.5		DC15
					Hexylamine (HA)	0.5		HA05
						1.0		HA10
						1.5		HA15
						2.0		HA20
PPG	HDI	HEA	TMPTA		4-(4-Aminophenyl) Benzonitrile (AB)	0.5		AB05
						1.0		AB10
						1.5		AB15
						2.0		AB20

[a]DC – Dispersed virgin clay
PUA:TMPTA:EHA = 4:4:2 by weight

2.4. Measurements

A Jasco Fourier Transform Infrared (FT-IR) 430 Spectrophotometer was used to observe the chemical modification of the clay at a resolution of 2 cm^{-1}. Clay was grounded into KBr powder and pressed into discs prior to being placed in the FT-IR for scanning.

Transmitted light intensity was measured with a photodiode. The reference transmitted light intensity was obtained with blank cell of glass substrate. The output from a function generator was amplified and used to drive the shutter. The drive signal and the response of the photodiode were monitored with a digital storage oscilloscope (Hitachi VC-6023) at ambient temperature. Morphology of the films was studied using scanning electron microscopy (SEM, Hitachi S430). For this, UV cured cells were fractured in liquid nitrogen and LC was extracted in ethanol for 24 h [16]. Contact angle of the resin surface with a drop of LC has been measured using a contact angle meter (G-1, Erma). X-ray diffraction (XRD) patterns for LC-modified clay system were recorded with symmetric reflection mode by using Rigaku X-ray Diffractometer (30 kV, 25 Ma). A monochromatic CuK_α radiation was used. For each scanning interval of 2°/min, diffracted X-ray intensity was automatically recorded.

3. Results and discussion

3.1. XRD profiles

Figure 2 shows XRD profiles of the virgin clay, hexylamine modified clay and 4-(4-aminophenyl) benzonitrile modified clay. The reflection peak at $2\theta = 7.31°$ gives the interlayer spacing (*d*-spacing) of 12.07 Å for the natural clay, which was calculated by Bragg's law (Equation (1)):

$$\lambda = 2d \cdot \sin\theta \tag{1}$$

where θ is the wavelength of X-rays, *d* is the spacing between the platelets of clay and θ is the diffraction angle. It is seen that the *d*-spacing is increased with the modified clay which is a direct indication of intercalation of LC molecules into the

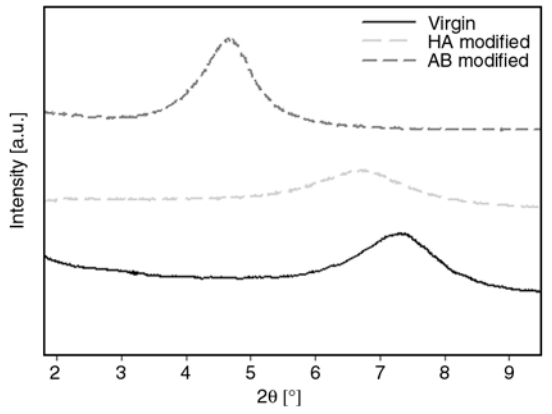

Figure 2. X-ray diffraction patterns of virgin clay, hexylamine (HA) modified and 4-(4-aminophenyl) benzonitrile (AB) modified clay

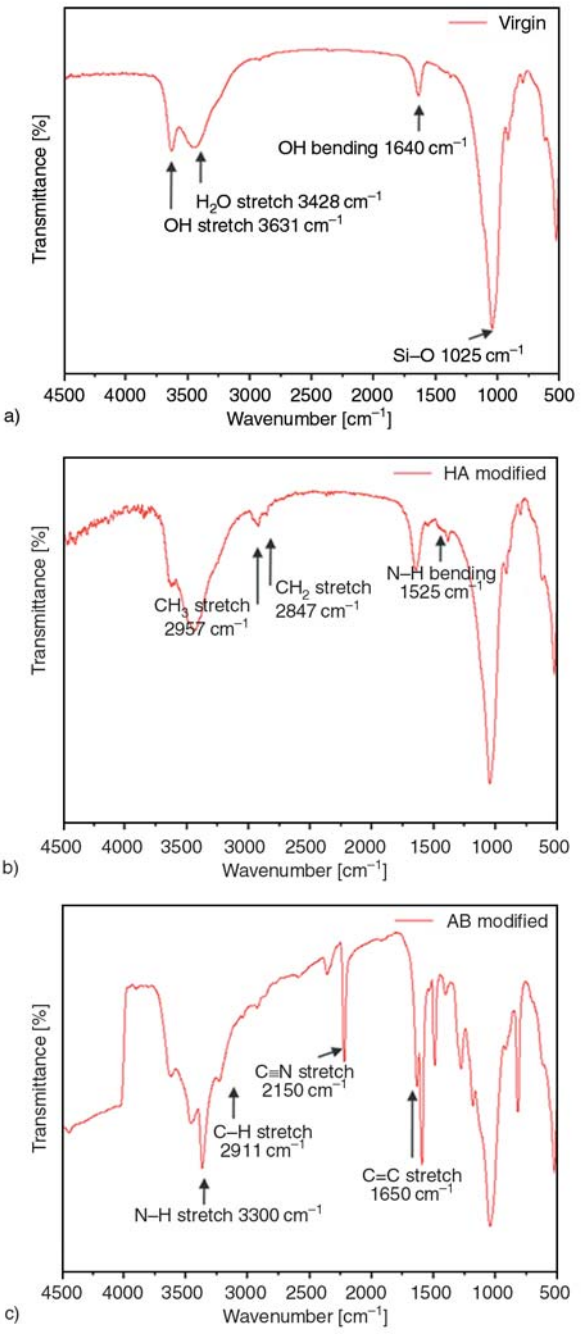

Figure 3. FT-IR spectra of virgin clay (a), hexylamine (b) and 4-(4-aminophenyl) benzonitrile modified clay (c)

layered structures of clay. It is also seen that the effect is more pronounced with AB than with HA due to the larger molecular size of the former.

3.2. FT-IR spectra

The FT-IR spectra of the virgin and modified clays are shown in Figure 3. For the virgin Na-MMT (Figure 3a), the broad absorption band centered at 1025 cm^{-1} corresponds to different crystallographic sets of Si-Al-O layers. Also, the absorption bands of OH bending (1640 cm^{-1}) and stretching (3400–3700 cm^{-1}) vibrations are due to the hydroxyl groups of modified clay and absorbed water.

For hexylamine modified clay (Figure 3b), absorption bands with peak positions at 2847, 2957 and 3300 cm^{-1} are assigned to stretching of CH_2, CH_3 and NH groups, respectively. The IR absorption spectra of 4-(4-aminophenyl) benzonitrile modified clay (Figure 3c) contain the bands of C=C (1650 cm^{-1}), C–H (2911 cm^{-1}) stretching vibrations of benzene ring and CN (2150 cm^{-1}) stretching.

3.3. Contact angle

Contact angles of polymer matrix with an LC drop have been measured as a function of modified clay content and are given in Figure 4 which show that contact angle decreases with the addition and increasing amount of modified clay. It is also noted that the contact angle of AB modified clay is smaller than the HA modified one, implying that the biphenyl group commonly appearing in clay and LC molecules contribute to miscibility.

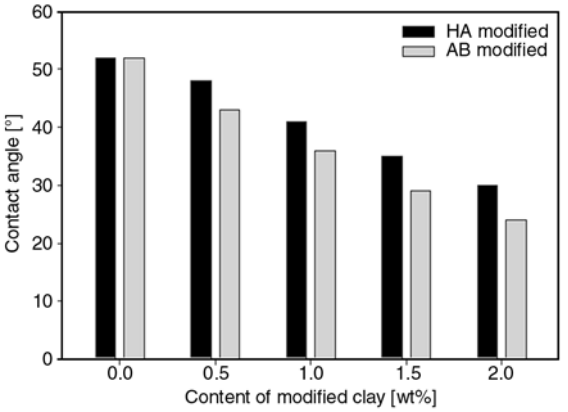

Figure 4. Contact angle of the film with LC drop

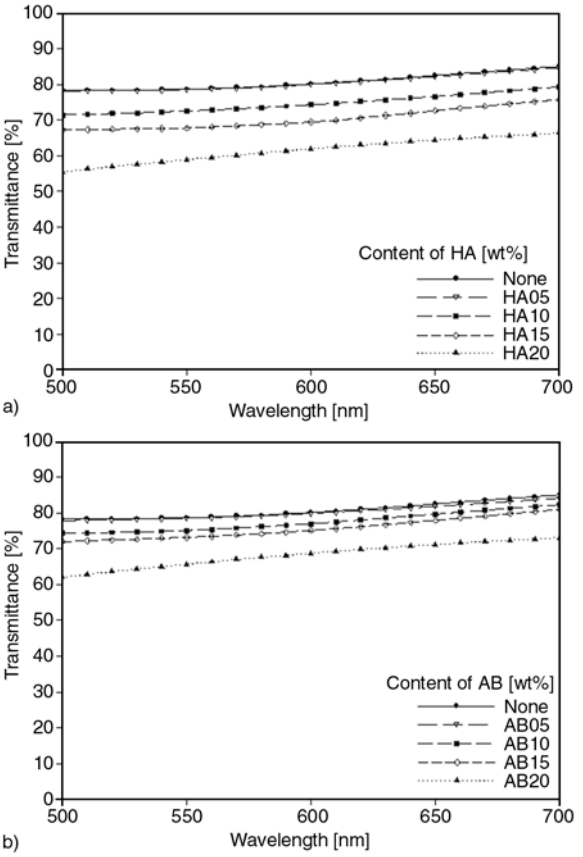

Figure 5. Visible spectra of various contents of HA (a) and AB (b)

3.4. Visible transmittance

Visible transmittance of the films with different resin compositions is shown in Figure 5 for various contents of modified clay. It is seen that the transmittance is slightly decreased with addition and increasing amount of modified clay. Also, the transmittance of AB is higher than HA due to the better dispersion of AB in LC.

3.5. Electro-optical properties

3.5.1. Driving voltage and memory effect

Typical switching characteristics of the film are shown in Figure 6 for various modifier contents, and parameters governing the effect are given in Table 2.

In the Table 2 memory parameter was defined by Equation (2):

$$M = \frac{T_m - T_0}{T_s - T_0} \tag{2}$$

where T_0, T_s and T_m are the initial transmittance of the sample, the transmittance of saturation in an

electric field and the residual transmittance after removing the field, respectively [17]. So, higher *M* gives greater memory effect. It is seen that the memory effect increases with the addition and increasing amount of modifier, and the effect is more pronounced with AB.

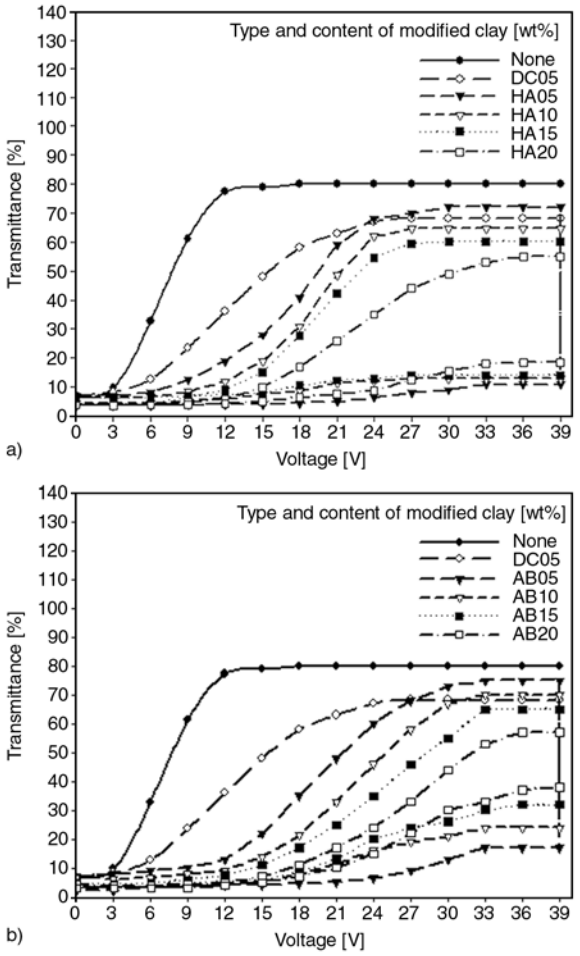

Figure 6. Transmittance vs. applied voltage at various contents of HA (a) and AB (b) (The upper and lower lines of the same caption respectively designate on state and off state transmittance. It is seen that films without clay and with virgin clay show no memory effect.)

Table 2. Memory effects of the film vs. type and content of clay

Type and content of modifier	Memory parameter (M)
None	0.00
DC05	0.00
HA05	0.11
HA10	0.14
HA15	0.15
HA20	0.29
AB05	0.22
AB10	0.33
AB15	0.48
AB20	0.66

It is seen that the driving voltage increases with the addition and increasing amount of modified clay due to the decreased droplet size to follow, which on the other hand is caused by the increased viscosity [18]. And the effect is more pronounced with AB than HA modifier.

3.5.2. Response times

The rise time is defined as the time required for the transmittance to increase from 10 to 90% points of the wave form upon turn on and the decay time is defined as the time required for the transmittance to fall from 90 to 10% upon turn off [19]. It is known that the reorientation field scales inversely with droplet size because the small liquid crystal domains produce high free energy of elastic deformations within the liquid crystal [20].

Typical response times of the films are shown in Figure 7, Table 3 and Table 4 for different types of clay and clay contents. Rise time and decay time increases with the addition and increasing amount of modified clay. These are due both to the decreased droplet size of LC (increased interfacial

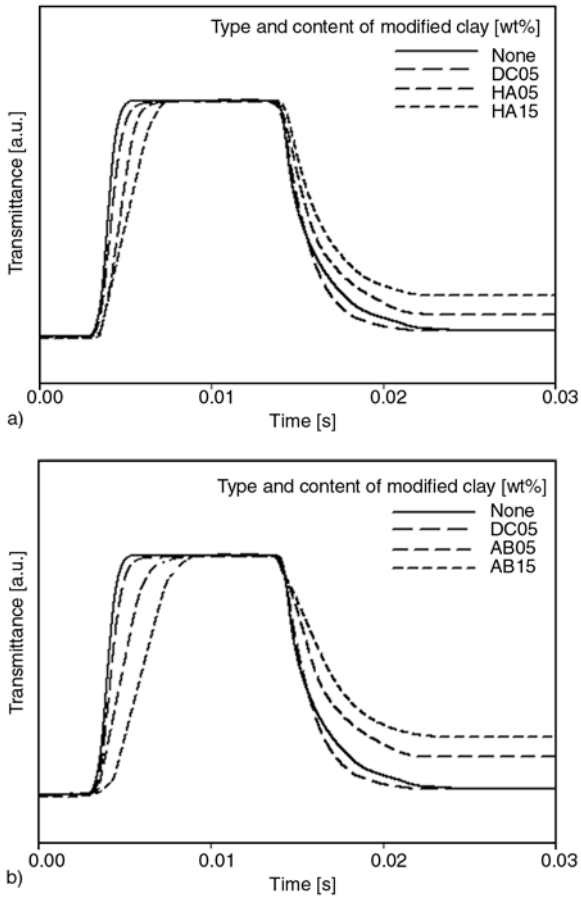

Figure 7. Response time vs. content of HA (a) and AB (b)

area) and increased anchoring strength. The response time of AB is longer than HA due mainly to the higher viscosity of AB. Virgin clay (DC) increases rise time over the None (AB00 and HA00) due to the increased viscosity, while the decay time decreased due mainly to the decreased droplet size of LC.

Surprisingly, the transparent state was maintained upon removal of the electric field, thus exhibiting memory effect. Upon field on, chain segments of modification are likely to orient along the field direction with LC molecules. Even after the field is off, the transmittance of the film remains high with modified clays and the effect is more pronounced with AB than HA modification. This implies that the modified clay maintains their orientation due to their bulkiness. Among the two types of modification, the pendant cyano-biphenyl group is expected

Table 3. Response time of the film vs. HA content (30 V)

Type and content of modify agent	Rise time [ms]	Decay time [ms]
None	2.04	8.26
HA05	2.77	10.04
HA15	3.42	10.48
DC15	2.17	8.02

Table 4. Response time of the film vs. AB content (30 V)

Type and content of modify agent	Rise time [ms]	Decay time [ms]
None	2.04	8.26
AB05	3.02	10.51
AB15	3.91	10.82
DC15	2.17	8.02

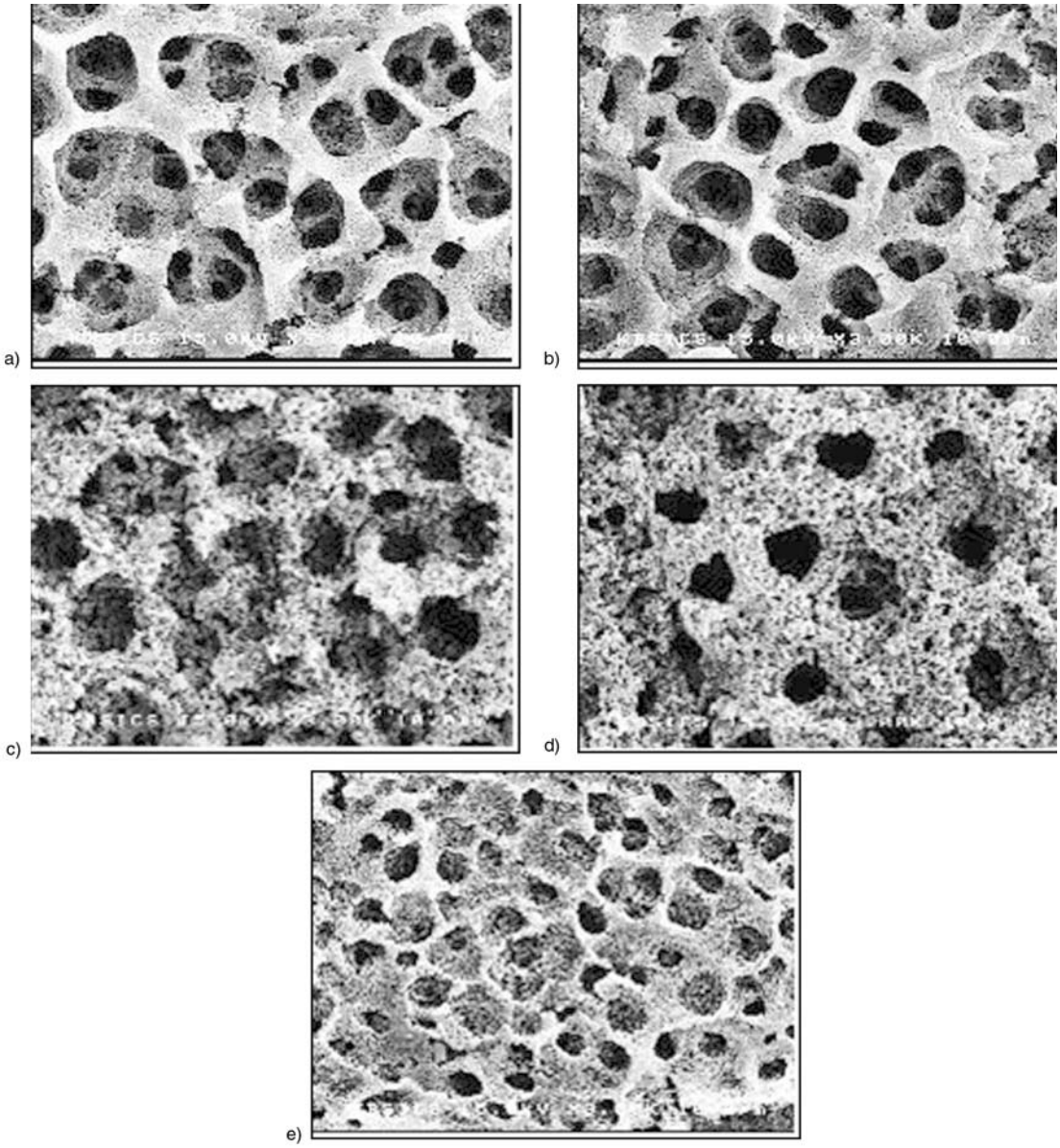

Figure 8. SEM image of the PDLC films vs. content of HA: 0 wt% (a), 0.5 wt% (b), 1.0 wt% (c), 1.5 wt% (d) and 2.0 wt% (e)

to show greater effect than the straight alkyl chain (HA) in terms of bulkiness and viscosity. The driving voltage of AB is higher than HA due to its smaller droplet size by high viscosity.

3.6. Morphology

Figure 8 and Figure 9 show SEM morphology with 3.00 K magnification of the PDLC films as a function of the type and content of the modified clay. With the addition and increasing amount of modified clay, droplet size of LC monotonically decreases due to their high viscosity. The AB shows smaller droplet size of LC than HA. This implies that miscibility of AB with LC molecules is greater than HA. At the same content of dispersed phase smaller droplet gives larger viscosity due to the larger effective volume of the droplet.

4. Conclusions

The addition of clay to the conventional polymer dispersed liquid crystals (PDLC) introduced significant effects in terms of morphology and electro-optical properties of the films. The memory effect exhibited by the modified clay is rather unusual since most of conventional nematic liquid crystals do not exhibit such effect.

With the addition and increasing amount of modified clay driving voltage and memory effect simul-

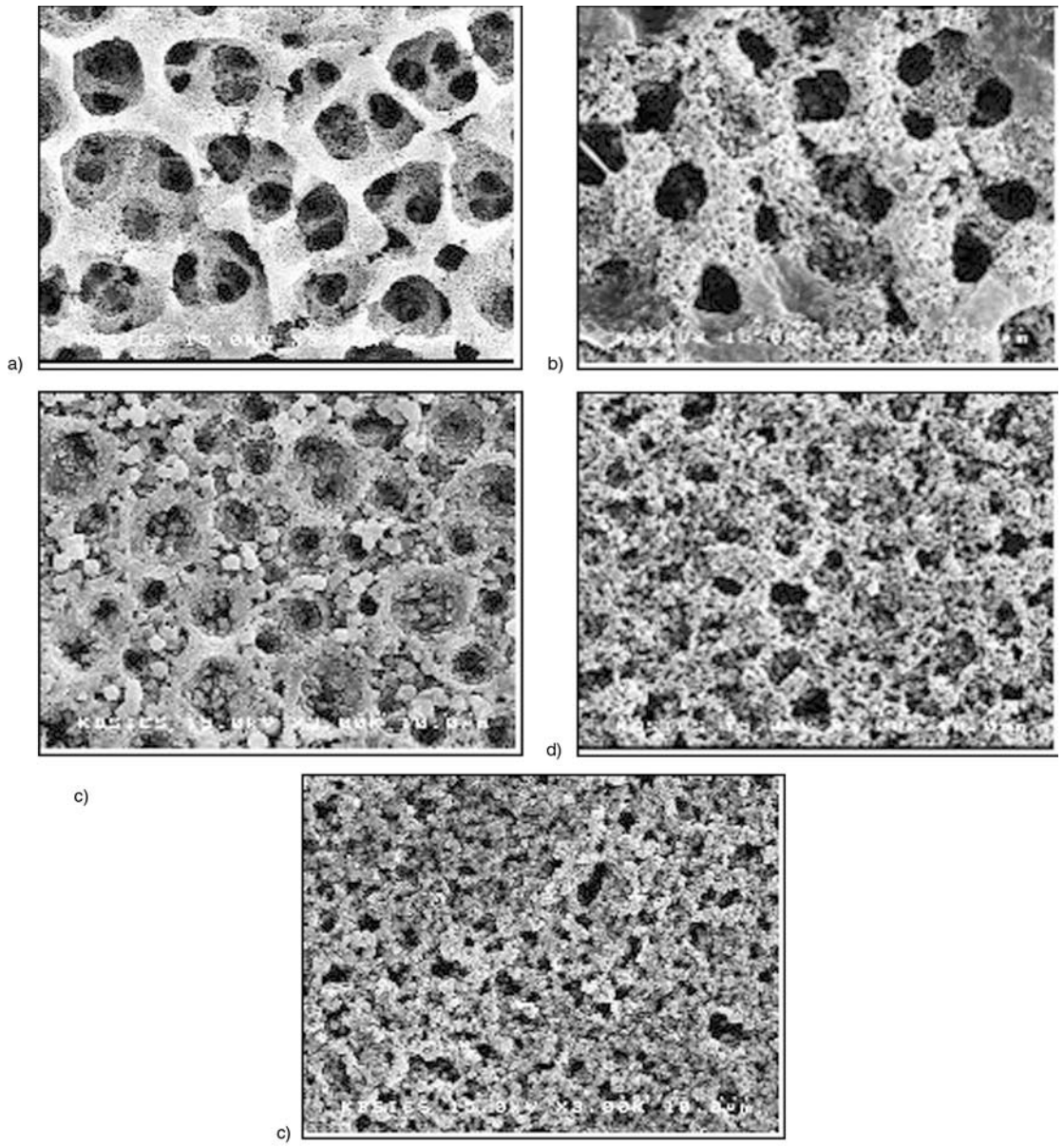

Figure 9. SEM image of the PDLC films vs. content of AB: 0 wt% (a), 0.5 wt% (b), 1.0 wt% (c), 1.5 wt% (d) and 2.0 wt% (e)

taneously increased due to the increased viscosity. Among the two types of modifier, AB gave finer dispersion of clay in LC due to the greater miscibility of AB in LC than HA. The greater miscibility is based on the similar chemical structure. So, AB gave greater viscosity, larger driving voltage and response time, and greater memory effect.

Acknowledgements

The research has been supported by the National Core Research Center at PNU.

References

[1] Drzaic P. S.: Polymer dispersed nematic liquid crystal for large area displays and light valves. Journal of Applied Physics, **60**, 2142–2148 (1986). DOI: 10.1063/1.337167

[2] Kawasumi M., Hasegawa N., Usuki A., Okuda A.: Nematic liquid crystal/clay mineral composites. Materials Science and Engineering: C, **6**, 135–143 (1998). DOI: 10.1016/S0928-4931(98)00045-9

[3] Bunning T. J., Natarajan L. V., Tondiglia V. P., Sutherland R. L.: Holographic polymer dispersed liquid crystals (H-PDLCs). Annual Review of Materials Science, **30**, 83–115 (2000). DOI: 10.1146/annurev.matsci.30.1.83

[4] Mucha M.: Polymer as an important component of blends and composites with liquid crystals. Progress in Polymer Science, **28**, 837–873 (2003). DOI: 10.1016/S0079-6700(02)00117-X

[5] Fan Y-H., Lin Y-H., Ren H., Gauza S., Wu S-T.: Fast-response and scattering-free polymer network liquid crystals for infrared light modulators. Applied Physics Letters, **84**, 1233–1235 (2004). DOI: 10.1063/1.1649816

[6] Nicoletta F. P., Chidichimo G., Cupelli D., Filpo G. D., Benedittis M. D., Gabriele B. G., Salerno A., Fazio A.: Electrochromic polymer-dispersed liquid-crystal film: A new bifunctional device. Advanced Functional Materials, **15**, 995–999 (2005). DOI: 10.1002/adfm.200400403

[7] Puchkovska G., Reznikov Yu., Yakubov A., Yaroshchuk O., Glushcheko A.: Molecular interaction and 'memory' of filled liquid crystals. Journal of Molecular Structure, **404**, 121–128 (1997). DOI: 10.1016/S0022-2860(96)09370-2

[8] Diorio N., Fisch M.: Filled liquid crystal depolarizers. Journal of Applied Physics, **90**, 3675–3678 (2001). DOI: 10.1063/1.1401799

[9] Kang D., Maclennan J., Clark N., Zakhidov A., Baughman R.: Electro-optic behavior of liquid-crystal-filled silica opal photonic crystals: Effect of liquid-crystal alignment. Physical Review Letters, **86**, 4052–4055 (2001). DOI: 10.1103/PhysRevLett.86.4052

[10] Glushchenko A., Kresse H., Puchkovska G., Reshetnyak V., Reznikov Yu., Yaoshchuk O.: Memory effect and structure of filled nematic liquid crystals. Molecular Crystals and Liquid Crystals, **321**, 15–30 (1998). DOI: 10.1080/10587259808025073

[11] Kawasumi M., Hasegawa N., Usuki A., Okada A.: Liquid crystal/clay mineral composites. Applied Clay Science, **15**, 93–108 (1999). DOI: 10.1016/S0169-1317(99)00029-0

[12] Glushchenko A., Kresse H., Reshetnyak V., Reznikov Yu., Yaroshchuk O.: Memory effect in filled nematic liquid crystals. Liquid Crystals, **23**, 241–246 (1997). DOI: 10.1080/026782997208505

[13] Kim B. K., Lee J. C.: Waterborne polyurethanes and their properties. Journal of Polymer Science Part A: Polymer Chemistry, **34**, 1095–1104 (1996) DOI: 10.1002/(SICI)1099-0518(19960430)34:6<1095::AID-POLA19>3.0.CO;2-2

[14] Kim B. K., Lee Y. H., Lee J. S.: Effect of polymer structure on the morphology and electro-optic properties of UV curable PNLCs. Polymer, **41**, 1325–1335 (2000). DOI: 10.1016/S0032-3861(99)00282-7

[15] Jung J. A., Kim B. K.: Controls of solubility parameter and crosslinking density in polyurethane acrylate based holographic polymer dispersed liquid crystal. Optics Communications, **247**, 125–132 (2005). DOI: 10.1016/j.optcom.2004.11.063

[16] Kim E. H., Kim B. K.: Diffraction gratings in non-crosslinked polymers. Journal of Polymer Science Part B: Polymer Physics, **42**, 613–620 (2004). DOI: 10.1002/polb.10743

[17] Puchkovskaya G., Reznikov Yu., Yakubov A., Yaroshchuk O., Glushchenko A.: Molecular interaction and 'memory' of filled liquid crystals. Journal of Molecular Structure, **404**, 121–128 (1997). DOI: 10.1016/S0022-2860(96)09370-2

[18] Mormile P., Musto P., Petti L., Ragosta G., Villano P.: Electro-optical properties of a PDLC based on unsaturated polyester resin. Applied Physics B: Lasers and Optics, **70**, 249–252 (2003). DOI: 10.1007/s003400050040

[19] Klosterman J., Natarajan L. V., Tondiglia V. P., Sutherland R. L., White T. J., Guymon C. A., Bunning T. J.: The influence of surfactant in reflective HPDLC gratings. Polymer, **45**, 7213–7218 (2004). DOI: 10.1016/j.polymer.2004.08.043

[20] Wu B-G., Erdmann J. H., Doane J. W.: Response times and voltages for PDLC light shutters. Liquid Crystals, **5**, 1453–1465 (1989). DOI: 10.1080/02678298908027783

eXPRESS Polymer Letters Vol.4, No.1 (2010) 47–53
Available online at www.expresspolymlett.com
DOI: 10.3144/expresspolymlett.2010.8

Nanofibre-assisted alignment of carbon nanotubes in macroscopic polymer matrix via a scaffold-based method

Z. J. Chang[1], *X. Zhao*[1], *Q. H. Zhang*[1], *D. J. Chen*[1,2*]

[1]State Key Laboratory for Modification of Chemical Fibers and Polymer Materials Shanghai 201620, People's Republic of China
[2]College of Materials Science and Engineering, Donghua University Shanghai 201620, People's Republic of China

Received 19 September 2009; accepted in revised form 28 October 2009

Abstract. A facile way for alignment of carbon nanotubes in macroscopic polymer matrix was developed by combining electrospinning and *in-situ* polymerization. The approach is based on the formation of nanofibre scaffolds with well-aligned arrays, which is filled with carbon nanotubes (CNTs). CNTs will be well aligned in macroscopic polymer matrix when the aligned nanofibre scaffold containing CNTs has been incorporated into the poly(methyl methacrylate) (PMMA) matrix by *in-situ* polymerization. We demonstrate that this scaffold approach is broadly applicable and allows for the fabrication of nanocomposites with accurately aligned nanofillers. The results presented in this report show that the approach is ideal by using polyacrylonitrile (PAN) nanofibres as a scaffold of multiwalled carbon nanotubes (MWNTs), and PMMA as the macroscopic polymer matrix. The tensile strength (7.2 wt% MWNTs/PAN nanofibres loadings) reaches 48.61 MPa, 87% higher than that pure PMMA, and the tensile modulus is increased by 175%.

Keywords: *nanocomposites, electrospinning, nanofibres, carbon nanotubes, alignment*

1. Introduction

Carbon nanotubes (CNTs) possess high intrinsic strength, stiffness, flexibility, high thermal and electrical conductivity, and are being incorporated in polymers to obtain composites with unique properties. Since the discovery of CNTs by Iijima [1], carbon nanotube-based polymer composites have become a focal point of nanocomposite research [2–4].

The state of dispersion, alignment, assembly and load stress transfer of CNTs is crucially important to the performance of nanocomposites [5]. Because of their small size, CNTs usually have high specific surface areas, resulting in a strong tendency for aggregation, so it is difficult to assemble them in polymer matrix. The dispersion and alignment of CNTs in macroscopic polymer matrix are the bigger challenges for the development of polymer nanocomposites. Over the past years, many groups have studied the dispersion of CNTs in various polymer matrices. Several processing methods are available for producing nanotube/polymer composites include: melt-mixing, solution processing, *in-situ* polymerization, gelation/crystallization method. Although these methods are different, all of them try to disperse CNTs in polymer matrix.

Electrospinning is a highly versatile method for processing solutions or melts, mainly of polymers, into continuous fibres with diameters ranging from nano- to microscale. Like nanofillers mentioned above, nanofibres also show several amazing several characteristics such as surface area to volume ratio, flexibility in surface functionalities, and superior mechanical performance compared with conventional fibres. However, the aspect ratio of nanofibres is much larger than that of general

*Corresponding author, e-mail: cdj@dhu.edu.cn

nanofillers which makes its assembling much easier. This outstanding property makes nanofibres to be optimal candidates for many important applications, including reinforcement, tissue engineering, energy and environment. In the previous research, pure random electrospun nanofibres tended to display enhanced mechanical properties in polymer matrix [6, 7]. Recently, polymer nanofibres containing carbon nanotubes [8–11], clay [12, 13], ceramics [14] and metals [15, 16] have been fabricated by several research groups. At the same time, research on nanofibre assemblies explored various structures and methods, including aligned fibres [17–20], patterned fibres [21, 22], and helical fibres [23].

In this report, we developed a general approach for the creation of polymer nanocomposites with alignment of CNTs. The processing scheme showed the initial fabrication process of the aligned polymer nanofibres with CNTs via controlled deposition of electrospun nanofibres. The polymer nanofibres become a scaffold of CNTs. CNTs will be confined in nanofibre environments, and can be aligned in nanofibre axial direction. This scaffold containing well aligned CNTs was immersed in the monomer solution. Then, the intended nanocomposite was obtained by *in-situ* polymerization. After polymerization, CNTs can be aligned within macroscopic polymer matrix. The approach, which is much easier than that in the previous methods, has a broad application and allows for the fabrication of materials with good thermal and mechanical properties. To examine the approach being facile, we used aligned polyacrylonitrile (PAN) nanofibres as a scaffold of multiwalled carbon nanotubes (MWNTs) to fabricate aligned MWNTs/PAN composite nanofibres (ACNs) firstly, and then used poly(methyl methacrylate) (PMMA) as the macroscopic polymer matrix of ACNs. Schematics of the process are shown in Figure 1.

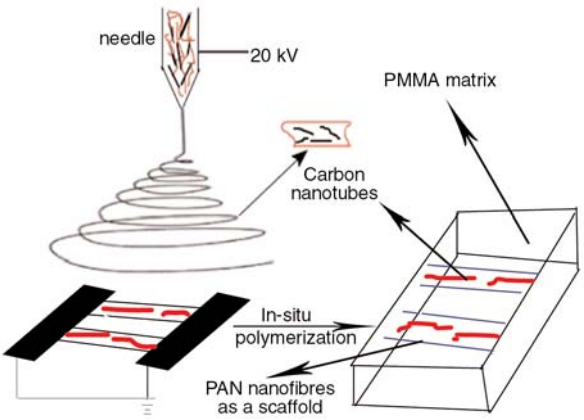

Figure 1. Alignment of MWNTs in PMMA matrix by a nanofibre scaffold

2. Experimental section

2.1. Materials

MWNTs with a purity of >95% were supplied from Shenzhen Nanotech Port Co. Ltd, China. Triton X-100, t–Oct–C_6H_4–$(OCH_2CH_2)_n$OH (n = 9–10), was purchased from Aldrich. HNO_3, $SOCl_2$ and dimethyl formamide (DMF) were purchased from Sinopharm Chemical Reagent Co. Ltd, China. The monomer, methyl methacrylate (MMA), 2,2'-azobisisobutyronitrile (AIBN) as the initiator and methanol were purchased from Sinopharm Chemical Reagent Co. Ltd, China. The AIBN was purified by re-crystallization from methanol before use. The other chemicals were used directly without further purification.

2.2. Electrospun MWNTs/PAN composite nanofibres

The MWNTs/PAN composites nanofibres were prepared according to the reported procedures [24]. The synthesis procedure can be briefly described as follows: MWNTs were functionalized by a mixture of concentrated sulfuric and nitric acids (3:1, by volume). As a result, many carboxylic acid groups (–COOH) were created in MWNTs. Then, the MWNT–COOH mixture was suspended in $SOCl_2$ and stirred for 24 h at 65°C to produce MWNT–COCl. The above MWNT–COCl and Triton X-100 was stirred under N_2 atmosphere at 120°C for 48 h. The MWNT–Triton (f-MWNTs) was thus obtained after washing and drying. For the fabrication of PAN/f-MWNT solution, 0.38 g of PAN (average molecular weight 70 000) and 0.02 g of MWNT–Triton were separately dissolved in 5 ml of DMF, and then the above solutions were mixed using an ultrasonicator. Well-aligned composite nanofibres containing PAN and f-MWNTs were prepared by electrospinning in dimethyl formamide solution, and a collector consisting of two parallel copper sheets was used to catch the nanofibres. The distance between parallel electrodes is 4 cm.

2.3. Preparation of polymer nanocomposites

MMA and purified AIBN were mixed together (20 ml of MMA:0.05 g of AIBN). A portion of the above solution was added to a glass mold. Then the nanofibre scaffold with the isolated MWNTs, which were well aligned along the nanofibre axes, was gently immersed in the solution. The mold was sealed with argon balloons after nitrogen was purged for 10 min. The polymerization was carried out in a water bath at 90°C for 15 min. Then it was polymerized at 55°C, for 16 h. After polymerization, the mold was broken. The PMMA/ACNs nanocomposites were taken out and cut some fringe sections, which did not contain ACNs.

2.4. Characterization

Thermogravimetric analysis (TGA) measurements were performed on Netzsch STA 490 under a nitrogen atmosphere from room temperature to 500°C. Wide angle X-ray diffraction (WAXD) intensity profiles of the sample were recorded with a diffractometer (D/Max-2550 PC, Rigaku, Japan). The molecular weight and molecular weight distributions of PMMA matrix from composite, using GPC (BI-MwA from Waters, LS). The solution was made by dissolving the samples in high-pressure liquid chromatography (HPLC)-grade tetrahydrofuran (THF) and filtered twice though 0.2 μm filters. The morphology and the alignment of the nanofibre scaffold in matrix were observed on a JSM-5600LV scanning electron microscope at an accelerating voltage of 10 kV, gold-sputtered prior to observation. The embedding and morphology of MWNTs within the nanofibres was measured on a Hitachi H-800 transmission electron microscope at 250 kV. Tensile tests were carried out on a Universal material testing machine (DXL-2000) at room temperature with a crosshead speed of 0.5 mm/min. The specimen gauge length was 4 cm and the width was 0.5 cm. In all cases, five samples were tested from which the standard deviations were calculated. The humidity of the laboratory was about 65%.

3. Results and discussion

MWNTs were functionalized by grafting Triton X-100 on their surface to improve their dispersion in the solution of PAN. The grafting yield is about 25 wt% by TGA data (Figure 2). Well-aligned composite nanofibres containing PAN with f-MWNTs were prepared by electrospinning in dimethyl formamide solution, and a collector consisting of two pieces of electrode was used to catch the nanofibres. SEM was used to observe the morphology of the nanofibres. Figure 3 shows the uniaxially aligned nanofibres. Figure 4 showed TEM images of the composite nanofibres in which the surface functionalized MWNTs grafted with Triton X-100 are embedded within the PAN nanofibre matrix. TEM observation showed a MWNT was parallel and oriented along the axes of the nanofibre.

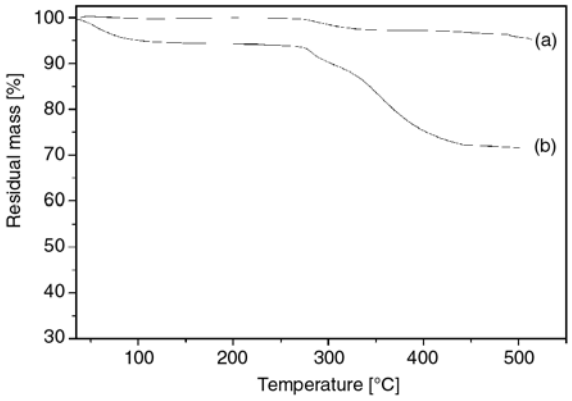

Figure 2. TGA of MWNTs (a) and MWNTs with grafted Triton X-100 (b)

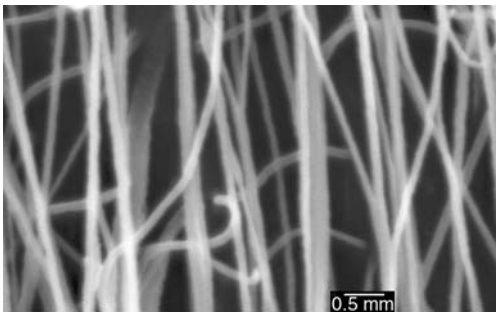

Figure 3. SEM images of the uniaxially aligned nanofibres with MWNTs

To determine whether the nanofibres influence the polymerization process, the GPC results indicate that average M_w is $5.6 \cdot 10^5$, the polydispersity of PMMA matrix (~2.18), as to pure PMMA with the average M_w ($6.7 \cdot 10^5$) and polydispersity (=1.82). The addition of ACNs shows a lower average molecular weight and a larger distribution of molecular weights. It can be concluded from these results that ACNs influence the *in-situ* polymerization of PMMA, by changing the polydispersity and molecular weight.

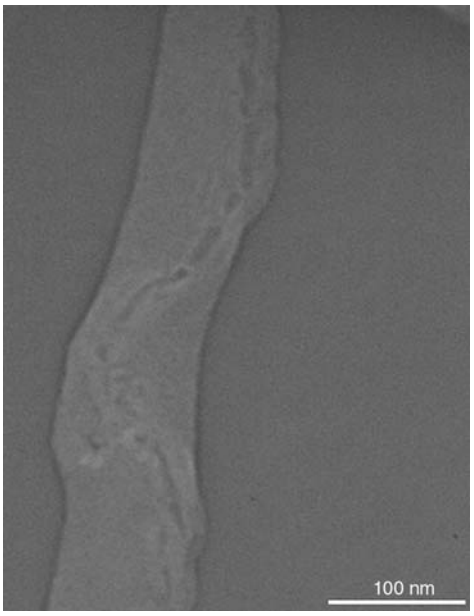

Figure 4. TEM image of nanofibre with well-oriented MWNT along the axis of nanofibre

The WAXD spectra obtained from electrospun pure aligned PAN nanofibre are presented in Figure 5a, where a characteristic diffraction peak at 16.8° and a weak peak at 28.7° were observed. These two peaks of diffraction can be assigned as (200) and (020) crystal planes of PAN. The composites sample (Figure 5b) showed a strong diffraction peak at 26.3°, was recognized as the diffraction of the (002) crystal planes of MWNTs. The weak peak is (101) at 44.3°. The result shows no significant difference from the diffraction pattern of composite nanofibres and pure PAN nanofibres, meaning that the 5 wt% f-MWNTs do not have much influence on the crystal morphology of PAN [9].

SEM was used to check the morphologies of ACNs in polymer matrix. In order to observe the morphology of ACNs in PMMA matrix, we stick them to

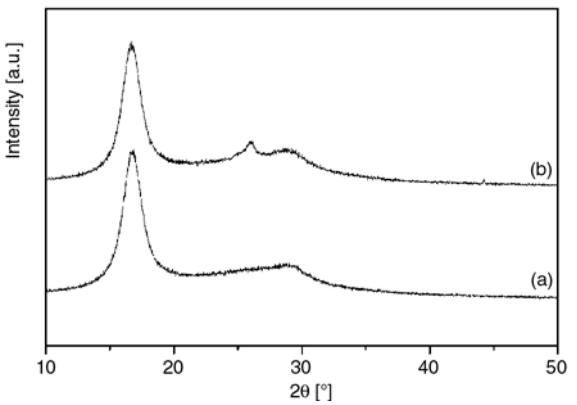

Figure 5. WAXD spectra of pure PAN nanofibres (a), and PAN-MWNTs composite nanofibres containing f-MWNTs of 5% by weight (b)

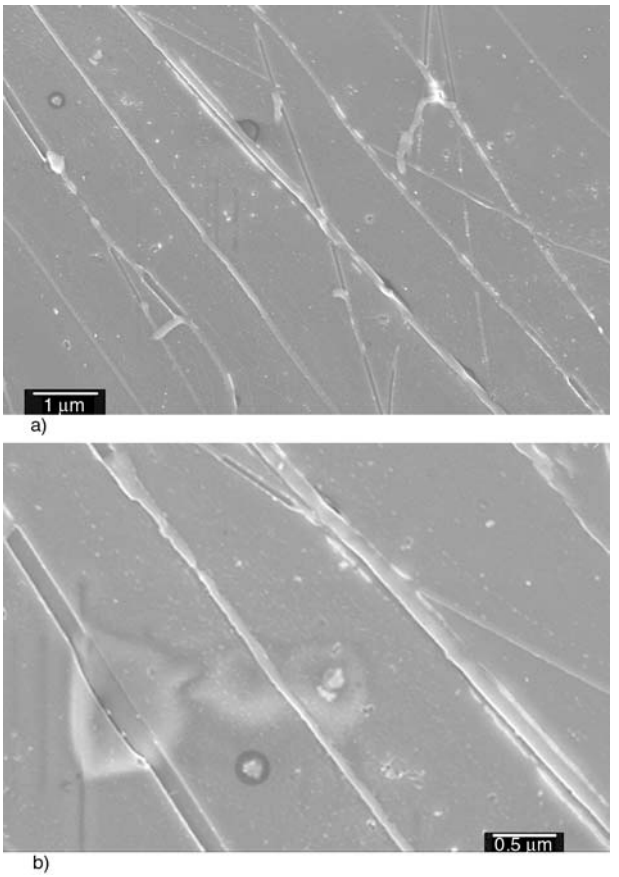

Figure 6. SEM images with different magnifications of the PMMA matrix with low-volume fraction of ACNs

bottom of the glass mold. Most of ACNs were embedded in matrix after *in-situ* polymerization. A part of ACNs embedded in polymer matrix from the bottom of the glass mold were exposed. Figure 6a gives an image with a low magnification of ACNs in PMMA matrix; a few of them are not parallel with the most of composite nanofibres but cross the ACNs. As shown in Figure 6b, the image with high magnification clearly shows that the ACNs are embedded in the PMMA matrix. Similar to existing macro-fibre composites, the ideal morphology nanocomposite has a high volume fraction of aligned, collinear nanotubes homogeneously dispersed in a surrounding matrix. By mechanically densifying ACNs, variable control of MWNTs volume fraction is easily obtained. Combined with polymer monomer into the nanofibre scaffold via simple capillarity-driven wetting along the axis of the MWNTs, nanocomposites are formed by *in-situ* polymerization. Figure 7a shows that the ultrahigh-volume-fraction ACNs were embedded in PMMA matrix. The clear morphology is shown by high magnification in Figure 7b.

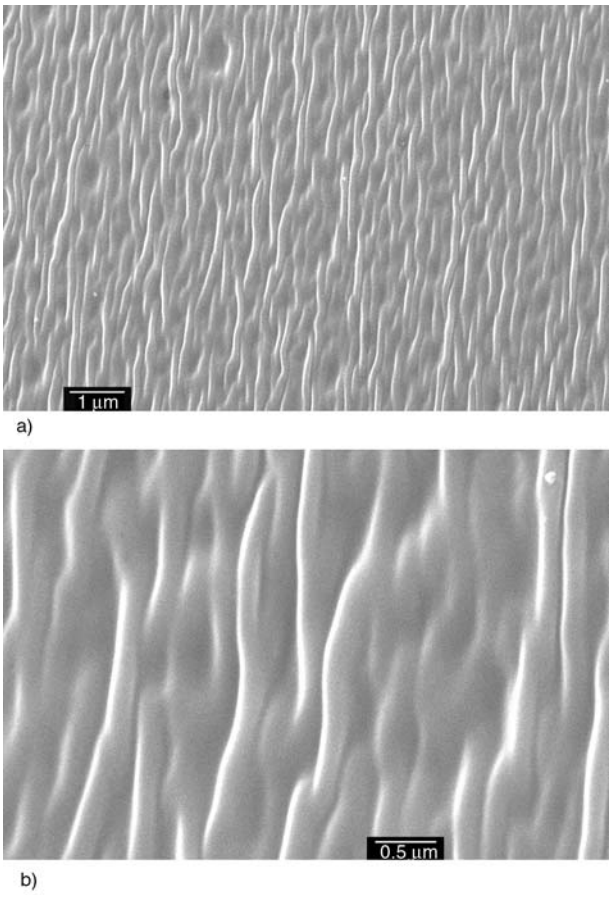

Figure 7. SEM images with different magnifications of the PMMA matrix with ultrahigh-volume fraction of ACNs

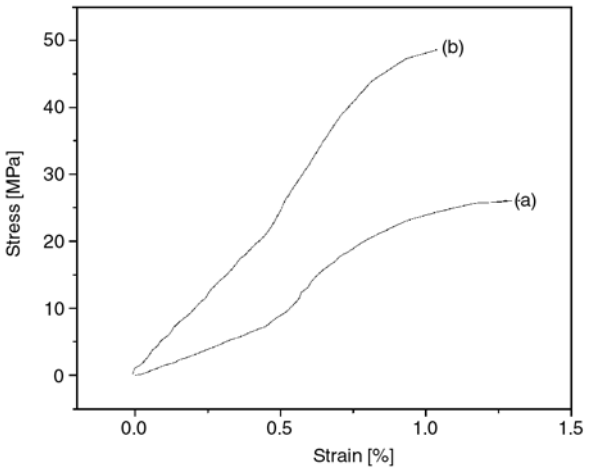

Figure 8. Stress–strain profiles of pure PMMA (a) and the composite with 7.2 wt% ACNs loadings (b)

Table 1. Tensile properties of PMMA and PMMA nanocomposites with ACNs

	Tensile strength [MPa]	**Tensile modulus [GPa]**	**Strain at break [%]**
Pure PMMA	26.04 ± 0.32	1.40 ± 0.21	1.29 ± 0.51
7.2 wt% ACNs	48.61 ± 0.75	3.86 ± 0.53	1.04 ± 0.37

Figure 8 shows the typical stress-strain curves of pure PMMA (a) and the PMMA/ACNs nanocomposites (b). The tensile strength, the tensile modulus and the strain at break values are summarized in Table 1. Pure PMMA shows a tensile strength of 26.04 MPa, and tensile modulus of 1.40 GPa, while the nanocomposite with the loading of ACNs (7.2 wt%) shows a strength of 48.61 MPa, and a tensile modulus of 3.86 GPa (axial direction of ACNs). This corresponds to an increase of about 87 and 175%, verifying the validity of introducing the aligned f-MWNTs as reinforcing fillers to PMMA matrix.

A wide variety of theoretical work has been carried out since the 1950s with the aim of modeling the mechanical properties of fibre-reinforced composites. There are the rule of mixtures and the Halpin-Tsai equations [25]. The Halpin-Tsai equation is used in the nanocomposites, which is known to fit some data very well at low volume fractions of fillers. In the equation, E_m is the tensile modulus of the matrix of ACNs, V_f is the MWNTs (in ACNs) volume fraction, l_f, d_f are length and diameter of MWNTs, respectively, l_f/d_f is the aspect ratio of MWNTs.

E_f of MWNT was taken as 450 GPa [26], whereas the volume fraction $V_f = 2.0\%$ was calculated from the measured weight fraction (5.0 wt%) of f-MWNTs, based on the MWNTs density (2.16 g/cm^3), Triton X-100 density (1.07 g/cm^3) and the PAN density (1.16 g/cm^3). For the E_m, we use $E_m \approx 27$ GPa [27, 28]. The aspect ratio of MWNTs was 15, using measurements from transmission electron microscopy images. Since electrospun fibre formation imposes an axial orientation of the nanotubes, the composite modulus (E_{fibre}) can be calculated by Equation (1), resulting in a value of 38.8 GPa for ACNs containing 5 wt% f-MWNTs:

$$E_{fibre} = E_m \frac{1 + 2\frac{l_f}{d_f}\eta V_f}{1 - \eta V_f} \tag{1}$$

where

$$\eta = \frac{\frac{E_f}{E_m} - 1}{\frac{E_f}{E_m} + 2\frac{l_f}{d_f}} \tag{2}$$

The Halpin-Tsai equation is known to fit some data very well at low volume fractions but to underestimate stiffness at high volume fraction of nanofillers. The rule of mixtures can be used to model the ACNs/PMMA nanocomposites with high volume fraction of ACNs . In the simplest possible case a composite can be modeled as an isotropic, elastic matrix filled with aligned elastic fibres that span the full length of the specimen [29]. We use the rule of mixtures modeling properties of ACNs reinforced composites by Equation (3), where E_{fibre} is the ACNs modulus, E'_m is the matrix modulus, and V'_f is the ACNs volume fraction:

$$E_c = (E_{fibre} - E'_m)V'_f + E'_m \quad (3)$$

In Equation (3), E'_m of PMMA was taken as 1.40 GPa from experiment data, and the volume fraction $V'_f = 7.1\%$ was calculated from the measured weight fraction (7.2 wt%) of ACNs, based on ACNs weight put into the reacting solution and the PMMA density (1.17 g/cm^3). The calculated modulus (E_c = 4.05 GPa) is close agreement with the experimental modulus (3.86 GPa), which indicates f-MWNTs are isolated and aligned in PMMA matrix.

4. Conclusions

In conclusion, the aligned PAN nanofibre scaffold containing MWNTs was introduced to PMMA matrix to control the alignment of MWNTs in PMMA matrix. MWNTs can be well aligned within macroscopic PMMA matrix via a scaffold of aligned PAN nanofibres. The reinforcement effect of ACNs has been clearly demonstrated. The approach can be broadly used for the fabrication of nanocomposites with better alignment and much higher volume fraction of nanofillers.

Acknowledgements

This work has been supported by the Fund of Innovation Project on Doctoral Dissertation of Donghua University and Supported by the Programme of Introducing Talents of Discipline to Universities (111-2-04).

References

[1] Iijima S.: Helical microtubules of graphitic carbon. Nature, **354**, 56–58 (1991). DOI: 10.1038/354056a0

[2] Moniruzzaman M., Winey K. I.: Polymer nanocomposites containing carbon nanotubes. Macromolecules, **39**, 5194–5205 (2006). DOI: 10.1021/ma060733p

[3] Zhang Q. H., Rastogi S., Chen D. J., Lippits D., Lemstra P. J.: Low percolation threshold in single-walled carbon nanotube/high density polyethylene composites prepared by melt processing technique. Carbon, **44**, 778–785 (2006). DOI: 10.1016/j.carbon.2005.09.039

[4] Zhang Q. H., Lippits D. R., Rastogi S.: Dispersion and rheological aspects of SWNTs in ultrahigh molecular weight polyethylene. Macromolecules, **39**, 658–666 (2006). DOI: 10.1021/ma051031n

[5] Schaefer D. W., Justice R. S.: How nano are nanocomposites? Macromolecules, **40**, 8501–8517 (2007). DOI: 10.1021/ma070356w

[6] Bergshoef M. M., Vancso G. J.: Transparent nanocomposites with ultrathin, electrospun nylon-4,6 fiber reinforcement. Advanced Materials, **11**, 1362–1365 (1999). DOI: 10.1002/(SICI)1521-4095(199911)11:16<1362::AID-ADMA1362>3.0.CO;2-X

[7] Kim J-S., Reneker D. H.: Mechanical properties of composites using ultrafine electrospun fibers. Polymer Composites, **20**, 124–131 (1999). DOI: 10.1002/pc.10340

[8] Ayutsede J., Gandhi M., Sukigara S., Ye H. H., Hsu C. M., Gogotsi Y., Ko F.: Carbon nanotube reinforced *Bombyx mori* silk nanofibers by the electrospinning process. Biomacromolecules, **7**, 208–214 (2006). DOI: 10.1021/bm0505888

[9] Hou H. Q., Ge J. J., Zeng J., Li Q., Reneker D. H., Greiner A., Chen S. Z. D.: Electrospun polyacrylonitrile nanofibers containing a high concentration of well-aligned multiwall carbon nanotubes. Chemistry of Materials, **17**, 967–973 (2005). DOI: 10.1021/cm0484955

[10] McCullen S. D., Stevens D. R., Roberts W. A., Ojha S. S., Clarke L. I., Gorga R. E.: Morphological, electrical, and mechanical characterization of electrospun nanofiber mats containing multiwalled carbon nanotubes. Macromolecules, **40**, 997–1003 (2007). DOI: 10.1021/ma061735c

[11] Heikkilä P., Harlin A.: Electrospinning of polyacrylonitrile (PAN) solution: Effect of conductive additive and filler on the process. Express Polymer Letters, **3**, 437–445 (2009). DOI: 10.3144/expresspolymlett.2009.53

[12] Ji Y., Li B. Q., Ge S. R., Sokolov J. C., Rafailovich M. H.: Structure and nanomechanical characterization of electrospun PS/clay nanocomposite fibers. Langmuir, **22**, 1321–1328 (2006).
DOI: 10.1021/la0525022

[13] Kim G-M., Michler G. H., Ania F., Calleja F. J. B.: Temperature dependence of polymorphism in electrospun nanofibres of PA6 and PA6/clay nanocomposite. Polymer, **48**, 4814–4823 (2007).
DOI: 10.1016/j.polymer.2007.05.082

[14] Shao C., Kim H-Y., Gong J., Ding B., Lee D-R., Park S-J.: Fiber mats of poly(vinyl alcohol)/silica composite via electrospinning. Materials Letters, **57**, 1579–1584 (2003).
DOI: 10.1016/S0167-577X(02)01036-4

[15] Lee H. K., Jeong E. H., Baek C. K., Youk J. H: One-step preparation of ultrafine poly(acrylonitrile) fibers containing silver nanoparticles. Materials Letters, **59**, 2977–2980 (2005).
DOI: 10.1016/j.matlet.2005.05.005

[16] Wang Y. Z., Li Y. X., Sun G., Zhang G. L., Liu H., Du J. S., Yang S. A., Bai J., Yang Q. B.: Fabrication of Au/PVP by electrospinning nanofiber composites by electrospinning. Journal of Applied Polymer Science, **105**, 3618–3622 (2007).
DOI: 10.1002/app.25003

[17] Li D., Wang Y. L., Xia Y. N.: Electrospinning of polymeric and ceramic nanofibers as uniaxially aligned arrays. Nano Letters, **3**, 1167–1171 (2003).
DOI: 10.1021/nl0344256

[18] Matthews J. A., Wnek G. E., Simpson D. G., Bowlin G. L.: Electrospinning of collagen nanofibers. Biomacromolecules, **3**, 232–238 (2002).
DOI: 10.1021/bm015533u

[19] Teo W. E., Ramakrishna S.: Electrospun fibre bundle made of aligned nanofibres over two fixed points. Nanotechnology, **16**, 1878–1884 (2005).
DOI: 10.1088/0957-4484/16/9/077

[20] Theron A., Zussman E., Yarin A. L.: Electrostatic field-assisted alignment of electrospun nanofibres. Nanotechnology, **12**, 384–390 (2001).
DOI: 10.1088/0957-4484/12/3/329

[21] Li D., Ouyang G., McCann J. T., Xia Y. N.: Collecting electrospun nanofibers with patterned electrodes. Nano Letters, **5**, 913–916 (2005).
DOI: 10.1021/nl0504235

[22] Zhang D. M., Chang J.: Patterning of electrospun fibers using electroconductive templates. Advanced Materials, **19**, 3664–3667 (2007).
DOI: 10.1002/adma.200700896

[23] Yu J., Qiu Y. J., Zha X. X., Yu M., Yu J. L., Rafique J., Yin J.: Production of aligned helical polymer nanofibers by electrospinning. European Polymer Journal, **44**, 2838–2844 (2008).
DOI: 10.1016/j.eurpolymj.2008.05.020

[24] Zhang Q. H., Chang Z. J., Zhu M. F., Mo X. M., Chen D. J.: Electrospun carbon nanotube composite nanofibres with uniaxially aligned arrays. Nanotechnology, **18**, 115611/1–115611/6 (2007).
DOI: 10.1088/0957-4484/18/11/115611

[25] Mallick P. K.: Fiber-reinforced composites: Materials, manufacturing, and design. Marcell Dekker, New York (1993).

[26] Liu L-Q., Tasis D., Prato M., Wagner H. D.: Tensile mechanics of electrospun multiwalled nanotube/poly(methyl methacrylate) nanofibers. Advanced Materials, **19**, 1228–1233 (2007).
DOI: 10.1002/adma.200602226

[27] Yuya P. A., Wen Y. K., Turner J. A., Dzenis Y. A., Li Z.: Determination of Young's modulus of individual electrospun nanofibers by microcantilever vibration method. Applied Physics Letters, **90**, 111909/1–111909/3 (2007).
DOI: 10.1063/1.2713128

[28] Gu S-Y., Wu Q-L., Ren J., Vancso G. J.: Mechanical properties of a single electrospun fiber and its structures. Macromolecular Rapid Communications, **26**, 716–720 (2005).
DOI: 10.1002/marc.200400667

[29] Callister W. D.: Materials science and engineering: An introduction. Wiley, New York (2003).